Open Quantum System Studies of Optical Lattices and Nonlinear Optical Cavities: A Comprehensive Development of Atomtronics

by

Ronald A. Pepino

B.S., University of Connecticut, 2003

A thesis submitted to the

Faculty of the Graduate School of the

University of Colorado in partial fulfillment

of the requirements for the degree of

Doctor of Philosophy

Department of Physics

2011

This thesis entitled:
Open Quantum System Studies of Optical Lattices and Nonlinear Optical Cavities:
A Comprehensive Development of Atomtronics
written by Ronald A. Pepino
has been approved for the Department of Physics

Murray Holland

Ana Maria Rey

Date

The final copy of this thesis has been examined by the signatories, and we find that both the content and the form meet acceptable presentation standards of scholarly work in the above mentioned discipline.

Pepino, Ronald A. (Ph.D., Physics)

Open Quantum System Studies of Optical Lattices and Nonlinear Optical Cavities:

A Comprehensive Development of Atomtronics

Thesis directed by Prof. Murray Holland

A generalized open quantum theory that models the transport properties of bosonic systems is derived from first principles. This theory is shown to correctly describe the long-time behavior of a specific class of non-Markovian system-reservoir interactions. Starting with strongly-interacting bosons in optical lattices, we use this theory to construct a novel, one-to-one analogy with electronic systems, components, and devices. Beginning with the concept of a wire, we demonstrate theoretically the ultracold boson analog of a semiconductor diode, a field-effect transistor, and a bipolar junction transistor. In a manner directly analogous to electronics, we show that it is possible to construct combinatorial logic structures from the fundamental electronic-emulating devices just described. In this sense, our proposal for atomtronic devices is a useful starting point for arrangements with more complex functionality. In addition we show that the behavior of the proposed diode should also be possible utilizing a weakly-interacting, coherent bosonic drive.

After demonstrating the formal equivalence between systems comprised of bosons in optical lattices and photons in nonlinear cavity networks, we use the formalism to extend the ideas and concepts developed earlier in ultracold boson systems to nonlinear optical systems. We adapt the open quantum system theory to this new physical environment, and demonstrate theoretically how a few-photon optical diode can be realized in a coupled nonlinear cavity system. An analysis of different practical cavity quantum electrodynamics systems is presented and experimentally-viable candidates are evaluated.

Dedication

To my family, including Jen and Scooter, with much love.

Acknowledgements

Although some people do perform science in vacuum. Science—in general—is not done in a vacuum. It would be hard for me to imagine completing this work with out the good fortune to have interacted with the following people.

First, I would like to thank my brilliant, talented, and charismatic high school physics teacher Dr. James Volo. This man introduced me to the discipline of physics as well as ignited in me the passion that kept me in the field for the last thirteen years.

Next, I would like to thank my professors/mentors/friends at the University of Connecticut. From these faculty members, I acquired the fundamental skills needed to think about and analyze physical problems.

I would also like to thank Vasili Kharchenko and Alex Dalgarno at ITAMP. Under their guidance, I honed my research skills, learned how to program, as well as write scientific papers.

I would like to thank the faculty here at the University of Colorado. The outstanding faculty that I had a chance to overlap with have all been great educators/mentors. I am especially grateful to Paul Beale, Ana Maria Rey, Dana Anderson and Robert Parson for sitting on my dissertation committees. Poor Professor Beale also suffered through my second comprehensive exam process, where he was very helpful in guiding my learning of renormalization group methods in understanding critical phenomena.

I am grateful to have met so many talented, interesting, and fun colleagues and friends here at CU, especially my fellow members of the Holland group: Rajiv, Brian, Jochen, Brandon, Merit, Jami, Boris, Sarah, David, and Dominic. These people have all contributed to this thesis in some

way.

I owe much gratitude to John (a.k.a. Jinks) Cooper. From the very beginning of my work in Murray's group, Jinks has always made himself available to me. I was a great benefactor of Jinks' piercing physical intuition. Despite the fact that Jinks would probably regard myself as a Markov process from time to time, he has patiently remained a pain in the ass, who refused to settle for an imprecise explanation on just about anything. He also saw to it that I left Colorado knowing many of the standard quantum optics analytical 'tricks of the trade'. Our interaction, has helped make me a better, more careful, and thorough scientist.

Finally—and most of all—I would like to thank (full) Professor Murray Holland, who allowed me be part of his group, financially supported me (even over himself when funding became an issue), and provided me with intellectual freedom, as well as guidance, when I needed it. Equipped with a wealth of creative scientific ideas, as well as keen physical insight, Murray has been an excellent scientific mentor to me over the past few years. He is also one of the best public speakers/lecturers that I have ever seen. Observing him, as well as listening to his suggestions regarding my own presentations, I feel that my own lecture style has improved greatly. Additionally, in Brandon's absence, Murray became the editor-in-chief for this thesis. And, although Murray loves atomtronics, I have a sneaking suspicion that upon the third read/overhaul of this work, his enthusiasm was starting to fade a bit. On top of all of these things, Murray has also been a good friend as well as an exceptional scientific and personal role model.

Contents

Chapter

Tables

Table

Figures

Figure

Chapter 1

Introduction

The advent of laser cooling and trapping of neutral atoms and ions [1] has revolutionized the field of atomic physics in several ways. From the standpoint of spectroscopy, the absorption lines of trapped, virtually stationary ultracold atoms or ions can be resolved without spectral lines undergoing shifts or broadening due to time dilation and Doppler effects. Additionally, the extended observation times allow the unshifted, unbroadened features to be resolved with greater precision. These ultracold, trapped atomic systems, along with our improved spectroscopic knowledge of them, have led to great advances in the field of metrology as well. For example, this technology has allowed improvement in the accuracy of atomic clocks by orders of magnitude, and matter-wave interferometry of ultracold atomic beams has made ultrasensitive accelerometers and thus gravimeter and gravity gradient detectors. The impact that laser cooling has had on atomic physics as a field of research goes well-beyond enhancements in high-resolution spectroscopy, time standards, and metrological technologies.

Today, cold atoms can be prepared (via optical pumping techniques for example) in specific quantum states, precisely manipulated, and even entangled [2]. Entanglement, manipulation, and storage of quantum states in atomic systems has played a significant role in the emergence of the field of quantum information science.

Ultracold atomic systems have also proven to be effective quantum simulators: many-body quantum phase transitions such as Bose-Einstein condensation (BEC) [3] and the Bose-Einstein condensation to Bardeen-Cooper-Schrieffer (BEC-BCS) cross-over [4] have been demonstrated and

studied in these systems. The fact that ultracold atoms can be stored in virtually defect-free crystals known as optical lattices [5] also makes them great quantum simulators for condensed matter models such as the Bose-Hubbard model [6]. Perhaps the most striking demonstration of applying Bose-Hubbard physics to ultracold gases was the recent observation of the Mott insulator-to-superfluid phase transition [7].

Over the past two decades, our ability to manipulate and control quantum systems has increased profoundly. This precise level of control has inspired the idea of atomtronics, which is the topic of this thesis. The goal of atomtronics is to realize the behavior of electronic components and devices in atom-optical systems. Micheli *et al.* originally proposed the idea of a single atom transistor [8], where the transport of bosons in an optical lattice can be allowed, or inhibited, based on the spin orientation of a single fermion 'impurity' atom. This system is illustrated in Figure 1.1(a). Stickney, Anderson and Zozuya [9] proposed transistor-like behavior in a different system, consisting of a BEC trapped in the left most well of a three-well system. In their model, depicted in Figure 1.1(b-c), the transport of atoms from the left well to the right well is controlled

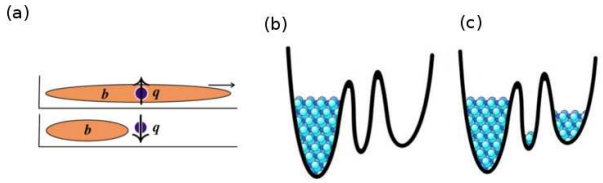

Figure 1.1: (a) The single atom transistor, proposed by Micheli *et al.* involves a BEC trapped on the left side of an optical lattice where its transport to the right side of the lattice is controlled by a single fermionic atom (labeled as q). If q is spin down, then the BEC remains fully on the left-hand side where quantum interference effects inhibit the wave function from existing on the right-hand side of the lattice. If q is spin up, there is no interference, and the BEC can traverse the lattice. Reprinted with permission from reference [8]. (b) A three well BEC transistor device, proposed by Stickney *et al.* Here a BEC is stored in the left well of the three well system. If no atoms are in the middle well, then there is a chemical potential mismatch between the central and the first well containing the atoms. The mismatch prevents the atoms from tunneling to the third well. (c) On the other hand, in this configuration, adding atoms to the middle well raises the chemical potential, bringing it closer to the chemical potential of the left well. When a resonance is achieved between the left and middle wells, the atoms can cross and populate the right-most well.

by the chemical potential of the middle well. If atoms are added to the middle well, its chemical potential is raised. As the chemical potential of the middle well approaches the chemical potential of the well containing the BEC, a resonance is enabled, allowing atoms in the BEC to tunnel through to the right well in the system. The general qualitative behavior of both of these proposed devices is consistent with the device characteristics exhibited by a conventional electronic semiconductor transistor.

In this thesis, we present a different approach to atomtronics. We consider a much closer analog to electronic circuitry than the systems mentioned above. Our approach involves atomtronic devices composed of optical lattices that are driven by reservoirs of ultracold, neutral atomic gases. These systems are direct analogs of traditional electronic components driven by a voltage source, where the atoms traversing the lattice resemble electrons moving in a semiconductor crystal.

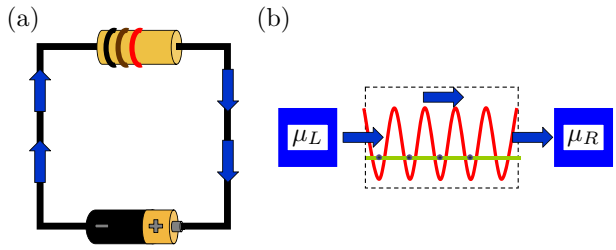

Figure 1.2: Illustration of the analogy between (a) the electronic circuit of a wire (with some inherent resistance) connected to a battery and (b) its atomtronic counterpart.

The analogy is illustrated in Figure 1.2, where we have the simple circuit of a resistive wire connected to a battery. In this example, the electric potential difference between the two battery terminals that is responsible for generating an electronic flux through the wire is replaced by a chemical potential difference between two reservoirs, which enable an atomic flux through the system. The wire itself, which could be for example a copper lattice where electrons hop from atom-to-atom, is replaced by an optical lattice with finite site-to-site tunneling. The electronic current measured in amperes is replaced by an atomic flux measured in particles per second through the optical lattice system. The motivation to construct and study these particular atomtronic analogs of electronic systems comes from several directions.

First, the experimental atomtronic realizations promise to be extremely clean. Imperfections such as lattice defects or phonons can be essentially eliminated if desired. This allows one to study an idealized system from which all inessential complications have been stripped. Interest in such complexity-reduced systems lies parallel to the recent research efforts in single electron transistors in mesoscopic systems [10] and molecules [11], where many themes common with atomtronics emerge. A consequence of the near ideal experimental conditions for optical lattice systems is that theoretical descriptions for atomtronic systems can be developed from first principles. This allows theorists to develop detailed models that can reliably predict the properties of devices.

Second, atomtronics systems are intrinsically richer than their electronic counterparts because atoms can possess more complex internal structure than electrons. Whereas electrons can only be spin-up or spin-down, atoms can be either bosons or fermions, possessing many internal states, and the interactions between atoms can be widely varied from short to long range, from strong to weak, and from isotropic to anisotropic. This can lead to behavior that is qualitatively different to that of electronics [12, 13, 14, 15]. Consequently, one can study repulsive, attractive, or even non-interacting atoms in the same experimental setup. Additionally, current experimental techniques allow for the detection of atoms with fast, state-resolved meters that operate at near unit quantum efficiency [16]. Thus it is possible, in principle, to follow the dynamics of an atomtronic system in real time.

Third, neutral atoms in optical lattices can be well-isolated from the environment, reducing the negative effects of decoherence. They combine a powerful means of state readout and preparation with methods for entangling atoms [17]. Such systems have all the necessary ingredients to be the building blocks of quantum signal processors. The close analogies with electronic devices can serve as a guide in the search for new quantum information architectures, including novel types of quantum logic gates that are closely tied with the conventional architecture in electronic computers.

Fourth and finally, recent experiments studying transport properties of ultracold atoms in optical lattices [18, 19, 20] can be discussed in the context of the atomtronics framework. In particular, one can model the short-time transport properties of an optical lattice with the open

quantum system formalism discussed here.

This thesis is structured as follows. In Chapter 2, we review background physical concepts used throughout this work. We discuss the basic physics involved in trapping atoms in optical lattices, and consider how the system of ultracold bosonic atoms trapped in an optical lattice is related to the Bose-Hubbard model. We then derive a simple coupled cavity quantum electrodynamics (QED) model and discuss the implication of inserting a nonlinear Kerr medium into the cavity. As we see, this system is an alternative physical realization of the Bose-Hubbard model. We conclude this chapter with a review of electromagnetically-induced transparency (EIT) and an extension thereof. Such systems are shown to exhibit large Kerr nonlinear response with minimal absorption.

In Chapter 3, we review the master equation treatment of open quantum systems. We derive the standard second-order Born-Markov master equation as well as an all-orders kinetic theory description of the formalism. After demonstrating that under the same approximations, the two formalisms are equivalent, we generalize the kinetic theory description to model system Hamiltonians that are time-dependent.

In Chapter 4, we demonstrate the possible breakdown of the Born-Markov formalism when the reservoirs in the model have sharp boundaries in their density of states. We then derive a non-Markovian master equation that is capable of modeling these exotic reservoirs. The validity of this non-Markovian theory is confirmed by comparing its behavior at a sharp reservoir boundary to the behavior of a large, closed quantum system model that can be solved exactly.

In Chapter 5, we develop atomtronics components in the context of bosonic atoms trapped in optical lattices. Assuming a fermionized bosonic reservoir model, we propose a series of atomtronic devices that emulate the electronic behavior of a semiconductor diode, field-effect transistor, and bipolar junction transistor. We show that basic discrete logic behavior can be realized in these systems. Afterwords, an alternative reservoir model, where the lattice system is driven by a coherent BEC is considered. Assuming this reservoir model, the basic atomtronic diode behavior is recovered.

In Chapter 6 we discuss the progress that we have made to extending the atomtronics theory

to encompass sequential logic devices. After the set-reset flip-flop is reviewed, the time-dependent master equation is used to demonstrate the enhancement of transport across off-resonant lattices. This is done in the context of developing and understanding bistable atomtronic circuitry, which is at the heart of implementing sequential logic behavior.

In Chapter 7 we discuss a distinct realization of the atomtronic components in a nonlinear optical cavity context. We present models for various driving mechanisms, and perform simulations that evaluate the parameter regime where the characteristics of the diode could potentially be realized. We then explore possible experimental implementations of this device in high-finesse etalon cavities, toroidal microcavities, and photonic band-gap nanocavities.

Finally, in Chapter 8 we draw conclusions, and consider potential avenues for future research directions.

Chapter 2

Background and Physical Concepts

Our goal in this thesis is to realize electronic behavior in atom-optical systems, specifically atoms in optical lattices and photons in optical cavities. Here we provide a brief review of established physical concepts that will be utilized throughout this thesis. We first discuss optical lattices and their connection to the Bose-Hubbard model. Afterwords we derive a simple coupled cavity theory consisting of cascaded one-dimensional etalons containing a nonlinear $\chi^{(3)}$ material. We find that the Hamiltonian for this nonlinear etalon cavity theory, in second-quantized form, amounts to another realization of the Bose-Hubbard model with on-site interactions. For this reason, the Bose-Hubbard model plays a central role throughout this thesis. Finally, we review the basic characteristics of three-level and four-level electromagnetically-induced transparency (EIT) systems. These systems have the capability of generating large Kerr nonlinearities with minimal dissipation.

2.1 Atoms in Optical Lattices

Optical lattices, in the simplest sense, are periodic crystals of light created by interfering counterpropagating laser beams. The resulting standing-wave is a spatially-periodic array of strong and weak electric and magnetic fields. Single atoms predominantly interact with the electric component of this light field, where they can either be attracted to the field maxima or minima depending on whether the wavelength of the light field is detuned to a frequency either above or below the atomic transition. If the potential energy of the atom-lattice coupling is large compared to the thermal

energy of the atoms themselves, the atoms become localized on the lattice sites, with the ability to tunnel to neighboring sites. In the limit that the lattice potential goes towards infinity, the atoms lose the ability to tunnel even to nearest neighboring sites, and thus remain frozen in place.

Optical lattices are near-perfect crystal structures. They are free of lattice vibrations, they can be perfectly regular, *i.e.* defect-free structures, and, if desired, they can be constructed with precisely-located 'defect' features. They are also energy-conserving systems, which makes them suitable for quantum information applications. Furthermore, these lattices can be constructed in one-dimension, two-dimensions, or three-dimensions by utilizing the appropriate number of counter-propagating pairs of lasers in orthogonal directions. This is illustrated schematically in Figure 2.1.

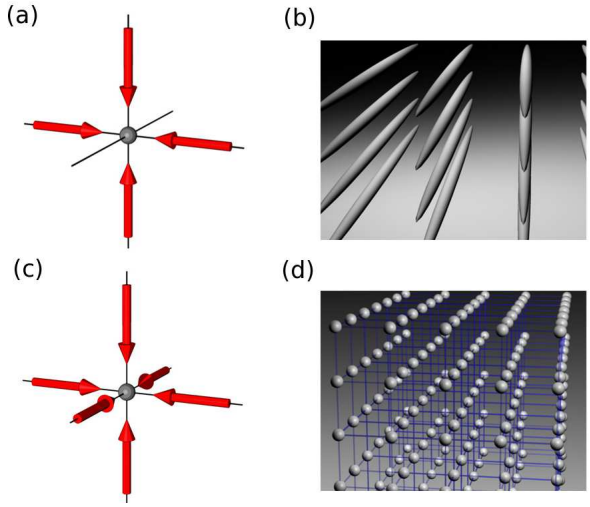

Figure 2.1: Illustration of a BEC confined by (a) two orthogonal sets of counterpropagating lasers, which generate a two-dimensional lattice of tube-like BEC distributions (b). (c) The addition of a third mutually orthogonal set of counterpropagating lasers generates a three-dimensional light crystal, confining the atoms to point-like sites (d). Reprinted with permission from reference [21].

Jaksch *et al.* [22] suggested that the dynamics of an ultracold gas of bosons trapped in an optical lattice could be well-described by the Bose-Hubbard model [6]. The Bose-Hubbard model utilizes a Hamiltonian that describes a system of bosons confined to sites of a crystal lattice, where the bosons can interact with each other, and can tunnel in the lowest band to the nearest neighboring

sites. This minimalistic model exhibits a quantum phase transition as a function of the lattice depth known as the Mott insulator-to-superfluid phase transition. In their work, Jaksch *et al.* proposed that this quantum phase transition could be realized in this atom-optical system. These ideas were subsequently experimentally implemented and confirmed by Greiner *et al.* in 2002 [7]. The success of this experiment, depicted in Figure 2.2, demonstrated that optical lattice systems can be ideal realizations for a variety of strongly-correlated condensed matter models. Among many other implementations, these lattices are currently used in both theoretical and experimental contexts to study analogs of high-temperature superconductivity via the so-called t-J-U Hamiltonian [23], and Tonks-Girardeau gases, where a strongly-interacting one-dimensional Bose gas can exhibit some fermionic properties [24].

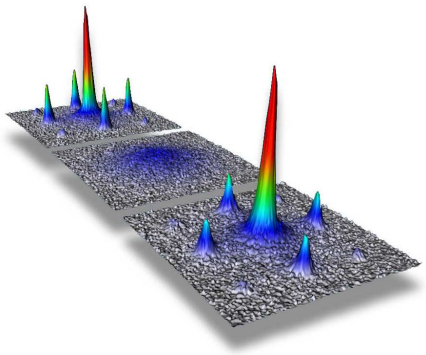

Figure 2.2: Experimental realization of the Mott insulator-to-superfluid quantum phase transition. Reprinted with permission from reference [21].

Experimentalists have made great strides in their ability to create, manipulate, and resolve the behavior of ultracold gasses trapped in optical lattices. Today, instead of simply using counter-propagating lasers to obtain a uniform lattice structure, site-by-site custom optical lattices can be constructed with great precision by illuminating a holographic mask with a light source [25, 26]. As can be seen in Figure 2.3, cutting-edge experimental technology also makes it possible to resolve single atoms in the lattice [25, 27, 28] as well as to address single sites at the sub-micron level [29, 30]. The lack of energetic dissipation, the extreme tunability of the Bose-Hubbard systems, and the ability to resolve single atoms, make optical lattices excellent candidates for the study and possible

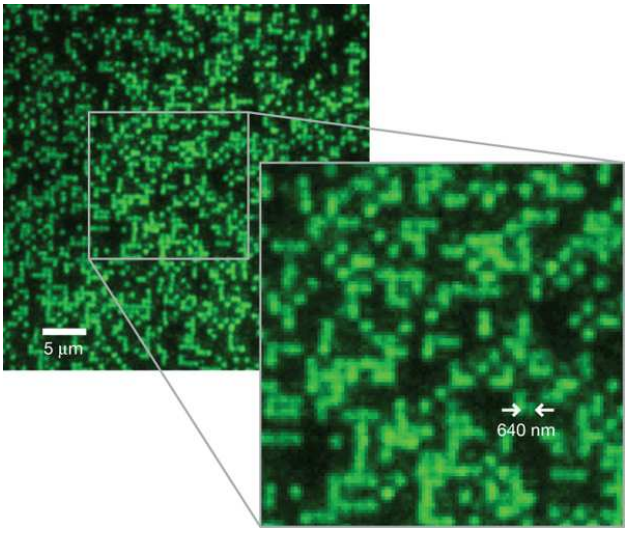

Figure 2.3: An actual experimental image of site-resolved 640 nm optical lattice. Here, single atoms, holes, and even adjacent atoms are resolved. Reprinted with permission from reference [16].

realization of the atomtronic components, as we propose in this thesis.

In this section, we introduce the basic physics behind trapping atoms in optical lattices, and provide a brief derivation of the Bose-Hubbard model for atoms in optical lattices. For simplicity, these calculations are performed in one-dimension. In principle at least, extending these ideas to higher dimensions is straightforward.

2.1.1 Interaction of an atom with a standing electromagnetic wave

Consider the one-dimensional problem of a two-level atom interacting with the electromagnetic field that is generated by two counter-propagating lasers that are both characterized by the wave vector k. The electric field for this system can be written as

$$\begin{aligned} E(t) &= E_0 \left(\cos(kx - \omega t) + \cos(kx + \omega t)\right) \\ &= E_0 \cos(kx) \left(\mathrm{e}^{i\omega t} + \mathrm{e}^{-i\omega t}\right) \end{aligned} \tag{2.1}$$

where E_0 is the magnitude of the electric field and ω is the frequency of the laser field. The atoms interact with the electric field through their electric dipole moment μ. The corresponding

Hamiltonian for a two-level atom interacting with this electric field is

$$\hat{H} = \hbar\omega_0|1\rangle\langle 1| + \mu E_0 \cos(kx)\Big(|0\rangle\langle 1| + |1\rangle\langle 0|\Big)\left(\mathrm{e}^{i\omega t} + \mathrm{e}^{-i\omega t}\right). \tag{2.2}$$

Transforming into an interaction picture that rotates with the frequency of the laser field, the corresponding Hamiltonian in the interaction picture $\tilde{H}$ is

$$\begin{aligned}\tilde{H} &= \hbar\Delta|1\rangle\langle 1| + \mu E_0 \cos(kx)\Big(|0\rangle\langle 1|\mathrm{e}^{-i\omega t} + |1\rangle\langle 0|\mathrm{e}^{i\omega t}\Big)\left(\mathrm{e}^{-i\omega t} + \mathrm{e}^{i\omega t}\right) \\ &\simeq \hbar\Delta|1\rangle\langle 1| + \mu E_0 \cos(kx)\Big(|0\rangle\langle 1| + |1\rangle\langle 0|\Big)\end{aligned} \tag{2.3}$$

where $\Delta = \omega_0 - \omega$, and we have made the rotating wave approximation by dropping the rapidly-oscillating terms of frequency $\simeq 2\omega$. This approximation is justified since, for optical frequencies $\sim 10^{15}$ Hz, these terms average to zero rapidly compared to their stationary counterparts.

If $|\hbar\Delta| \sim |\mu E_0|$, the atom may absorb photons from the laser field, and then spontaneously emit them. Such dissipative dynamics can be suppressed by working in the regime where $|\hbar\Delta| \gg |\mu E_0|$, which causes the atom to essentially remain in its ground state. Additionally, this regime allows us to treat the dipole term perturbatively since, by construction, it is much smaller in magnitude than $\hbar\Delta$. Perturbation theory gives the following second order correction to the ground state energy:

$$\begin{aligned}\varepsilon_0^{(2)}(x) &= -\frac{\mu^2 E_0^2}{\hbar\Delta}\cos^2(kx) \\ &\equiv V_0 \cos^2(kx)\end{aligned} \tag{2.4}$$

This is known as the alternating current (AC) Stark shift. From this energetic correction, we see that the atom experiences a spatially periodic potential through its interaction with the oscillating electric component of the standing wave. It is through this potential that the atom becomes confined to sites on the optical lattice. For $\omega > \omega_0$, *i.e.* 'blue-detuning', the atoms experience a potential minimum whenever $\cos^2(kx) = 0$. Alternatively, when $\omega < \omega_0$, *i.e.* 'red-detuning', the atoms experience a minimum whenever $\cos^2(kx) = 1$. Since the atoms will localize at the potential minima, blue detuning localizes the atoms at the field minima, while red detuning localizes atoms at the field maxima.

2.1.2 The Bose-Hubbard model

In recent experiments, the relative minima of individual lattice sites can be shifted up or down in energy with respect to one another. We can include this effect in our model by adding a site-dependent energy term $\epsilon(\boldsymbol{x})$ to the Hamiltonian, which defines the relative local minima of the lattice. Using the AC-Stark shift result from Section 2.1.1, the corresponding Hamiltonian for a two-level atom trapped in a three-dimensional optical lattice can be written as

$$\tilde{H} = \frac{\hat{p}^2}{2m} + V_0 \left(\cos^2(kx) + \cos^2(ky) + \cos^2(kz)\right) + \epsilon(\boldsymbol{x}). \tag{2.5}$$

where $\hat{p}$ is the kinematic momentum, m is the mass, and we have assumed the the frequency and intensity of all of the counterpropagating laser beams are identical for simplicity. If $\epsilon(\boldsymbol{x})$ is neglected, then the periodicity of $V_0 \cos^2(kx)$ implies that the complete set of wave functions that are eigenmodes of the Hamiltonian are Bloch functions. These Bloch functions can be expressed as a site-localized set of orthonormal basis states known as Wanier states. Assuming that all of the atoms are in the lowest band, and that their kinetic energies are much smaller than the second band excitation energies, we can expand the wave function solutions in the lowest band Wanier states alone. In a second quantized description, the field operators are then

$$\hat{\psi}(\boldsymbol{x}) = \sum_j \hat{a}_j w_0(\boldsymbol{x} - \boldsymbol{x}_j) \tag{2.6}$$

where $\hat{a}_j$ annihilates an atom on site j and $w_0(\boldsymbol{x} - \boldsymbol{x}_j)$ is the lowest band Wanier state centered on site j.

Assuming that the ultracold atoms interact with each other through an s-wave scattering contact potential, the atom-atom interaction can be written as [31]

$$U(\boldsymbol{x}_j, \boldsymbol{x}_k) \simeq \frac{4\pi\hbar^2 a_s}{m} \delta(\boldsymbol{x}_j - \boldsymbol{x}_k) \tag{2.7}$$

where a_s is the scattering length and $\boldsymbol{x}_j$ and $\boldsymbol{x}_k$ are the positions of atoms indexed by j and k. The second quantized Hamiltonian for the many atom system [32] is then

$$\begin{aligned}\hat{H} &= \int d\boldsymbol{x}\ \hat{\psi}^\dagger(\boldsymbol{x})\left(\frac{\hat{p}^2}{2m} + V_0\left(\cos^2(kx)+\cos^2(ky)+\cos^2(kz)\right)+\epsilon(\boldsymbol{x})\right)\hat{\psi}(\boldsymbol{x}) \\ &\quad + \frac{2\pi\hbar^2 a_s}{m}\int d\boldsymbol{x}\hat{\psi}^\dagger(\boldsymbol{x})\hat{\psi}^\dagger(\boldsymbol{x})\hat{\psi}(\boldsymbol{x})\hat{\psi}(\boldsymbol{x}) \\ &= \sum_{j,k}\hat{a}_j^\dagger\hat{a}_k\int d\boldsymbol{x}\ w_0(\boldsymbol{x}-\boldsymbol{x}_j)\left(\frac{p^2}{2m} + V_0\left(\cos^2(kx)+\cos^2(ky)+\cos^2(kz)\right)+\epsilon(\boldsymbol{x})\right)w_0(\boldsymbol{x}-\boldsymbol{x}_k) \\ &\quad + \frac{2\pi\hbar^2 a_s}{m}\sum_{jklm}\hat{a}_j^\dagger\hat{a}_k^\dagger\hat{a}_l\hat{a}_m\int d\boldsymbol{x}\ w_0(\boldsymbol{x}-\boldsymbol{x}_j)w_0(\boldsymbol{x}-\boldsymbol{x}_k)w_0(\boldsymbol{x}-\boldsymbol{x}_l)w_0(\boldsymbol{x}-\boldsymbol{x}_m).\end{aligned} \tag{2.8}$$

Restricting ourselves to the tight-binding regime, where the magnitude of the lattice potential guarantees that a non-negligible overlap of Wanier states occurs for nearest neighbor lattice sites alone, we get

$$\hat{H} = \sum_j\left(\hbar\omega_j\hat{a}_j^\dagger\hat{a}_j + \frac{U_j}{2}\hat{a}_j^\dagger\hat{a}_j^\dagger\hat{a}_j\hat{a}_j\right) - \sum_{\langle j,k\rangle}J_{jk}\hat{a}_j^\dagger\hat{a}_k \tag{2.9}$$

where

$$\hbar\omega_j = \int d\boldsymbol{x}\ w(\boldsymbol{x}-\boldsymbol{x}_j)^2\epsilon(\boldsymbol{x}), \tag{2.10}$$

$$U_j = \frac{4\pi\hbar^2 a_s}{m}\int d\boldsymbol{x}\ w_0(\boldsymbol{x}-\boldsymbol{x}_j)^4, \tag{2.11}$$

and

$$J_{jk} = -\int d\boldsymbol{x}\ w_0(\boldsymbol{x}-\boldsymbol{x}_j)\left(\frac{-\hbar^2}{2m}\nabla^2 + V_0\left(\cos^2(kx)+\cos^2(ky)+\cos^2(kz)\right)\right)w_0(\boldsymbol{x}-\boldsymbol{x}_k). \tag{2.12}$$

The sum $\langle j,k\rangle$ is exclusively taken over nearest neighboring sites.

Equation (2.9) is known as the the Bose-Hubbard model. The parameters $\hbar\omega_j$ and U_j are the zero point and on-site interaction energies for lattice site j, and J_{jk} is the tunneling energy between sites j and k. In this thesis, we will make great use of this Hamiltonian in a variety of open quantum system settings. The definition of an 'open quantum system', as well as the mathematical apparatus needed to describe them, is provided in detail in the following chapter.

2.2 Photons in coupled optical cavities

An alternative system to atoms in optical lattices is coupled arrays of high quality optical cavities. In this section, we provide a classical field analysis of such coupled etalons. Quantization

of the cavity mode field is straightforward [33, 34, 35] and implemented afterwords. We show that this simple system is all that's needed to introduce the cavity parameters that will be discussed later in this thesis.

We then consider the effect of inserting a material with a Kerr nonlinearity into the cavity. This material generates an effective nonlinear photon-photon interaction. This interaction term, in a second-quantized representation, is formally equivalent to the on-site interaction energy of two atoms trapped on the same lattice site. With the inclusion of the Kerr-type material in the cavity, the resulting second quantized form of this cavity QED system Hamiltonian is another realization of the Bose-Hubbard Hamiltonian.

2.2.1 Simple cavity theory

We first consider a single etalon cavity comprised of two parallel mirrors driven by electromagnetic plane waves. Figure 2.4(a) depicts this scenario where an incident wave $E_i^{(+)}$ approaches the etalon from the left side. For simplicity, we assume that the mirrors have the same transmission and reflection coefficients (t, r). The field inside the cavity as a function of frequency can be determined from the continuity of the boundary conditions as the field propagates through the etalon

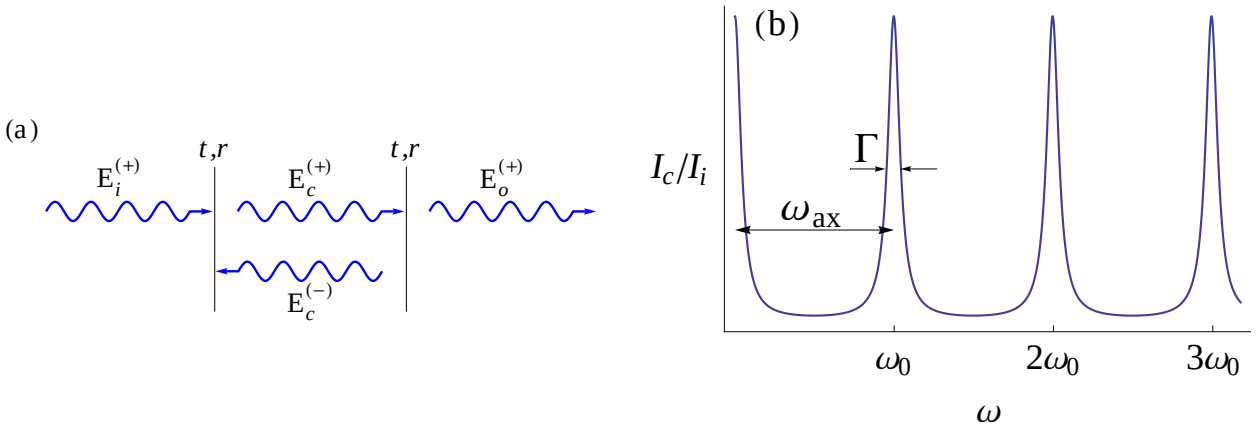

Figure 2.4: (a) An illustration of light incident, inside and leaving an etalon with reflection and transmission coefficients r and t. (b) The generic response of an etalon driven by a laser with frequency ω and fundamental cavity mode ω_0. The axial mode spacing ω_{ax} and linewidth Γ are labeled.

system:

$$E_c^{(+)} = itE_i^{(+)} + rE_c^{(-)}e^{i\frac{\varphi}{2}} \tag{2.13}$$

$$E_c^{(-)} = rE_c^{(+)}e^{i\frac{\varphi}{2}} \tag{2.14}$$

$$E_o^{(+)} = itE_c^{(+)}e^{i\frac{\varphi}{2}} \tag{2.15}$$

where the sign designates the field traveling in the positive or negative direction for the incident field E_i, the cavity field E_c, and the field transmitted through the cavity E_o. The reflection and transmission coefficients r and t are constrained by $|r|^2 + |t|^2 = R + T = 1$, where R and T are the reflectance and transmittance of the cavity, and φ is the round trip phase shift that the electromagnetic wave acquires in the cavity. From these expressions, the ratio of the intensity of the field inside the cavity to the input intensity is

$$\begin{aligned}\frac{I_c^{(+)}}{I_i^{(+)}} &= \frac{T}{1 - 2R\cos(\varphi) + R^2} \\ &= \frac{\frac{T}{(1-R)^2}}{1 + \frac{4R}{(1-R)^2}\sin^2\left(\frac{\varphi}{2}\right)}.\end{aligned} \tag{2.16}$$

This function is plotted in Figure 2.4(b), where we have labeled the axial mode spacing by ω_{ax} and the cavity bandwidth (or linewidth) by Γ. From equation (2.16), the axial mode spacing (or free spectral range) can be determined:

$$\varphi = 2\pi = k \cdot l = \omega_{ax}\frac{\lambda_0}{c} \tag{2.17}$$

where $l = \lambda_0$ is the round trip path length, or fundamental wavelength of the cavity and c is the speed of light. The cavity linewidth, which is the full-width half maximum (FWHM) of the periodic peaks of equation (2.16), can be obtained by asserting

$$\frac{4R}{(1-R)^2}\sin^2\left(\frac{\varphi}{2}\right) = 1. \tag{2.18}$$

Here φ corresponds to the half width half maximum (HWHM) of the linewidth. Assuming that $R \simeq 1$, it follows from equation (2.18) that

$$\varphi = k \cdot \lambda_0 = \omega_{\mathrm{HWHM}}\frac{\lambda_0}{c} = \pi\frac{2\omega_{\mathrm{HWHM}}}{\omega_{ax}} \equiv \pi\frac{\Gamma}{\omega_{ax}} \simeq \frac{1-R}{\sqrt{R}} \tag{2.19}$$

or simply

$$\Gamma = \frac{\omega_{ax}}{\mathcal{F}} \tag{2.20}$$

where

$$\mathcal{F} \equiv \frac{\pi\sqrt{R}}{1-R} \tag{2.21}$$

is the finesse of the cavity. Since $T = 1 - R$ is the fractional power loss in the cavity, the cavity linewidth is directly related to the cavity decay rate. Since $R \to 1$, implies $\mathcal{F} \to \infty$, more reflective cavity mirrors lead to a higher value of finesse. For this reason, finesse is a common cavity parameter used to characterize how 'good' a cavity is. In modern cavity QED experiments, finesse values greater than 4×10^5 have been achieved [36, 37]. An alternative way to quantify the quality of a cavity is through its quality factor, or Q factor. The Q factor of a cavity is defined as the ratio of the cavity driving frequency over the cavity linewidth. Thus

$$\mathcal{F} = \frac{\omega_{ax}}{\omega_0} Q \tag{2.22}$$

where ω_0 is the frequency of the driven cavity mode.

For high finesse cavities, the axial modes are well-separated, and a single mode description of the cavity field is possible. The corresponding Hamiltonian for a particular cavity mode with energy ω_1 can be expressed in the following second quantized form:

$$\hat{H}_{\text{cav}} = \hbar\omega_1 \hat{a}^\dagger \hat{a}. \tag{2.23}$$

The cavity field amplitude for this mode is

$$\hat{E}(z) = \varepsilon_{\omega_1} \left(\hat{a} + \hat{a}^\dagger\right) \sin\left(k_1 z\right) \tag{2.24}$$

where z is the direction of propagation of the field, $k_1 = \omega_1/c$, and

$$\varepsilon_{\omega_1} = \sqrt{\frac{\hbar\omega_1}{\epsilon_0 V}} \tag{2.25}$$

is the electric field per photon in the cavity, where ϵ_0 is the permittivity of free space and V is the effective mode volume [34].

The mirrors that make up the cavity in practice are typically spherical mirrors as illustrated in Figure 2.5. The cavity mode within the Rayleigh range and under the paraxial approximation [38] is a Gaussian standing wave of the form

$$\psi(x, y, z) = \sin(k_1 z)\mathrm{e}^{-(x^2+y^2)/\mathrm{w}_0^2} \tag{2.26}$$

where the standing wave is in the z-direction, and w_0 is the cavity mode waist [38]. The cavity waist, depicted in Figure 2.5, is an important cavity parameter as it restricts the effective mode volume of the cavity. As the effective mode volume is reduced, the electric field per photon is enhanced. Since the atom-cavity field coupling is proportional to the electric field, smaller cavity mode volumes lead to greater atom-field coupling strengths.

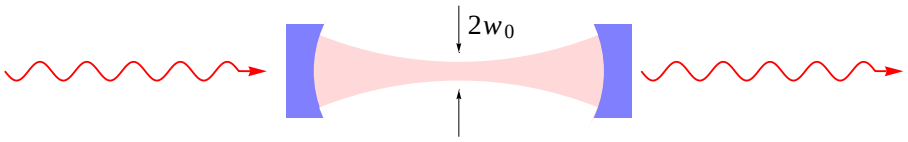

Figure 2.5: An illustration of a driven etalon cavity with characteristic mode waist w_0.

2.2.2 Classical treatment of cavity input-output theory

Here we relate the classical input-output parameters of a cavity to its quantum mechanical counterpart. This is achieved by comparing the response of a driven classical oscillator to the response of a driven cavity mode. This comparison allows us to determine which etalon parameters correspond to the oscillator damping and detuning. As we see, the etalon result in this form agrees exactly with the quantum input-output theory of Gardiner and Collett [39]. This is not surprising since the quantized cavity mode is merely an oscillator itself.

To start with, consider a classically driven damped harmonic oscillator whose equation of motion is

$$\frac{d^2X_1}{dt^2} + \beta\frac{dX_1}{dt} + \omega_1^2 X_1 = A\mathrm{e}^{-i\omega t} \tag{2.27}$$

where X_1 is the position of the oscillator, β is the damping coefficient, ω_1 is the oscillator frequency, A is the driving strength, and ω is the driving frequency. A particular solution to equation (2.27) is

$$X_1(t) = \alpha e^{-i\omega t} \tag{2.28}$$

with

$$\alpha = \frac{A}{(\omega_1 - \omega)(\omega_1 + \omega) - i\beta\omega_1}. \tag{2.29}$$

For near resonant driving, $\omega_1 \simeq \omega$, this reduces to

$$\alpha \simeq \frac{A}{-\delta_1 2\omega_1 - i\beta\omega_1} \tag{2.30}$$

where $\delta_1 = \omega - \omega_1$. The ratio of the oscillator excitation to the drive is then,

$$\frac{X_1(t)}{Ae^{-i\omega t}} = \frac{i\frac{1}{2\omega_1}}{\frac{\beta}{2} - i\delta_1}. \tag{2.31}$$

We now use these results for a mechanical oscillator to assist with understanding the analogous optical system. Consider a near-perfect etalon cavity whose mirrors have different reflection coefficients $r_1 = 1 - \epsilon_1$ and $r_2 = 1 - \epsilon_2$ where $0 < \epsilon_{1,2} \ll 1$. Performing the same analysis as in Section 2.2.1, we find

$$\frac{E_c^{(+)}}{E_i^{(+)}} = i\frac{t_1}{1 - r_1 r_2 e^{i\varphi}}. \tag{2.32}$$

where ω is the frequency of the driving laser, ω_{ax} is the axial mode spacing of of the cavity and $\delta = \omega - \omega_1$ is the detuning of the driving laser from the cavity mode ω_1. If the driving field is near-resonant to the Nth mode of the cavity, then

$$e^{i\varphi} = e^{i\frac{2\pi\omega}{\omega_{ax}}} = e^{i\frac{2\pi}{\omega_{ax}}(N\omega_{ax}+\delta)} = e^{i\frac{2\pi}{\omega_{ax}}\delta} \simeq 1 + i\frac{2\pi}{\omega_{ax}}\delta. \tag{2.33}$$

Since the transmission coefficient $t_1 = \sqrt{1 - r_1^2} \simeq \sqrt{2\epsilon_1}$, taking equation (2.32) to first order in ϕ, ϵ_1, and ϵ_2, implies

$$\begin{aligned} \frac{E_c^{(+)}}{E_i^{(+)}} &\simeq i\frac{\sqrt{\frac{\epsilon_1}{\pi}}\omega_{ax}}{\frac{\omega_{ax}}{2\pi}(\epsilon_1 + \epsilon_2) - i\delta} \\ &= i\frac{\sqrt{\gamma_1}\sqrt{\omega_{ax}}}{\frac{1}{2}(\gamma_1 + \gamma_2) - i\delta}. \end{aligned} \tag{2.34}$$

Since the cavity decay rate is equal to the cavity linewidth, equation (2.20) implies $\gamma_x = \epsilon_x \omega_{ax}/\pi$. This is the decay rate out of mirror x. Comparing the denominators of this expression to that of equation (2.31) we see that the oscillator decay rate β corresponds to the etalon decay rate $\gamma_1 + \gamma_2$ [35].

2.2.3 Cascaded optical cavities

When two cavities are coupled together, as depicted in Figure 2.6, a photon in one cavity can tunnel to the other. Here we characterize that tunneling rate by performing the same classical analysis above. We call this coupling parameter J because it is analogous to the hopping parameter in the Bose-Hubbard Hamiltonian.

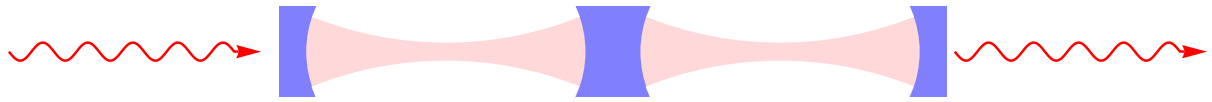

Figure 2.6: Illustration of a driven, coupled etalon system.

Here we consider two coupled oscillators with different damping rates and frequencies, where oscillator 1 is driven at frequency ω and coupled to oscillator 2. The equations of motion for the coupled system are

$$\frac{d^2X_1}{dt^2} + \beta_1 \frac{dX_1}{dt} + \omega_1^2 X_1 = A e^{-i\omega t} + \omega_1 J X_2 \tag{2.35}$$

$$\frac{d^2X_2}{dt^2} + \beta_2 \frac{dX_2}{dt} + \omega_2^2 X_2 = \omega_2 J X_1. \tag{2.36}$$

Particular solutions to these equations are $X_1(t) = \alpha_1 e^{-i\omega t}$ and $X_2(t) = \alpha_2 e^{-i\omega t}$. Substituting these solutions into the equations of motion yields for the excitation amplitude of oscillator 2

$$\begin{aligned} \alpha_2 &= \frac{AJ\omega_1}{[(\omega_1-\omega)(\omega_1+\omega) - i\beta_1\omega]\,[(\omega_2-\omega)(\omega_2+\omega) - i\beta_2\omega] - \omega_1\omega_2 J^2} \\ &\simeq \frac{-A\frac{J}{4\omega_2}}{(\frac{\beta_1}{2} - i\delta_1)(\frac{\beta_2}{2} - i\delta_2) + \frac{J^2}{4}} \end{aligned} \tag{2.37}$$

Here we have assumed that $\delta_1 \ll \omega$, and $\delta_2 \ll \omega$.

The ratio of the excitation of oscillator 2 to the drive of oscillator 1 is then

$$\frac{X_2(t)}{A\mathrm{e}^{-i\omega t}} = \frac{-\frac{J}{4\omega_2}}{(\frac{\beta_1}{2} - i\delta_1)(\frac{\beta_2}{2} - i\delta_2) + \frac{J^2}{4}}. \tag{2.38}$$

We now consider two coupled etalons as shown in Figure 2.7. Matching boundary conditions for this system yields

$$E_1^{(+)} = it_1 E_i^{(+)} + r_1 E_1^{(-)} \mathrm{e}^{i\frac{\varphi_1}{2}} \tag{2.39}$$

$$E_1^{(-)} = itE_2^{(-)} \mathrm{e}^{i\frac{\varphi_2}{2}} + rE_1^{(+)} \mathrm{e}^{i\frac{\varphi_1}{2}} \tag{2.40}$$

$$E_2^{(+)} = itE_1^{(+)} \mathrm{e}^{i\frac{\varphi_1}{2}} + rE_2^{(-)} \mathrm{e}^{i\frac{\varphi_2}{2}} \tag{2.41}$$

$$E_2^{(-)} = r_2 E_2^{(+)} \mathrm{e}^{i\frac{\varphi_2}{2}} \tag{2.42}$$

$$E_o^{(+)} = it_2 E_2^{(+)} \mathrm{e}^{i\frac{\varphi_2}{2}} \tag{2.43}$$

where t_1 (r_1), t (r), and t_2 (r_2) are the transmission (reflection) coefficients for the left, center, and right mirrors respectively, E_i, E_1, E_2, and E_o are the electric fields that are incident on the left cavity mirror, inside cavity 1, inside cavity 2, and exiting cavity 2 from the right. The corresponding sign determines the direction of propagation, and ϕ_1 and ϕ_2 are the round trip phases in cavity 1 and 2. Here, we get

$$\frac{E_2^{(+)}}{E_i^{(+)}} = \frac{t_1 t \mathrm{e}^{i\varphi_1}}{(1 - rr_1\mathrm{e}^{i\varphi_1})(1 - rr_2\mathrm{e}^{i\varphi_2}) + t^2 r_1 r_2 \mathrm{e}^{i(\varphi_1+\varphi_2)}} \tag{2.44}$$

Since equation (2.38) is second order in δ and β, we take equation (2.44) to second order in $\delta_{1,2}$ and $\epsilon_{1,2}$. As we demonstrate here, second order in $\epsilon_{1,2}$ implies first order in ϵ.

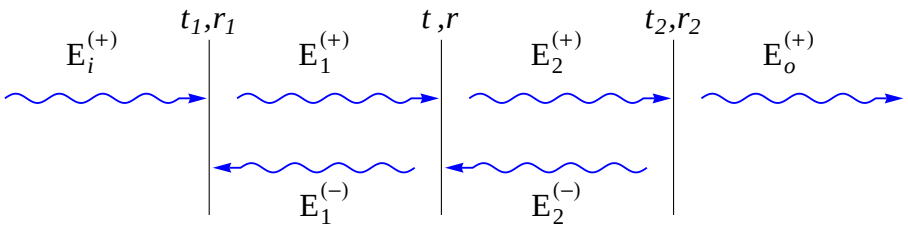

Figure 2.7: Illustration of a driven, coupled etalon system. The electric fields propagating in both directions that are incident on the system, in cavity 1, in cavity 2 and leaving the system labeled as well as the transmission and reflection coefficients for all three mirrors.

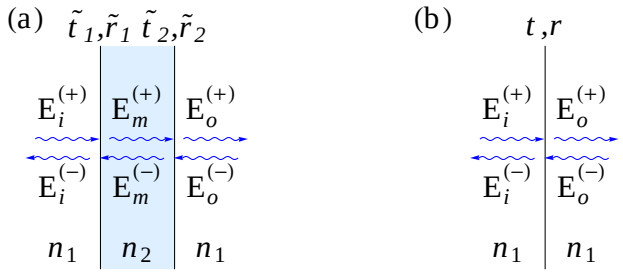

Figure 2.8: (a) Illustration of a finite width dielectric boundary with index of refraction n_2, and transmission and reflection coefficients $\tilde{t}_1$, $\tilde{r}_1$, and $\tilde{t}_2$, $\tilde{r}_2$ four boundaries 1 and 2 respectively. All propagating fields are labeled, and it is assumed that $n_2 > n_1$. (b) The infinitely-thin counterpart to the finite width dielectric with effective transmission and reflection coefficients t and r.

The infinitely-thin central barrier in Figure 2.7 with coefficients r and t is a schematic for a dielectric barrier with a finite width (Figure 2.8(a)). The effective coefficients r and t actually correspond to the net reflection and transmission through this barrier (Figure 2.8(b)). Here we derive the effective transmission and reflection coefficients by solving the continuity boundary conditions in the three regions of space depicted in Figure 2.8(a), and map them onto the infinitely thin system reflection and transmission coefficients depicted in Figure 2.8(b). The incident electromagnetic wave passes through a medium with index of refraction $n_2 > n_1$ with entry and exit coefficients of reflection and transmission $(\tilde{r}_1, \tilde{t}_1)$ and $(\tilde{r}_2, \tilde{t}_2)$.

The boundary conditions for the finite width boundary with $n_2 > n_1$ are

$$E_i^{(-)} = \tilde{r}_1 E_i^{(+)} + i\tilde{t}_1 e^{i\frac{\varphi}{2}} E_m^{(-)} \tag{2.45}$$

$$E_m^{(+)} = \tilde{t}_1 E_i^{(+)} - i\tilde{r}_1 e^{i\frac{\varphi}{2}} E_m^{(-)} \tag{2.46}$$

$$E_m^{(-)} = \tilde{t}_2 E_o^{(-)} - i\tilde{r}_2 e^{i\frac{\varphi}{2}} E_m^{(+)} \tag{2.47}$$

$$E_o^{(+)} = i\tilde{t}_2 e^{i\frac{\varphi}{2}} E_m^{(+)} + \tilde{r}_2 E_o^{(-)}, \tag{2.48}$$

where E_i, E_m, and E_o are the incident, intra-medium and outgoing fields in regions traveling in the positive or negative directions, $(\tilde{r}_1, \tilde{t}_1)$ and $(\tilde{r}_2, \tilde{t}_2)$ are the reflection and transmission coefficients of the left and right sides of the barrier, and φ is the round-trip phase shift that the light wave acquires from traveling inside the barrier.

We guarantee that no field is stored in the medium by asserting $\phi = \pi$. Eliminating the intra-medium field in terms of the incident and outgoing field yields

$$E_i^{(-)} = \frac{\tilde{r}_1 + \tilde{r}_2}{1 + \tilde{r}_1\tilde{r}_2} E_i^{(+)} \equiv r E_i^{(+)} \tag{2.49}$$

$$E_o^{(+)} = -i\frac{\tilde{t}_1\tilde{t}_2}{1 + \tilde{r}_1\tilde{r}_2} E_i^{(+)} \equiv it E_i^{(+)}. \tag{2.50}$$

From equation (2.50), given $t \simeq \tilde{t}_1\tilde{t}_2$ we conclude that second order in $\tilde{t}_1, \tilde{t}_2$ implies first order in t.

Taking equation (2.44) to second order in $\delta_{1,2}$, second order in $\epsilon_{1,2}$, and first order in ϵ,

$$\begin{aligned}
\frac{E_2^{(+)}}{E_i^{(-)}} &\simeq \frac{t_1 t \mathrm{e}^{i\varphi_1}}{2\epsilon + (\epsilon_1 - i\varphi_1)(\epsilon_2 - i\varphi_2)} \\
&= \frac{\sqrt{\gamma_1} t \sqrt{\frac{\omega_{ax_1}\omega_{ax_2}}{(2\pi)^2}} \sqrt{\frac{\omega_{ax_2}}{2\pi}}}{(\frac{\gamma_1}{2} - i\delta_1)(\frac{\gamma_2}{2} - i\delta_2) + t^2 \frac{\omega_{ax_1}\omega_{ax_2}}{(2\pi)^2}} \\
&\equiv \frac{\sqrt{\gamma_1} t \sqrt{\frac{\omega_{ax_2}}{2\pi}} \frac{J}{2}}{(\frac{\gamma_1}{2} - i\delta_1)(\frac{\gamma_2}{2} - i\delta_2) + \frac{J^2}{4}}
\end{aligned} \tag{2.51}$$

where comparison with equation (2.38) implies

$$J = \frac{t\sqrt{\omega_{ax_1}\omega_{ax_2}}}{\pi} \simeq \frac{\sqrt{2\epsilon}\sqrt{\omega_{ax_1}\omega_{ax_2}}}{\pi}. \tag{2.52}$$

This is our classical estimate for the second quantized photon tunneling rate through two coupled cavities. This rate is Hermitian: the rate of tunneling out of cavity 1 into cavity 2 is equal to the rate of tunneling out of cavity 2 into cavity 1, and the phase shifts are conjugate. The corresponding second quantized coupled cavity interaction Hamiltonian term is then simply given by

$$\hbar J(\hat{a}_1^\dagger \hat{a}_2 + \hat{a}_1 \hat{a}_2^\dagger). \tag{2.53}$$

Utilizing equation (2.20), we see that for two identical coupled cavities

$$\Gamma \simeq J \tag{2.54}$$

where Γ is the individual cavity linewidth.

For the etalon cavity system modeled here J is fixed and unalterable. In alternative cavity systems discussed in later chapters, such as toroidal microcavities coupled with a tapered fiber via evanescent waves, and photonic band gap nanocavities, the value of J becomes potentially modifiable, allowing a range of parameter values to be explored.

2.2.4 Effect of a nonlinear media in a cavity

If a nonlinear medium is inserted into the cavity, the cavity, in general, experiences a shift of the mode frequency, and the light inside the cavity picks up a nonlinear phase shift that depends on the mode intensity. Here we derive the second quantized description of the cavity mode field when such a medium is present.

Consider a classical nonlinear material with first and third order contributions to the polarization

$$\mathbf{P} = \epsilon_0 \left(\chi^{(1)} + |E|^2 \chi^{(3)} \right) \mathbf{E}. \tag{2.55}$$

Here $\mathbf{E}$ is the electric field vector with magnitude $|E|$. The total energy generated from the interaction of the medium with the light field inside the cavity would then be

$$\begin{aligned} H_{\text{int}} &= V\ \mathbf{P} \cdot \mathbf{E} \\ &= \epsilon_0 V \left(\chi^{(1)} |E|^2 + \chi^{(3)} |E|^4 \right) \end{aligned} \tag{2.56}$$

where we have assumed that the nonlinear material fills the cavity mode volume for simplicity. Since the electric field amplitude in the cavity is defined by equation (2.24), $\hat{H}_{\text{int}}$ generates terms in the cavity Hamiltonian proportional to $\hat{a}^\dagger \hat{a}$ and $\hat{a}^\dagger \hat{a}^\dagger \hat{a} \hat{a}$ [35]. A lossless $\chi^{(1)}$ medium, induces a shift of the cavity resonance, while a lossless $\chi^{(3)}$ medium causes an effective photon-photon nonlinear interaction exactly of the collisional type given in the Bose-Hubbard form. In Section 2.3, we will derive in detail these terms in a second quantized framework. For now, we acknowledge that the effect of including a $\chi^{(3)}$ medium in the cavity can yield the following Hamiltonian term

$$\frac{U}{2} \hat{a}^\dagger \hat{a}^\dagger \hat{a} \hat{a}, \tag{2.57}$$

where U is determined by properties of the medium and the cavity geometry.

2.2.5 The effective system Hamiltonian

Putting everything from this section together, we obtain the following Hamiltonian for N coupled, nonlinear cavities:

$$\hat{H}_S = \sum_j^N \hbar\omega_j \hat{a}_j^\dagger \hat{a}_j + \frac{U_j}{2}\hat{a}_j^\dagger \hat{a}_j^\dagger \hat{a}_j \hat{a}_j + \sum_{\langle j,k\rangle} \hbar J_{jk}\left(\hat{a}_j^\dagger \hat{a}_k + \hat{a}_j \hat{a}_k^\dagger\right), \tag{2.58}$$

which is, again, the Bose-Hubbard model. The qualitative difference here being the operators $\hat{a}_j$ annihilate photons in a mode defined by the cavity boundaries. Here U_j and $\hbar J_{jk}$ are the interaction energy per photon pair, and the photon hopping matrix element respectively.

2.2.6 Cavity QED experiments

Recently, the field of cavity QED has been spurred on by a growing interest in experiments involving toroidal microresonators coupled to atoms [40, 41, 42]. The toroidal microcavity system has a few advantages over standard etalon cavities. First, the effective mode volume of the microcavity can be $\sim 50\ \mu\text{m}^3$, which is ~ 500 times smaller than its etalon counterpart. This leads to an increase in the atom-field coupling strength by a factor ~ 20. Second, it is the whispering gallery mode of the cavity that is excited. This can lead to extraordinarily high Q-factors, which have exceeded 10^{10}. Finally, improved development techniques have made the fabrication of many identical toroidal microcavities relatively easy compared to the construction of just one etalon. Obviously cascaded identical, multi-layer dielectric etalon cavities are even more difficult to make.

Another contemporary avenue of cavity QED research involves photonic crystal nanocavities [43]. These cavities are constructed in semiconductor slabs where etching or lithography are used to isolate their relative location and size. The finesse of these cavities is not as impressive as that of the toroidal cavities. Nanocavities, however, can have mode volumes $\sim 0.03\ \mu\text{m}^3$. These nanocavities are also easy to consistently fabricate. It is even possible to enhance the $\chi^{(3)}$ characteristics of the cavities by doping them with quantum dots [44], or possibly electromagnetically-induced transparency (EIT) atoms, which have been successfully embedded into semiconductor crystals while maintaining their EIT characteristics [45, 46].

2.3 Electromagnetically-induced transparency and the giant Kerr nonlinearity

There is a major issue with bulk nonlinear media: the third order $\chi^{(3)}$ nonlinear response is generally dwarfed by the first order $\chi^{(1)}$ linear response. If the $\chi^{(1)}$ response was purely real, this would not be such a problem, since the term would merely shift the cavity's resonant mode. In practice, the imaginary component of $\chi^{(1)}$ dominates the $\chi^{(3)}$ nonlinearity [47], which leads to loss and absorption. As an alternative to obtaining a Kerr nonlinearity from bulk material. We examine systems that acquire their nonlinear response using electromagnetically-induced transparency (EIT) atoms and also quantum dots.

In the 1990s, the pioneering work of researchers such as Harris and Imamoğlu led to an extensive understanding of EIT [48, 49, 50, 51]. One of the remarkable properties of the EIT system, is that a $\chi^{(3)} \gg \chi^{(1)}$ is obtainable. Later, Schmidt and Imamoğlu [47] demonstrated that a slightly more exotic atomic system can yield a 'giant' Kerr nonlinearity, where $\chi^{(3)}$ is predicted to be nine orders of magnitude greater than the original EIT scheme while maintaining a negligible $\chi^{(1)}$ response. This theoretical effort was instrumental to the success of the slow light experiments [52]. This work was later extended to cavity QED systems [53, 54, 55, 56, 57], where a 'photon blockade' effect was predicted. Roughly ten years later, in an experiment using a high finesse multi-layer dielectric cavity, the photon blockade effect was realized [37]. In this section, we review the physics behind EIT and the giant Kerr nonlinearity.

2.3.1 EIT Kerr nonlinearity

EIT involves an ensemble of three-level atoms prepared in their ground state. A possible EIT level structure, known as the lambda structure, is illustrated in Figure 2.9 with states $|1\rangle$ (ground), $|2\rangle$, and $|3\rangle$. The transitions $|1\rangle \rightarrow |3\rangle$ and $|2\rangle \rightarrow |3\rangle$ are dipole allowed transitions while the $|1\rangle \rightarrow |2\rangle$ transition is forbidden. If a probe laser incident on the otherwise undisturbed ensemble is resonant with the $|1\rangle \rightarrow |3\rangle$ transition, the light is efficiently absorbed and scattered by the atomic

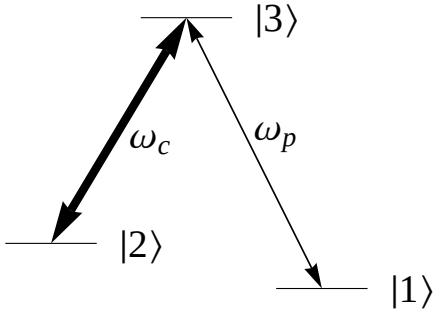

Figure 2.9: Schematic of a three-level EIT atom with $|1\rangle \rightarrow |3\rangle$ and $|2\rangle \rightarrow |3\rangle$ dipole-allowed transitions with corresponding frequencies ω_p and ω_c.

sample. However, if a coupling laser resonant with the $|2\rangle \rightarrow |3\rangle$ transition is also applied, then a quantum mechanical interference phenomenon can lead to the probe laser passing straight through with minimal absorption *i.e.* with virtually $\mathrm{Im}\left[\chi^{(1)}\right] = 0$. In other words, the coupling laser makes the once opaque sample transparent to the probe laser. This general behavior is the fundamental concept behind EIT.

For the system described above, the Hamiltonian for the doubly-driven three-level system under the rotating wave approximation is

$$\hat{H} = \hbar\left[\omega_{21}\hat{\sigma}_{22} + \omega_{31}\hat{\sigma}_{33} + g\left(\hat{\sigma}_{13}\mathrm{e}^{i\omega_p t} + \hat{\sigma}_{31}\mathrm{e}^{-i\omega_p t}\right) + \Omega_c\left(\hat{\sigma}_{23}\mathrm{e}^{i\omega_c t} + \hat{\sigma}_{32}\mathrm{e}^{-i\omega_c t}\right)\right] \tag{2.59}$$

where $\hat{\sigma}_{nm} = |n\rangle\langle m|$, $\omega_{nm} = \omega_n - \omega_m$ is the frequency difference between states $|n\rangle$ and $|m\rangle$, g is twice the Rabi frequency (taken to be real) of the probe field with frequency ω_p, and Ω_c (also taken to be real) is twice the Rabi frequency of the coupling field with frequency ω_c.

Transforming to an interaction picture that rotates with the drive frequencies ω_p and ω_c, a transformation defined by the unitary operator

$$\hat{U}(t) = \mathrm{e}^{-i(\omega_p\hat{\sigma}_{33} + (\omega_p - \omega_c)\hat{\sigma}_{22})t}, \tag{2.60}$$

yields

$$\tilde{H} = \hbar\left[(\omega_{21} - \omega_p + \omega_c)\hat{\sigma}_{22} + (\omega_{31} - \omega_p)\hat{\sigma}_{33} + g\left(\hat{\sigma}_{13} + \hat{\sigma}_{31}\right) + \Omega_c\left(\hat{\sigma}_{23} + \hat{\sigma}_{32}\right)\right]. \tag{2.61}$$

Letting $\delta = \omega_{31} - \omega_p$ and taking ω_c to be resonant with the $|2\rangle \rightarrow |3\rangle$ transition leads to

$$\tilde{H} = \hbar \left[\delta\hat{\sigma}_{22} + \delta\hat{\sigma}_{33} + g\left(\hat{\sigma}_{13} + \hat{\sigma}_{31}\right) + \Omega_c\left(\hat{\sigma}_{23} + \hat{\sigma}_{32}\right) \right]. \tag{2.62}$$

In order to correctly include dissipation from level $|3\rangle$ to levels $|2\rangle$ and $|1\rangle$, we need to construct a quantum master equation for this system. This formalism is described in detail in the next chapter. Here we ascribe $\hat{\rho}_S$ to be the reduced density operator of the three-level system, and then the inclusion of decay from state $|3\rangle$ to states $|2\rangle$ and $|1\rangle$ gives rise to the following master equation:

$$\begin{aligned} \frac{d\hat{\rho}_S}{dt} &= -\frac{i}{\hbar}[\tilde{H}, \hat{\rho}_S] - \frac{\gamma_1}{2}\left(\hat{\sigma}_{31}\hat{\sigma}_{13}\hat{\rho}_S + \hat{\rho}_S\hat{\sigma}_{31}\hat{\sigma}_{13} - 2\hat{\sigma}_{13}\hat{\rho}_S\hat{\sigma}_{31}\right) \\ &\quad -\frac{\gamma_2}{2}\left(\hat{\sigma}_{32}\hat{\sigma}_{23}\hat{\rho}_S + \hat{\rho}_S\hat{\sigma}_{32}\hat{\sigma}_{23} - 2\hat{\sigma}_{23}\hat{\rho}_S\hat{\sigma}_{32}\right) \\ &= -\frac{i}{\hbar}[\hat{H}, \hat{\rho}_S] - \gamma\left(\hat{\sigma}_{33}\hat{\rho}_S + \hat{\rho}_S\hat{\sigma}_{33}\right) + \gamma_1\hat{\sigma}_{13}\hat{\rho}_S\hat{\sigma}_{31} + \gamma_2\hat{\sigma}_{23}\hat{\rho}_S\hat{\sigma}_{32}, \end{aligned} \tag{2.63}$$

where γ_1, γ_2 are the decay rates from $|3\rangle \rightarrow |1\rangle, |2\rangle$ respectively, and $\gamma = (\gamma_1 + \gamma_2)/2$.

As discussed in references [58, 59, 60, 61], this master equation can be unraveled into wave functions (or trajectories) which evolve under an effective non-Hermitian Hamiltonian, undergoing 'quantum jumps' according to the Monte Carlo wave function method. Such trajectories can be averaged over to reconstruct the proper evolution of the master equation. The non-Hermitian Hamiltonian for this particular EIT case would be

$$\hat{H}_{\text{eff}} = \hbar \left[\delta\hat{\sigma}_{22} + (\delta - i\gamma)\hat{\sigma}_{33} + g\left(\hat{\sigma}_{13} + \hat{\sigma}_{31}\right) + \Omega_c\left(\hat{\sigma}_{23} + \hat{\sigma}_{32}\right) \right] \tag{2.64}$$

In the perturbative limit, where $\Omega_c \gg g$, a system that is initially in its ground state, for the most part, does not undergo quantum jumps. As a result, in this limit, we can use the effective non-Hermitian Hamiltonian to extract the relevant information to explain EIT [48]. As discussed in the next chapter, this is a special case—dissipation cannot universally be introduced into quantum mechanical situations by compromising the Hermiticity of the Hamiltonian. The validity here relies on the property that any particular trajectory has a low probability for undergoing quantum jumps.

Assuming that the system is in its ground state, and that $\Omega_c \gg g$, we look for steady-state

solutions to the Schrödinger equation involving $\hat{H}_{\rm eff}$:

$$i\hbar\frac{\partial}{\partial t}|\psi\rangle = \hat{H}_{\rm eff}|\psi\rangle. \tag{2.65}$$

Since $|\psi\rangle$ is going to remain in its ground state with near-unit probability, we seek out solutions of the form

$$|\psi\rangle \simeq |1\rangle + c_2|2\rangle + c_3|3\rangle. \tag{2.66}$$

In steady-state

$$\begin{aligned} 0 &= \delta c_2 + \Omega_c c_3 \\ 0 &= (\delta - i\gamma)c_3 + g + \Omega_c c_2, \end{aligned} \tag{2.67}$$

which implies

$$c_2 = \frac{g\Omega_c}{\delta^2 - \Omega_c^2 - i\gamma\delta}\ , \qquad c_3 = -\frac{g\delta}{\delta^2 - \Omega_c^2 - i\gamma\delta}. \tag{2.68}$$

Note that the normalization condition on $|\psi\rangle$ gives $1 + c_2^2 + c_3^2 \simeq 1$, asserting that $|c_{2,3}| \ll 1$. This constraint is consistent with the approximation made above, namely $|g|/|\Omega_c| \ll 1$. Once $|\psi\rangle$ is known, the density matrix for a single atom in the Schrödinger picture can be constructed,

$$\hat{\rho}(t) = \hat{U}(t)|\psi\rangle\langle\psi|\hat{U}^\dagger(t) \tag{2.69}$$

where $\hat{U}(t)$ is defined by equation (2.60). The polarization $\mathbf{P}(t)$ can be expressed as

$$\mathbf{P}(\mathbf{t}) = \frac{N}{V}\mathrm{Tr}\{\hat{\rho}(t)\left(\boldsymbol{\mu}_{13}\hat{\sigma}_{13} + \boldsymbol{\mu}_{23}\hat{\sigma}_{23} + \mathrm{H.c}\right)\} = \epsilon_0\chi^{(1)}\mathbf{E}(t) \tag{2.70}$$

where N is the number of atoms in the volume V, and $\hbar g = \mathbf{E}_p \cdot \boldsymbol{\mu}_{13}$ and $\hbar\Omega_c = \mathbf{E}_c \cdot \boldsymbol{\mu}_{23}$. Keeping track of the terms that rotate with $\mathrm{e}^{-i\omega_p t}$ implies

$$\chi^{(1)} = -\frac{N}{V}\frac{\hbar g^2}{\epsilon_0|E|^2}\frac{\delta}{\delta^2 - \Omega_c^2 - i\gamma\delta}. \tag{2.71}$$

The real (blue, solid) and imaginary (red, dashed) parts of $\chi^{(1)}$ are plotted in Figure 2.10, where it is seen that both go to zero as the detuning $\delta \to 0$.

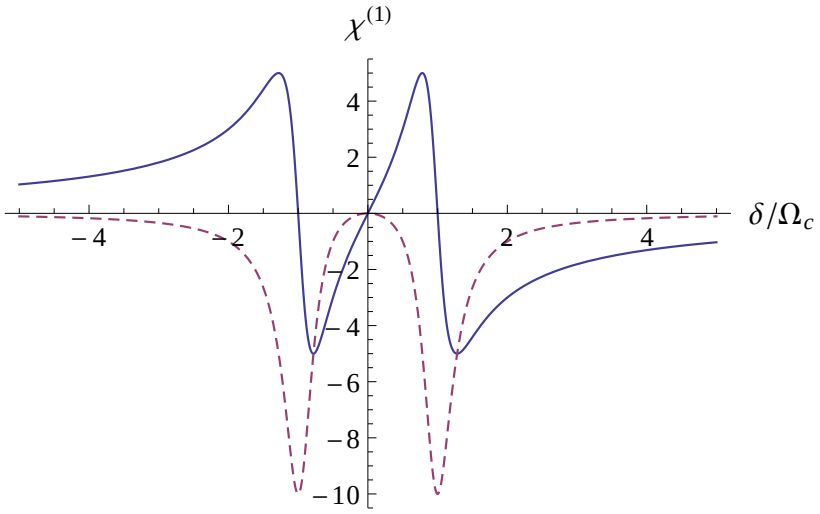

Figure 2.10: The real (solid blue) and imaginary (dashed red) $\chi^{(1)}$ responses of an EIT atom as a function of probe laser detuning in the presence of a resonant coupling drive.

For EIT systems in the $\delta \to 0$ limit, the probe laser experiences a maximum $\chi^{(3)}$ phase shift [48] of the form

$$\chi^{(3)}(\delta \to 0) \propto \frac{N}{V}\frac{2g}{3\epsilon_0\hbar^3|E|^2}\frac{1}{\Omega^2}. \tag{2.72}$$

Thus, one can use EIT atoms to generate $\chi^{(3)}$ nonlinear media with a vanishing $\chi^{(1)}$ at the resonant driving frequency.

2.3.2 Giant EIT-like Kerr nonlinearity

In 1996 Schmidt and Imamoğlu [47] suggested that much larger $\chi^{(3)}$ nonlinearities can be achieved by adding an additional atomic level to the EIT scheme. This four-level system, depicted in Figure 2.11(a), still has a virtually zero $\chi^{(1)}$ component, allowing photons to experience a large effective Kerr interaction with minimal energetic shift and loss.

Since we are ultimately concerned with a nonlinear cavity, we derive this theory for a cavity containing a single atom. We consider a cavity whose driven mode is detuned from the $|1\rangle \to |3\rangle$ atomic transition by δ. The coupling laser drives the atom in a direction orthogonal to the cavity mode as illustrated in Figure 2.11(b), and is resonant with the $|2\rangle \to |3\rangle$ transition. The

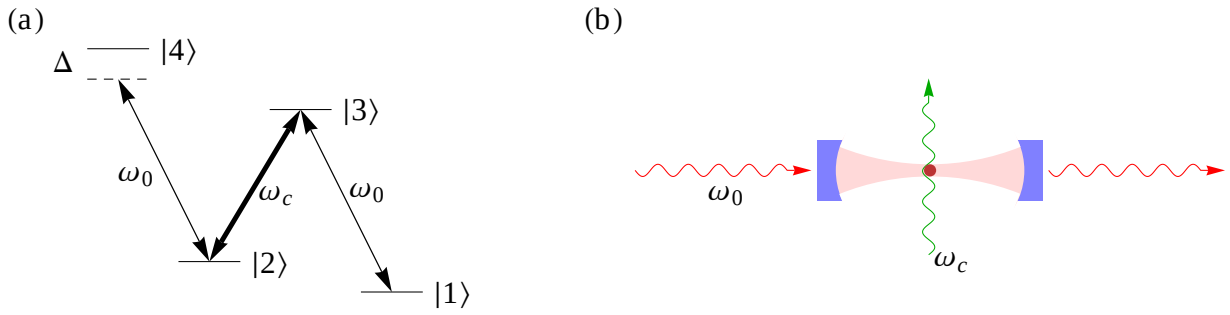

Figure 2.11: (a) The level structure and allowed dipole transitions of a four-level giant Kerr nonlinearity scheme. (b) An experimental schematic of the driven four-level system, where the coupling laser is driven orthogonal to the cavity mode/probe field.

Hamiltonian for this scenario under the rotating wave approximation is

$$\begin{aligned}\hat{H} &= \hbar\Big[(\omega_0-\delta)\hat{a}^\dagger\hat{a}+\omega_{21}\hat{\sigma}_{22}+\omega_0\hat{\sigma}_{33}+(\omega_{21}+\omega_0+\Delta)\hat{\sigma}_{44}+g_{13}(\hat{a}^\dagger\hat{\sigma}_{13}+\hat{a}\hat{\sigma}_{31}) \\ &\quad + g_{24}(\hat{a}^\dagger\hat{\sigma}_{24}+\hat{a}\hat{\sigma}_{42})+\Omega_c\left(\hat{\sigma}_{32}\mathrm{e}^{-i\omega_c t}+\hat{\sigma}_{23}\mathrm{e}^{i\omega_c t}\right)\Big] \end{aligned} \tag{2.73}$$

where $\omega_0-\delta$ is the cavity mode frequency, ω_{21}, $\omega_{31}=\omega_0$, and $\omega_{42}=\omega_{21}+\omega_0+\Delta$ are the frequency differences between states $|1\rangle$ and $|2\rangle$, $|1\rangle$ and $|3\rangle$, and $|2\rangle$ and $|4\rangle$, and finally, g_{13}, Ω_c, and g_{24} are twice the Rabi frequencies for the $|1\rangle\rightarrow|3\rangle$, $|2\rangle\rightarrow|3\rangle$, and $|2\rangle\rightarrow|4\rangle$ transitions. Transforming into an interaction picture with

$$\hat{U}(t)=\mathrm{e}^{-i\left((\omega_0-\delta)\hat{a}^\dagger\hat{a}+(\omega_{21}-\delta)\hat{\sigma}_{22}+(\omega_0-\delta)\hat{\sigma}_{33}+(\omega_{21}+\omega_0-2\delta)\hat{\sigma}_{44}\right)} \tag{2.74}$$

yields

$$\tilde{H}=\hbar\left[\delta\hat{\sigma}_{22}+\delta\hat{\sigma}_{33}+(2\delta+\Delta)\hat{\sigma}_{44}+g_{13}(\hat{a}^\dagger\hat{\sigma}_{13}+\hat{a}\hat{\sigma}_{31})+g_{24}(\hat{a}^\dagger\hat{\sigma}_{24}+\hat{a}\hat{\sigma}_{42})+\Omega_c(\hat{\sigma}_{32}+\hat{\sigma}_{23})\right]. \tag{2.75}$$

Similar to the EIT system described above, this system will be operating in the perturbative regime $g_{13}, g_{24} \ll \Omega_c$, and the effects of atomic relaxation can be included in this model by means of the

effective non Hermitian Hamiltonian

$$\begin{aligned}\tilde{H}_{\text{eff}} &= \hbar\Big[\delta\hat{\sigma}_{22} + (\delta - i\gamma_3)\hat{\sigma}_{33} + (2\delta + \Delta - i\frac{\gamma_{42}}{2})\hat{\sigma}_{44} + g_{13}(\hat{a}^\dagger\hat{\sigma}_{13} + \hat{a}\hat{\sigma}_{31}) \\ &\quad + g_{24}(\hat{a}^\dagger\hat{\sigma}_{24} + \hat{a}\hat{\sigma}_{42}) + \Omega_c(\hat{\sigma}_{32} + \hat{\sigma}_{23})\Big] \end{aligned} \tag{2.76}$$

where $\gamma_3 = (\gamma_{31} + \gamma_{32})/2$ is the average decay rate out of state $|3\rangle$, and γ_{42} is the decay rate from state $|4\rangle$ to $|2\rangle$. Here we look for steady-state solutions of the atom in the n-photon manifold of the cavity:

$$|\psi\rangle_n = |n\rangle|1\rangle + c_2|n-1\rangle|2\rangle + c_3|n-1\rangle|3\rangle + c_4|n-2\rangle|4\rangle \tag{2.77}$$

where, once again, we have asserted that the system approximately remains in the ground state $|n\rangle|1\rangle$. In steady-state, we get the following system of equations from the H_{eff} Schrödinger equation:

$$0 = \delta c_2 + \Omega_c c_3 + \sqrt{n-1}\; g_{24}c_4 \tag{2.78}$$

$$0 = (\delta - i\gamma_3)c_3 + \sqrt{n}\; g_{13} + \Omega_c c_2 \tag{2.79}$$

$$0 = (2\delta + \Delta - i\frac{\gamma_{24}}{2})c_4 + \sqrt{n-1}\; g_{24}c_2, \tag{2.80}$$

which yields

$$c_2 = -\frac{\sqrt{n}g_{13}\Omega_c(i\frac{\gamma_{42}}{2} - 2\delta - \Delta)}{g_{24}^2(n-1)(i\gamma_3 - \delta) + (i\frac{\gamma_{42}}{2} - 2\delta - \Delta)\left((i\gamma_3 - \delta)\delta + \Omega_c^2\right)} \tag{2.81}$$

$$c_3 = \frac{\sqrt{n}g_{13}\Omega_c(i\frac{\gamma_{42}}{2} - 2\delta - \Delta)\left(\frac{\delta}{\Omega_c} + \frac{g_{24}^2(n-1)}{\Omega_c(i\frac{\gamma_{42}}{2} - 2\delta - \Delta)}\right)}{g_{24}^2(n-1)(i\gamma_3 - \delta) + (i\frac{\gamma_{42}}{2} - 2\delta - \Delta)\left((i\gamma_3 - \delta)\delta + \Omega_c^2\right)} \tag{2.82}$$

$$c_4 = \frac{\sqrt{n}\sqrt{n-1}g_{13}g_{24}\Omega_c}{g_{24}^2(n-1)(i\gamma_3 - \delta) + (i\frac{\gamma_{42}}{2} - 2\delta - \Delta)\left((i\gamma_3 - \delta)\delta + \Omega_c^2\right)} \tag{2.83}$$

Since the time-independent Schrödinger equation determines the eigenenergy E by $E|\psi\rangle = \hat{H}|\psi\rangle$, the energy for this system in the n-photon manifold is

$$E_n \simeq \hbar\sqrt{n}g_{13}c_3. \tag{2.84}$$

In the limit where the detuning $\delta \to 0$,

$$E_n = \hbar\frac{g_{13}^2 g_{24}^2}{i\gamma_3 g_{24}^2(n-1) + \Omega_c^2(i\frac{\gamma_{42}}{2} - \Delta)}n(n-1). \tag{2.85}$$

Thus,

$$\begin{aligned} E_n|\psi\rangle_n &= \hbar\frac{g_{13}^2 g_{24}^2}{i\gamma_3 g_{24}^2(n-1)+\Omega_c^2(i\frac{\gamma_{42}}{2}-\Delta)}n(n-1)|\psi\rangle_n \\ &= \hbar\frac{g_{13}^2 g_{24}^2}{i\gamma_3 g_{24}^2(n-1)+\Omega_c^2(i\frac{\gamma_{42}}{2}-\Delta)}\hat{a}^\dagger\hat{a}^\dagger\hat{a}\hat{a}|\psi\rangle_n \\ &\equiv \hat{H}_{\chi^{(3)}}|\psi\rangle_n \end{aligned} \tag{2.86}$$

where $\hat{H}_{\chi^{(3)}}$ is our effective photon-photon interaction Hamiltonian under the constraint that $|c_2|^2, |c_3|^2, |c_4|^2 \ll 1$. Our assertion that the atom remains effectively in its ground state eliminates the atomic degrees of freedom from the problem. In the limit that the atomic decays are negligible compared to Ω_c and Δ, the validity conditions for this system are

$$\left(\frac{g_{13}}{\Omega_c}\right)^2 \ll 1\ , \qquad \frac{g_{24}}{\Delta} \leq 1\ , \qquad \frac{g_{24}^2}{\Delta\Omega_c} \leq 1 \tag{2.87}$$

where we are assuming that the cavity is operating in the few photon regime. Assuming $g_{24} \ll \Omega_c$, equation (2.86) implies that the effective Kerr nonlinearity is then

$$\begin{aligned} \hat{H}_{\chi^{(3)}} &\simeq -\hbar\frac{g_{13}^2 g_{24}^2}{\Omega_c^2\Delta}\hat{a}^\dagger\hat{a}^\dagger\hat{a}\hat{a} \\ &\equiv U\hat{a}^\dagger\hat{a}^\dagger\hat{a}\hat{a}. \end{aligned} \tag{2.88}$$

Therefore, for $\delta = 0$ and $g_{24}^2 \ll \Omega_c^2$, this four-level system exhibits a high nonlinear response with $\chi^{(1)} = 0$. Furthermore,

$$\left|\frac{\mathrm{Re}\left[\chi^{(3)}\right]}{\mathrm{Im}\left[\chi^{(3)}\right]}\right| = \left|\frac{\Delta}{\gamma_{42}}\right|. \tag{2.89}$$

For typical alkali atoms, $\Delta \sim 10^9$ rad/sec and $\gamma_{42} \sim 10^7$ rad/sec [55]. That is, the nonlinearity is ~ 100 times the absorption for the system.

Chapter 3

Open Quantum Systems and the Master Equation Formalism

In quantum mechanics, the state of the system $|\psi\rangle$ evolves under the Schrödinger equation

$$i\hbar\frac{\partial|\psi\rangle}{\partial t} = \hat{H}|\psi\rangle, \tag{3.1}$$

where the Hermitian Hamiltonian $\hat{H}$ describes an isolated (closed) quantum system. The Hermiticity of $\hat{H}$ is crucial to the theory of quantum mechanics: It guarantees that the prediction of the quantum state energies are real, and that $|\psi\rangle$ evolves under a unitary transformation with a norm $|\psi\rangle$ that is preserved. Consequently, the dynamical evolution of $|\psi\rangle$ under the Schrödinger equation is completely reversible. That is, Schrödinger's equation describes the dynamics of dissipation-free, energy-conserving systems. Trying to incorporate a loss mechanism into quantum mechanics by compromising the Hermiticity of $\hat{H}$ can ultimately lead to a state $|\psi\rangle$ whose norm is not preserved. This could imply that after some time T, the system has zero probability to be in **any** state. This outcome indicates that attempting to include damping in a quantum mechanical framework by constructing a non-Hermitian Hamiltonian is, in general, incomplete. One consistent method of including dissipative effects into quantum mechanics is to couple the isolated Hermitian quantum system to a comparably vast reservoir. This approach is known as the quantum master equation formalism [34, 35, 62], which we derive here. Under the assumptions that the reservoir is in thermal equilibrium and is very large compared to the system, it is diagonal in its energy basis, and resides in a steady-state. If this reservoir is weakly-coupled to the small system, the small perturbations that it experiences via the coupling negligibly affect its thermal equilibrium [63, 64]. As we demonstrate

below, these simple and reasonable assumptions alone allow us to develop a theory that introduces dissipative, irreversible behavior into a quantum mechanical framework that is consistent with all of the fundamental postulates of quantum mechanics.

Since Schrödinger-type evolution is in general incapable of correctly describing dissipative processes, we derive the master equation from the density matrix representation. This construction leads to a theory where the trace of the reduced density matrix, and therefore the total probability of the mixed quantum state, is preserved.

In Section 3.1, we derive the master equation in a quantum optics theoretical framework. This derivation provides a general discussion of the key approximations that are necessary. The logical structure of this derivation follows that of reference [62]. In the following section, we discuss a kinetic theory approach to the master equation. This alternative method yields an all-orders form of the master equation that illuminates a way to relax major approximations that are commonly made. In doing so, we enable the formalism to accommodate the parameter regime of ultracold atom systems. After demonstrating that the two theoretical descriptions are equivalent when the same approximations are applied, we conclude this chapter by extending our open quantum system theory to model time-dependent system Hamiltonians.

3.1 The master equation formalism under the Born and Markov approximations

We start with the full detailed quantum mechanical description of a small system coupled to a reservoir. We assume that the reservoir is much larger than the system and in thermal equilibrium, so that it is diagonal in its energy basis and in steady-state. Finally, we assume that the interaction between the system and reservoir is weak.

The Hamiltonian for the full quantum mechanical system is

$$\hat{H} = \hat{H}_S + \hat{H}_R + \hat{H}_V, \tag{3.2}$$

where $\hat{H}_S$ is the Hamiltonian for the isolated system, $\hat{H}_R$ is the Hamiltonian for the isolated reservoir

and $\hat{H}_V$ is the system-reservoir interaction Hamiltonian. The generic interaction $\hat{H}_V$ in a second quantized framework involves the product of a creation operator of the system with an annihilation operator of one of the many modes of the reservoir plus the Hermitian conjugate term. Here, we denote the annihilation operator corresponding to the kth reservoir mode as $\hat{R}_k$. The two-time average correlation functions for each mode k of the reservoir $\langle \hat{R}_k^\dagger(\tau)\hat{R}_k(0)\rangle$, and $\langle \hat{R}_k(\tau)\hat{R}_k^\dagger(0)\rangle$ decay on a timescale τ_c that is determined by the inverse bandwidth of the reservoir spectrum. In the limit that the reservoir modes form a near-continuum, τ_c becomes considerably smaller than the timescale of appreciable evolution of the system, defined here as T_{sys}.

The corresponding von Neumann equation of motion for the density operator $\hat{\rho}$ is

$$\frac{d\hat{\rho}}{dt} = -\frac{i}{\hbar}[\hat{H}, \hat{\rho}]. \tag{3.3}$$

We transform the equations of motion of $\hat{\rho}(t)$ into the interaction picture, effectively rotating out the free rapid rotation arising from the free energies of the system and reservoir. Defining the free Hamiltonian as $\hat{H}_0 = \hat{H}_S + \hat{H}_R$ yields the following equation of motion in the interaction picture:

$$\frac{d\tilde{\rho}}{dt} = -\frac{i}{\hbar}[\tilde{H}_V(t), \tilde{\rho}] \tag{3.4}$$

where

$$\tilde{\rho} = \mathrm{e}^{\frac{i}{\hbar}\hat{H}_0 t}\hat{\rho}\mathrm{e}^{-\frac{i}{\hbar}\hat{H}_0 t}, \tag{3.5}$$

and

$$\tilde{H}_V(t) = \mathrm{e}^{\frac{i}{\hbar}\hat{H}_0 t}\hat{H}_V\mathrm{e}^{-\frac{i}{\hbar}\hat{H}_0 t}. \tag{3.6}$$

If the interaction H_V is sufficiently weak, then the evolution of $\tilde{\rho}_S(t)$ is slow compared to its Schrödinger picture counterpart. Under this condition, we can approximate the time derivative of $\tilde{\rho}_S$ as

$$\frac{d\tilde{\rho}}{dt} \simeq \frac{\tilde{\rho}(t+\Delta t) - \tilde{\rho}(t)}{\Delta t} \equiv \frac{\Delta\tilde{\rho}}{\Delta t}. \tag{3.7}$$

where $\tau_c \ll \Delta t \ll T_{sys}$. This is known as coarse-graining, where the microscopic evolution on the timescale τ_c is averaged over. Coarse-graining the equations of motion simplifies the system

dynamics, yielding an analytic open quantum system model. For this reason, we construct the equations of motion for the coarse-grained density matrix.

We begin the derivation of the coarse-grained equations of motion by integrating equation (3.3), and iterating to yield the first two terms of the Dyson expansion. Since $\hat{H}_V$ is weak, it is generally sufficient to truncate the expansion at second order,

$$\Delta\tilde{\rho}(t) \simeq -\frac{i}{\hbar}\int_t^{t+\Delta t} dt_1[\tilde{H}_V(t_1),\tilde{\rho}(t)] - \frac{1}{\hbar^2}\int_t^{t+\Delta t} dt_1 \int_t^{t_1} dt_2\Big[\tilde{H}_V(t_1),\Big[\tilde{H}_V(t_2),\tilde{\rho}(t)\Big]\Big] \tag{3.8}$$

where $\Delta\tilde{\rho}(t) \equiv \tilde{\rho}(t+\Delta t) - \tilde{\rho}(t)$. This weak-coupling approximation is known as the Born approximation.

It should be noted that we are typically interested in the dynamics of the small system only. Consequently, we are concerned with observables that are solely functions of system variables. This simplifies the calculation immensely. Consider the expectation value of any particular system observable $\hat{\Theta}_S$. Assuming that we have the solution for the full density matrix $\hat{\rho}$,

$$\langle\hat{\Theta}_S\rangle = \mathrm{Tr}_{SR}\left\{\hat{\Theta}_S\hat{\rho}\right\} \tag{3.9}$$

$$= \mathrm{Tr}_S\left\{\mathrm{Tr}_R\left\{\hat{\Theta}_S\hat{\rho}\right\}\right\} \tag{3.10}$$

where the trace is taken over the variables of the system and reservoir. Since $\hat{\Theta}_S$ is not a function of the reservoir degrees of freedom,

$$\langle\hat{\Theta}_S\rangle = \mathrm{Tr}_S\left\{\hat{\Theta}_S\mathrm{Tr}_R\left\{\hat{\rho}\right\}\right\} \tag{3.11}$$

$$= \mathrm{Tr}_S\left\{\hat{\Theta}_S\hat{\rho}_S\right\} \tag{3.12}$$

where $\hat{\rho}_S \equiv \mathrm{Tr}_R\{\hat{\rho}\}$ is known as the reduced density matrix of the system. Tracing over the reservoir degrees of freedom of equation (3.3), yields the equation of motion for $\hat{\rho}_S$. This equation of motion is a function of the system degrees of freedom alone, greatly reducing the complexity of the problem.

We assume the reservoir and system are initially uncorrelated. The reservoir's interaction with the system induces correlations as time evolves. However, these correlations decay on a

timescale of $\tau_c \ll \Delta t$. Consequently, for resolving times $\sim \Delta t$, the reservoir's reduced density operator effectively remains independent of the system evolution albeit coupled to it. Thus, for the coarse-grained equations of motion, the density operator can be approximately factorized at all times as

$$\tilde{\rho}(t) \simeq \tilde{\rho}_S(t) \otimes \tilde{\rho}_R(t). \tag{3.13}$$

where $\tilde{\rho}_R = \mathrm{Tr}_S\{\tilde{\rho}\}$ is the reduced density operator for the reservoir. This is known as the decorellation assumption and is equivalent to assuming that the system and reservoir degrees of freedom do not become entangled. The assumptions that the reservoir is vast, in thermal equilibrium, and weakly-coupled to the system, also imply that it approximately remains in its initial state, despite the system-reservoir interaction; *i.e.*

$$\tilde{\rho}(t) \simeq \tilde{\rho}_S(t) \otimes \tilde{\rho}_R(0). \tag{3.14}$$

Tracing over the reservoir degrees of freedom of equation (3.8) and changing the variable of integration from $t_2 \to t_1 - \tau$ yields

$$\Delta\tilde{\rho}_S(t) \simeq -\frac{1}{\hbar^2}\int_t^{t+\Delta t} dt_1 \int_0^{t_1-t} d\tau \mathrm{Tr}_R \left\{ \left[\tilde{H}_V(t_1), \left[\tilde{H}_V(t_1-\tau), \tilde{\rho}_S(t)\tilde{\rho}_R(0) \right] \right] \right\}. \tag{3.15}$$

The trace of the single commutator term in equation (3.8) is equal to zero due to the fact that $\hat{\rho}_R$ is diagonal and that $\tilde{H}_V$ is proportional to $\hat{R}_k$ and $\hat{R}_k^\dagger$.

Noting the geometry of the integration domain shown in Figure 3.1, the order of integration can be switched, implying

$$\Delta\tilde{\rho}_S(t) \simeq -\frac{1}{\hbar^2}\int_0^{\Delta t} d\tau \int_{\tau+t}^{t+\Delta t} dt_1 \mathrm{Tr}_R \left\{ \left[\tilde{H}_V(t_1), \left[\tilde{H}_V(t_1-\tau), \tilde{\rho}_S(t)\tilde{\rho}_R(0) \right] \right] \right\}. \tag{3.16}$$

Anticipating that the correlation functions that arise from the trace over the double commutator of the form $\langle \hat{R}(t_1)\hat{R}^\dagger(t_1-\tau)\rangle = \langle \hat{R}(\tau)\hat{R}^\dagger(0)\rangle$, and $\langle \hat{R}(t_1)\hat{R}(t_1-\tau)\rangle = \langle \hat{R}^\dagger(\tau)\hat{R}^\dagger(0)\rangle$ will decay on a timescale $\tau_c \ll T_{sys}$, without consequence we can remove the negligibly-small τ dependence of the t_1 integral limit. The rapid decay of the reservoir correlation functions compared to T_{sys} will additionally allow us to take the upper limit of the τ integral to infinity without compromising our

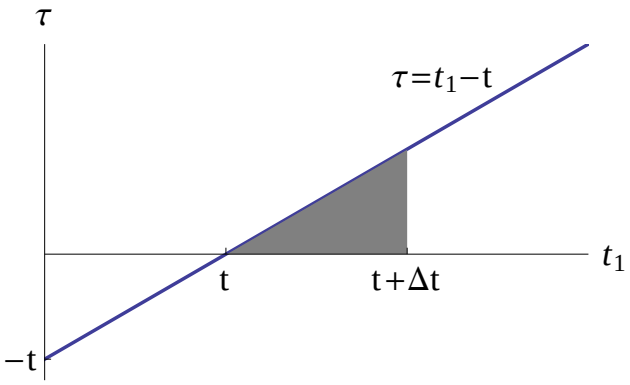

Figure 3.1: Graphical representation of the integration domain of the t_1 and τ integrals

result:

$$\Delta\tilde{\rho}_S(t) \simeq -\frac{1}{\hbar^2}\int_0^\infty d\tau \int_t^{t+\Delta t} dt_1 \mathrm{Tr}_R \left\{ \left[\tilde{H}_V(t_1), \left[\tilde{H}_V(t_1-\tau), \tilde{\rho}_S(t)\tilde{\rho}_R(0) \right] \right] \right\}. \tag{3.17}$$

This approximation is known as the Markov approximation. Physically, the rapid decay of the reservoir correlation functions imply that the system-reservoir interaction is effectively memoryless. Coarse-graining is consistent with the Markov approximation since time-averaging in steps $\Delta T \gg \tau_c$ leads to system evolution which lacks information of its past.

The rapid decay of the reservoir correlation functions imply that the remaining system operators in equation (3.17) can be removed from the τ integral retaining their initial value of $\tau = 0$. Additionally, since $\Delta t \ll T_{sys}$, we can approximate the remaining system variables, now solely a function of t_1, as a constant over the interval $[t, t+\Delta t]$. Thus,

$$\Delta\tilde{\rho}_S(t) \simeq -\frac{1}{\hbar^2}\Delta t \int_0^\infty d\tau \mathrm{Tr}_R \left\{ \left[\tilde{H}_V(t), \left[\tilde{H}_V(t-\tau), \tilde{\rho}_S(t)\tilde{\rho}_R(0) \right] \right] \right\}. \tag{3.18}$$

Equation (3.7) implies that the coarse-grained equation of motion for the reduced density operator in the interaction picture is

$$\frac{d\tilde{\rho}_S}{dt} \simeq -\frac{1}{\hbar^2}\int_0^\infty d\tau \mathrm{Tr}_R \left\{ \left[\tilde{H}_V(t), \left[\tilde{H}_V(t-\tau), \tilde{\rho}_S(t)\rho_R(0) \right] \right] \right\}, \tag{3.19}$$

or equivalently in the Schrödinger picture

$$\frac{d\hat{\rho}_S}{dt} = -\frac{i}{\hbar}\left[\hat{H}_S, \hat{\rho}_S\right] - \frac{1}{\hbar^2}\int_0^\infty d\tau \mathrm{Tr}_R \left\{ \left[\hat{H}_V, \left[\mathrm{e}^{-i\hat{H}_0\tau}\hat{H}_V \mathrm{e}^{i\hat{H}_0\tau}, \hat{\rho}_S(t)\hat{\rho}_R(0) \right] \right] \right\}. \tag{3.20}$$

This result is known as the master equation under the Born and Markov approximations. This equation is suitable for modeling a wide variety of quantum optics phenomena, such as the spontaneous emission of photons from atoms and molecules, and the emission of photons from an optical cavity.

3.2 A memory kernel approach to the master equation formalism

In this section we discuss the master equation from a kinetic theory standpoint where the equation of motion for $\hat{\rho}_S$ is derived in a Liouville representation. The formal solution that we obtain from this approach proves to be of critical importance in the next chapter when we examine reservoirs with a non-Markovian character.

For each part of $\hat{H} = \hat{H}_S + \hat{H}_R + \hat{H}_V$ we introduce the Liouville operation $\hat{\mathscr{L}}_x$, defined by its action on an arbitrary operator $\hat{\Theta}$ as

$$i\hat{\mathscr{L}}_x\hat{\Theta} = \frac{1}{i\hbar}[\hat{\Theta}, \hat{H}_x], \quad \text{where} \qquad x \in \{\mathrm{S},\ \mathrm{R},\ \mathrm{V}\}. \tag{3.21}$$

Additionally, we define the projection operator $\hat{\mathbb{P}}$ by

$$\hat{\mathbb{P}}\hat{\Theta} \equiv \hat{\rho}_R \otimes \mathrm{Tr}_R\{\hat{\Theta}\} \tag{3.22}$$

and its compliment by $\hat{\mathbb{Q}} = \hat{\mathbb{1}} - \hat{\mathbb{P}}$. Under these definitions, $\hat{\mathbb{P}}$ and $\hat{\mathbb{Q}}$ satisfy the usual projection operator relationships $\hat{\mathbb{P}}^2\hat{\Theta} = \hat{\mathbb{P}}\hat{\Theta}$, $\hat{\mathbb{Q}}^2\hat{\Theta} = \hat{\mathbb{Q}}\hat{\Theta}$, and $\hat{\mathbb{P}}\hat{\mathbb{Q}}\hat{\Theta} = \hat{\mathbb{Q}}\hat{\mathbb{P}}\hat{\Theta} = 0$. Using the projection operators, the reduced density matrix for the system can be written as

$$\hat{\rho}_S = \mathrm{Tr}_R\{\hat{\mathbb{P}}\hat{\rho}\}. \tag{3.23}$$

To find the equation of motion for $\hat{\rho}_S$, we start from the evolution of the full density matrix:

$$\frac{d\hat{\rho}}{dt} = -i\hat{\mathscr{L}}\hat{\rho}, \tag{3.24}$$

where $\hat{\mathscr{L}} = \hat{\mathscr{L}}_S + \hat{\mathscr{L}}_R + \hat{\mathscr{L}}_V$. Noting that $\hat{\mathbb{P}} + \hat{\mathbb{Q}} = \hat{\mathbb{1}}$, this equation can be written as

$$\frac{d\left(\hat{\mathbb{P}} + \hat{\mathbb{Q}}\right)\hat{\rho}}{dt} = -i\left(\hat{\mathbb{P}} + \hat{\mathbb{Q}}\right)\hat{\mathscr{L}}\left(\hat{\mathbb{P}} + \hat{\mathbb{Q}}\right)\hat{\rho}. \tag{3.25}$$

Acting on this equation with $\hat{\mathbb{P}}$ and $\hat{\mathbb{Q}}$ yields the the following coupled equations

$$\frac{d\hat{\mathbb{P}}\hat{\rho}}{dt} = -i\left[\hat{\mathbb{P}}\hat{\mathscr{L}}\hat{\mathbb{P}}\hat{\rho} + \hat{\mathbb{P}}\hat{\mathscr{L}}\hat{\mathbb{Q}}(\hat{\mathbb{Q}}\hat{\rho})\right], \tag{3.26}$$

$$\frac{d\hat{\mathbb{Q}}\hat{\rho}}{dt} = -i\left[\hat{\mathbb{Q}}\hat{\mathscr{L}}\hat{\mathbb{P}}\hat{\rho} + \hat{\mathbb{Q}}\hat{\mathscr{L}}\hat{\mathbb{Q}}(\hat{\mathbb{Q}}\hat{\rho})\right], \tag{3.27}$$

where we have used the fact that $\hat{\mathbb{Q}}^2\hat{\Theta} = \hat{\mathbb{Q}}\hat{\Theta}$. Equation (3.27) can be simplified since

$$\begin{aligned}\hat{\mathbb{Q}}\hat{\mathscr{L}}_S\hat{\mathbb{Q}}\hat{\rho} &= (\hat{\mathbb{1}} - \hat{\mathbb{P}})\hat{\mathscr{L}}_S(\hat{\mathbb{1}} - \hat{\mathbb{P}})\hat{\rho} \\ &= \hat{\mathscr{L}}_S\hat{\rho} - \hat{\mathscr{L}}_s\hat{\mathbb{P}}\hat{\rho} - \cancel{\hat{\mathbb{P}}\hat{\mathscr{L}}_S\hat{\rho}} + \cancel{\hat{\mathbb{P}}\hat{\mathscr{L}}_S\hat{\mathbb{P}}\hat{\rho}} \\ &= \hat{\mathscr{L}}_S\hat{\mathbb{Q}}\hat{\rho}\end{aligned} \tag{3.28}$$

where the last two terms cancel since $\hat{\mathscr{L}}_S$ is not a function of reservoir observables, and

$$\hat{\mathbb{Q}}\hat{\mathscr{L}}_R\hat{\mathbb{Q}}\hat{\rho} = \hat{\mathscr{L}}_R\hat{\mathbb{Q}} - \cancel{\hat{\mathbb{P}}\hat{\mathscr{L}}_R\hat{\rho}}^{\,0} + \cancel{\hat{\mathbb{P}}\hat{\mathscr{L}}_R\hat{\mathbb{P}}\hat{\rho}}^{\,0} \tag{3.29}$$

due to the diagonal and stationary assumptions respectfully. Therefore,

$$\hat{\mathbb{Q}}\hat{\mathscr{L}}\hat{\mathbb{Q}}\hat{\rho} = \hat{\mathscr{L}}_S + \hat{\mathscr{L}}_R + \hat{\mathbb{Q}}\hat{\mathscr{L}}_V\hat{\mathbb{Q}}. \tag{3.30}$$

The formal solution of equation (3.27) is then

$$\hat{\mathbb{Q}}\hat{\rho} = -i\int_0^t \mathrm{e}^{-i(\hat{\mathscr{L}}_S + \hat{\mathscr{L}}_R + \hat{\mathbb{Q}}\hat{\mathscr{L}}_V\hat{\mathbb{Q}})\tau}\hat{\mathbb{Q}}\hat{\mathscr{L}}\hat{\mathbb{P}}\hat{\rho}(t-\tau)d\tau. \tag{3.31}$$

where we have assumed that the system and reservoir are initially uncorrelated, *i.e.* $\hat{\mathbb{Q}}\hat{\rho}(0) = 0$. Using this result to eliminate $\hat{\mathbb{Q}}\hat{\rho}$ in equation (3.26), we get

$$\frac{d\hat{\mathbb{P}}\hat{\rho}}{dt} = -i\hat{\mathbb{P}}\hat{\mathscr{L}}\hat{\mathbb{P}}\hat{\rho} - \hat{\mathbb{P}}\hat{\mathscr{L}}\hat{\mathbb{Q}}\int_0^t \mathrm{e}^{-i(\hat{\mathscr{L}}_S + \hat{\mathscr{L}}_R + \hat{\mathbb{Q}}\hat{\mathscr{L}}_V\hat{\mathbb{Q}})\tau}\hat{\mathbb{Q}}\hat{\mathscr{L}}\hat{\mathbb{P}}\hat{\rho}(t-\tau)d\tau. \tag{3.32}$$

This equation can be simplified by considering the action of the projection operators. The operators $\hat{\mathbb{P}}$ and $\hat{\mathbb{Q}}$ operate on everything to their right. Therefore, we apply the right-most $\hat{\mathbb{P}}$ and $\hat{\mathbb{Q}}$ first, and work our way through them from right to left. Here we do so term-by-term. Consider the $\hat{\mathbb{P}}\hat{\mathscr{L}}\hat{\mathbb{P}}\hat{\rho}$ term in equation (3.32), the definition of $\hat{\mathbb{P}}$ implies

$$\hat{\mathbb{P}}\hat{\mathscr{L}}\hat{\mathbb{P}}\hat{\rho} = \hat{\mathbb{P}}(\hat{\mathscr{L}}_S + \hat{\mathscr{L}}_R + \hat{\mathscr{L}}_V)\hat{\rho}_S\hat{\rho}_R. \tag{3.33}$$

The fact that $\hat{\rho}_R$ is stationary also implies

$$\frac{d\hat{\rho}_R}{dt} = -i\hat{\mathscr{L}}_R\hat{\rho}_R = 0, \tag{3.34}$$

while the diagonal assumption of $\hat{\rho}_R$ gives

$$\hat{\mathbb{P}}\hat{\mathscr{L}}_V\hat{\rho}_R = \hat{\rho}_R\langle\hat{\mathscr{L}}_V\hat{\rho}_R\rangle = 0. \tag{3.35}$$

Therefore,

$$\hat{\mathbb{P}}\hat{\mathscr{L}}\hat{\mathbb{P}}\hat{\rho} = \hat{\rho}_R\hat{\mathscr{L}}_S\hat{\rho}_S. \tag{3.36}$$

Consider now

$$\hat{\mathbb{P}}\hat{\mathscr{L}}\hat{\mathbb{Q}}\mathrm{e}^{-i\hat{\mathbb{Q}}\hat{\mathscr{L}}\hat{\mathbb{Q}}\tau}\hat{\mathbb{Q}}\hat{\mathscr{L}}\hat{\mathbb{P}}\hat{\rho}. \tag{3.37}$$

This term is a bit more complicated. Here we break it down by first noting the fact that

$$\begin{aligned}
\hat{\mathbb{Q}}\hat{\mathscr{L}}\hat{\mathbb{P}}\hat{\rho} &= (\hat{\mathbb{1}} - \hat{\mathbb{P}})(\hat{\mathscr{L}}_S + \hat{\mathscr{L}}_R + \hat{\mathscr{L}}_V)\hat{\rho}_S\hat{\rho}_R \\
&= \cancel{\hat{\mathscr{L}}_S\hat{\rho}_S\hat{\rho}_R} + \cancelto{0}{\hat{\mathscr{L}}_R\hat{\rho}_S\hat{\rho}_R} + \hat{\mathscr{L}}_V\hat{\rho}_S\hat{\rho}_R - \cancel{\hat{\mathbb{P}}\hat{\mathscr{L}}_S\hat{\rho}_S\hat{\rho}_R} - \cancelto{0}{\hat{\mathbb{P}}\hat{\mathscr{L}}_R\hat{\rho}_S\hat{\rho}_R} - \cancelto{0}{\hat{\mathbb{P}}\hat{\mathscr{L}}_V\hat{\rho}_S\hat{\rho}_R} \\
&= \hat{\mathscr{L}}_V\hat{\rho}_S\hat{\rho}_R
\end{aligned} \tag{3.38}$$

where we have used equation (3.34) and equation (3.35). Now consider an arbitrary function $\hat{\mathcal{F}}$ of system and reservoir variables.

$$\begin{aligned}
\hat{\mathbb{P}}\hat{\mathscr{L}}\hat{\mathbb{Q}}\hat{\mathcal{F}}\hat{\rho}_R &= \hat{\mathbb{P}}(\hat{\mathscr{L}}_S + \hat{\mathscr{L}}_R + \hat{\mathscr{L}}_V)(\hat{\mathbb{1}} - \hat{\mathbb{P}})\hat{\mathcal{F}}\hat{\rho}_R \\
&= \hat{\mathbb{P}}\hat{\mathscr{L}}_S\hat{\mathcal{F}}\hat{\rho}_R + \hat{\mathbb{P}}\hat{\mathscr{L}}_R\hat{\mathcal{F}}\hat{\rho}_R + \hat{\mathbb{P}}\hat{\mathscr{L}}_V\hat{\mathcal{F}}\hat{\rho}_R - \hat{\mathbb{P}}\hat{\mathscr{L}}_S\hat{\mathbb{P}}\hat{\mathcal{F}}\hat{\rho}_R - \hat{\mathbb{P}}\hat{\mathscr{L}}_S\hat{\mathbb{P}}\hat{\mathcal{F}}\hat{\rho}_R - \hat{\mathbb{P}}\hat{\mathscr{L}}_S\hat{\mathbb{P}}\hat{\mathcal{F}}\hat{\rho}_R \\
&= \cancel{\hat{\mathscr{L}}_S\hat{\rho}_R\langle\hat{\mathcal{F}}\rangle} + \cancelto{0}{\hat{\mathbb{P}}\hat{\mathscr{L}}_R\hat{\mathcal{F}}\hat{\rho}_R} + \hat{\mathbb{P}}\hat{\mathscr{L}}_V\hat{\mathcal{F}}\hat{\rho}_R - \cancel{\hat{\mathbb{P}}\hat{\mathscr{L}}_S\hat{\rho}_R\langle\hat{\mathcal{F}}\rangle} - \cancelto{0}{\hat{\mathbb{P}}\hat{\mathscr{L}}_R\hat{\rho}_R\langle\hat{\mathcal{F}}\rangle} - \cancelto{0}{\hat{\mathbb{P}}\hat{\mathscr{L}}_V\hat{\rho}_R\langle\hat{\mathcal{F}}\rangle} \qquad (3.39) \\
&= \hat{\mathbb{P}}\hat{\mathscr{L}}_V\hat{\mathcal{F}}. \qquad (3.40)
\end{aligned}$$

The second term in equation (3.39) goes to zero since

$$\begin{aligned}
\hat{\mathbb{P}}\hat{\mathscr{L}}_R\hat{\mathcal{F}}\hat{\rho}_R &= \hat{\rho}_R\Big(\mathrm{Tr}[\hat{H}_R\hat{\mathcal{F}}\hat{\rho}_R] - \mathrm{Tr}[\hat{\mathcal{F}}\hat{\rho}_R\hat{H}_R]\Big) \\
&= \hat{\rho}_R\Big(\mathrm{Tr}[\hat{H}_R\hat{\mathcal{F}}\hat{\rho}_R] - \mathrm{Tr}[\hat{H}_R\hat{\mathcal{F}}\hat{\rho}_R]\Big) \\
&= 0.
\end{aligned} \tag{3.41}$$

Putting everything together we get,

$$\begin{aligned}\frac{d\hat{\mathbb{P}}\hat{\rho}}{dt} &= -i\hat{\mathbb{P}}\hat{\mathscr{L}}\hat{\mathbb{P}}\hat{\rho} - \hat{\mathbb{P}}\hat{\mathscr{L}}\hat{\mathbb{Q}}\int_0^t \mathrm{e}^{-i\hat{\mathbb{Q}}\hat{\mathscr{L}}\hat{\mathbb{Q}}\tau}\hat{\mathbb{Q}}\hat{\mathscr{L}}\hat{\mathbb{P}}\hat{\rho}(t-\tau)d\tau \\ &= \hat{\rho}_R\hat{\mathscr{L}}_S\rho_S - \int_0^t \hat{\mathbb{P}}\hat{\mathscr{L}}_V\mathrm{e}^{-i\hat{\mathbb{Q}}\hat{\mathscr{L}}\hat{\mathbb{Q}}\tau}\hat{\mathscr{L}}_V\hat{\rho}_S(t-\tau)\hat{\rho}_R d\tau. \end{aligned} \tag{3.42}$$

Finally, tracing over the reservoir degrees of freedom yields

$$\frac{d\hat{\rho}_S(t)}{dt} = -i\hat{\mathscr{L}}_S\hat{\rho}_S(t) + \int_0^t \mathscr{R}(\tau)\hat{\rho}_S(t-\tau)d\tau, \tag{3.43}$$

where we have defined the memory kernel

$$\mathscr{R}(\tau) = -\mathrm{Tr}_R\left\{\hat{\mathscr{L}}_V\mathrm{e}^{-i(\hat{\mathscr{L}}_S+\hat{\mathscr{L}}_R+\hat{\mathbb{Q}}\hat{\mathscr{L}}_V\hat{\mathbb{Q}})\tau}\hat{\mathscr{L}}_V\hat{\rho}_R\right\}. \tag{3.44}$$

The first term on the right hand side of equation (3.43) is the free system evolution while the second term describes the irreversible contribution due to the system-reservoir interaction.

Equation (3.43) is the exact master equation under the sole condition that the system and reservoirs are initially uncorrelated. All the dynamics due to the coupling to the reservoirs is encapsulated in $\mathscr{R}(\tau)$. Once the memory kernel is known, we can calculate the evolution of the reduced density matrix of the system. However, it turns out in general to be impossible to solve for the memory kernel exactly except for the most trivial situations, so approximations must be made to continue from this point.

3.3 Equivalence of the two formalisms

In this framework, we can recover the master equation under the Born and Markov approximations in two simple steps. First, the Born approximation can be made by taking equation (3.43) to second order in $\hat{H}_V$. This amounts to eliminating the $\hat{\mathbb{Q}}\hat{\mathscr{L}}_V\hat{\mathbb{Q}}$ term from the exponential in equation (3.44). Second, the memoryless (Markovian) nature can be asserted by taking the τ integral to infinity as well as assuming that, on the time scale of the rapid decay of the memory kernel, the backwards evolution of $\hat{\rho}_S$ is determined solely by the system evolution, *i.e.*

$$\hat{\rho}_S(t-\tau) \simeq \mathrm{e}^{i\hat{\mathscr{L}}_S\tau}\hat{\rho}_S(t). \tag{3.45}$$

Then,

$$\begin{aligned}
\frac{d\hat{\rho}_S(t)}{dt} &= -i\hat{\mathscr{L}}_S\hat{\rho}_S(t) - \int_0^\infty \mathrm{Tr}_R\left\{\hat{\mathscr{L}}_V \mathrm{e}^{-i(\hat{\mathscr{L}}_S+\hat{\mathscr{L}}_R+\hat{\mathbb{Q}}\hat{\mathscr{L}}_V\hat{\mathbb{Q}})\tau}\hat{\mathscr{L}}_V\hat{\rho}_R\right\}\hat{\rho}_S(t-\tau)d\tau \\
&\simeq -i\hat{\mathscr{L}}_S\hat{\rho}_S(t) - \int_0^\infty \mathrm{Tr}_R\left\{\hat{\mathscr{L}}_V \mathrm{e}^{-i(\hat{\mathscr{L}}_S+\hat{\mathscr{L}}_R)\tau}\hat{\mathscr{L}}_V\hat{\rho}_R\right\}\mathrm{e}^{-i\hat{\mathscr{L}}_S\tau}d\tau\hat{\rho}_S(t) \\
&= -i\hat{\mathscr{L}}_S\hat{\rho}_S(t) - \int_0^\infty \mathrm{Tr}_R\left\{\hat{\mathscr{L}}_V \mathrm{e}^{-i(\hat{\mathscr{L}}_S+\hat{\mathscr{L}}_R)\tau}\hat{\mathscr{L}}_V\hat{\rho}_R\right\}\mathrm{e}^{-i\hat{\mathscr{L}}_S\tau}d\tau\hat{\rho}_S(t) \\
&= -i\left[\hat{H}_S,\hat{\rho}_S(t)\right] - \int_0^\infty \mathrm{Tr}_R\left\{\left[\hat{H}_V,\left[\mathrm{e}^{-i\hat{H}_0\tau}\hat{H}_V\mathrm{e}^{i\hat{H}_0\tau},\hat{\rho}_S(t)\hat{\rho}_R(0)\right]\right]\right\}d\tau\hat{\rho}_S(t) \quad (3.46)
\end{aligned}$$

which is in agreement with equation (3.20).

3.4 Time-dependent master equation

We conclude our formal discussion of the master equation by considering the possibility of a time-dependent system Hamiltonian in an open quantum system setting. Later in this work, we use the results derived here to explore the properties of specific time-dependent Bose-Hubbard systems coupled to the environment. We perform this derivation using the projection operator method as well, and it follows closely the master equation derivation in Section 3.2. Due to this similarity, we go through this derivation rather quickly, taking for granted mathematical details established in Section 3.2.

Given a time dependent system, the full equation of motion for the density matrix for the system and reservoir is

$$\frac{d\hat{\rho}}{dt} = -i(\hat{\mathscr{L}}_S(t) + \hat{\mathscr{L}}_R + \hat{\mathscr{L}}_V)\hat{\rho}, \quad (3.47)$$

which yields

$$\begin{aligned}
\frac{d\hat{\mathbb{P}}\hat{\rho}}{dt} &= -i\left[\hat{\mathbb{P}}\hat{\mathscr{L}}(t)\hat{\mathbb{P}}\hat{\rho} + \hat{\mathbb{P}}\hat{\mathscr{L}}(t)\hat{\mathbb{Q}}(\hat{\mathbb{Q}}\hat{\rho})\right] \quad (3.48) \\
\frac{d\hat{\mathbb{Q}}\hat{\rho}}{dt} &= -i\left[\hat{\mathbb{Q}}\hat{\mathscr{L}}\hat{\mathbb{P}}\hat{\rho} + \hat{\mathbb{Q}}\hat{\mathscr{L}}\hat{\mathbb{Q}}(\hat{\mathbb{Q}}\hat{\rho})\right]. \quad (3.49)
\end{aligned}$$

The formal solution of equation (3.49) is

$$\hat{\mathbb{Q}}\hat{\rho} = -i\int_0^t \mathrm{e}^{i\left(\mathrm{T}\int_t^{t_2}\hat{\mathscr{L}}_S(t_1)dt_1 + \hat{\mathscr{L}}_R(t_2-t) + \hat{\mathbb{Q}}\hat{\mathscr{L}}_V\hat{\mathbb{Q}}(t_2-t)\right)}\hat{\mathscr{L}}_V\hat{\rho}_S(t_2)\hat{\rho}_R dt_2 \quad (3.50)$$

where the T signifies time-ordering for the integral in the exponential, and we have once again made the assumption that the system and reservoir are initially uncorrelated. Substituting this result into equation (3.48) yields

$$\frac{d\hat{\mathbb{P}}\hat{\rho}}{dt} = -i\hat{\mathbb{P}}\hat{\mathscr{L}}(t)\hat{\mathbb{P}}\hat{\rho} - \int_0^t \hat{\mathscr{L}}_V \mathrm{e}^{i\left(\mathrm{T}\int_t^{t_2}\hat{\mathscr{L}}_S(t_1)dt_1 + \hat{\mathscr{L}}_R(t_2-t) + \hat{\mathbb{Q}}\hat{\mathscr{L}}_V\hat{\mathbb{Q}}(t_2-t)\right)}\hat{\mathscr{L}}_V\hat{\rho}_S(t_2)\hat{\rho}_R dt_2. \tag{3.51}$$

We make the Born approximation by taking the $\hat{\mathscr{L}}_V$ term in the exponent to be zero. Since $[\hat{\mathscr{L}}_S(t_1), \hat{\mathscr{L}}_R] = 0$,

$$\mathrm{e}^{i\left(\mathrm{T}\int_t^{t_2}\hat{\mathscr{L}}_S(t_1)dt_1 + \hat{\mathscr{L}}_R(t_2-t)\right)} = \mathrm{e}^{i\mathrm{T}\int_t^{t_2}\hat{\mathscr{L}}_S(t_1)dt_1}\mathrm{e}^{i\hat{\mathscr{L}}_R(t_2-t)}. \tag{3.52}$$

Changing the variable of integration to $\tau = t - t_2$ implies

$$\frac{d\hat{\mathbb{P}}\hat{\rho}}{dt} = -i\hat{\mathbb{P}}\hat{\mathscr{L}}(t)\hat{\mathbb{P}}\hat{\rho} - \int_0^t \hat{\mathscr{L}}_V \mathrm{e}^{i\mathrm{T}\int_t^{t-\tau}\hat{\mathscr{L}}_S(t_1)dt_1}\mathrm{e}^{-i\hat{\mathscr{L}}_R\tau}\hat{\mathscr{L}}_V\hat{\rho}_S(t-\tau)\hat{\rho}_R d\tau \tag{3.53}$$

Finally, making the Markov approximation, and tracing over the reservoir degrees of freedom, we arrive at the master equation

$$\begin{aligned}\frac{d\hat{\rho}_S}{dt} &= -i\hat{\mathscr{L}}_S(t)\hat{\rho}_S \\ &\quad -\mathrm{Tr}_R\left\{\int_0^\infty \left[\hat{H}_V, \left[\mathrm{e}^{i\mathrm{T}\int_t^{t-\tau}\hat{H}_S(t_1)dt_1}\mathrm{e}^{-i\hat{H}_R\tau}\hat{H}_V\mathrm{e}^{-i\mathrm{T}\int_t^{t-\tau}\hat{H}_S(t_1)dt_1}\mathrm{e}^{-i\hat{\mathscr{L}}_R\tau}, \hat{\rho}_R\hat{\rho}_S(t)\right]\right]\right\}d\tau\end{aligned} \tag{3.54}$$

This equation is identical to equation (3.46), but with a time-ordered propagator for the system Hamiltonian. As we see later in this work when specific models are adopted for the system and reservoir, under the Markov approximation the rapid decay of the correlation functions in the memory kernel lead to a time-independent expression for the kernel. Under this condition, the only difference between equation (3.46), and equation (3.54) is $\hat{\mathscr{L}}_S\hat{\rho}_S \to \hat{\mathscr{L}}_S(t)\hat{\rho}_S$.

3.5 Conclusion

In this chapter, we reviewed the master equation formalism under the Born and Markov approximations. Afterwords, an all-orders kinetic theory approach was presented. In the next chapter we will use this theory to make approximations that go beyond the standard approximation. After

demonstrating that the two formalisms are equivalent when the Born and Markov approximations are made to the memory kernel, we derived a generalized master equation that is capable of treating time-dependent system Hamiltonians. This equation will find use in Chapter 6, when we discuss the progress that we have made in understanding sequential logic in atomtronic systems.

Chapter 4

Non-Markovian Open Quantum Systems

Most of the atomtronic systems that we apply the master equation approach to in this thesis involve reservoirs where zero-temperature Fermi-Dirac equilibrium statistics are assumed. At the start of this research effort, however, we found that such reservoir assumptions lead to various mathematical divergences when the standard Born-Markov master equation framework is employed. Here, in the context of a two-level atom coupled to a distribution of vacuum modes, we discuss the origin of these divergences, as well as derive a non-Markovian master equation theory to rectify the theoretical inconsistencies. As we demonstrate, the divergence only arises when system energy differences directly overlap with a sharp boundary in the reservoir structure. In order to properly quench this divergence, we go beyond the standard approximations. Using the memory kernel formulation derived in Section 3.2, we derive a modified master equation by introducing an ansatz for the full memory kernel. The resulting model is free of all divergences that are induced by the reservoir structure discontinuity. Our analysis reveals that the divergence is a consequence of the breakdown of the Markov assumption. We conclude this chapter by comparing the behavior of our modified master equation to exact results from a closed, isolated quantum system. These simulations confirm that our model correctly captures the steady-state dynamics around the quenched divergence.

4.1 Coupling an atom to the vacuum

Consider a two level atom coupled to the zero-temperature vacuum environment schematically depicted in Figure 4.1. The Hamiltonians for the system, reservoir and interaction are

$$\hat{H}_S = \frac{1}{2}\hbar\omega_0\hat{\sigma}^{(z)} \tag{4.1}$$

$$\hat{H}_R = \sum_j \hbar\bar{\omega}_j \hat{R}_j^\dagger \hat{R}_j \tag{4.2}$$

$$\hat{H}_V = \sum_k \hbar\left(g_k \hat{R}_k^\dagger \hat{\sigma}^{(-)} + g_k^* \hat{R}_k \hat{\sigma}^{(+)}\right) \tag{4.3}$$

where $\hat{\sigma}^{(z)}$, $\hat{\sigma}^{(-)}$, and $\hat{\sigma}^{(+)}$ are the Pauli spin matrices, $\hbar\omega_0$ is the energy of the two level atom, $\hat{R}_k^\dagger$ and $\hat{R}_k$ create and annihilate an excitation in the reservoir with energy $\hbar\bar{\omega}_k$, and g_k is the complex coupling between cavity mode k and the two level atom.

The standard Born Markov master equation is given by

$$\frac{d\hat{\rho}_S}{dt} = -\frac{i}{\hbar}\left[\hat{H}_S, \hat{\rho}_S\right] - \frac{1}{\hbar^2}\int_0^\infty d\tau \mathrm{Tr}_R\left\{\left[\hat{H}_V, \left[e^{-i\hat{H}_0\tau}\hat{H}_V e^{i\hat{H}_0\tau}, \hat{\rho}_S(t)\hat{\rho}_R(0)\right]\right]\right\}. \tag{4.4}$$

Here we examine in detail the integral

$$-\int_0^\infty d\tau \mathrm{Tr}_R\left\{\hat{H}_V e^{-i\hat{H}_0\tau}\hat{H}_V e^{i\hat{H}_0\tau}\hat{\rho}_S(t)\hat{\rho}_R\right\}. \tag{4.5}$$

The divergence that we discuss directly below is common to all four integrals in the second-order kernel that arise when the commutators are expanded. The remaining three integrals are treated in

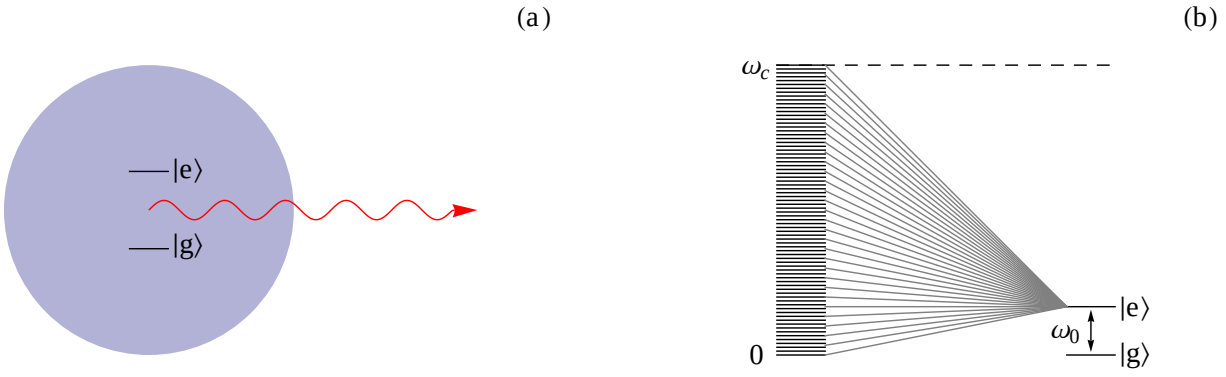

Figure 4.1: (a) Illustration of a two-level atom radiating a photon into the vacuum. (b) Schematic of a two-level atom coupled to a near-continuum of modes, which gives the atom the ability to decay into the vacuum.

exactly the same manner. The simple form of $\hat{H}_0 = \hat{H}_S + \hat{H}_R$ has the following two consequences:

$$\mathrm{e}^{-\frac{i}{2}\omega_0\hat{\sigma}^{(z)}\tau}\hat{\sigma}^{(-)}\mathrm{e}^{\frac{i}{2}\omega_0\hat{\sigma}^{(z)}\tau} = \hat{\sigma}^{(-)}\mathrm{e}^{i\omega_0\tau}, \tag{4.6}$$

$$\mathrm{e}^{-i\hat{H}_R\tau}\hat{R}_j\mathrm{e}^{i\hat{H}_R\tau} = \hat{R}_j\mathrm{e}^{i\bar{\omega}_j\tau}. \tag{4.7}$$

Thus,

$$\mathrm{e}^{-\frac{i}{\hbar}\hat{H}_0\tau}\hat{H}_V\mathrm{e}^{\frac{i}{\hbar}\hat{H}_0\tau} = \mathrm{e}^{-\frac{i}{\hbar}\hat{H}_0\tau}\left(\hbar\sum_k g_k\hat{R}_k^\dagger\hat{\sigma}^{(-)} + g_k^*\hat{R}_k\hat{\sigma}^{(+)}\right)\mathrm{e}^{\frac{i}{\hbar}\hat{H}_0\tau} \tag{4.8}$$

$$= \hbar\sum_k g_k\hat{R}_k^\dagger\hat{\sigma}^{(-)}\mathrm{e}^{i(\omega_0-\bar{\omega}_k)\tau} + g_k^*\hat{R}_k\hat{\sigma}^{(+)}\mathrm{e}^{-i(\omega_0-\bar{\omega}_k)\tau}. \tag{4.9}$$

When the assumption is made that the reservoir is in thermal equilibrium, the trace over the diagonal reservoir reduces the two sums over the reservoir degrees of freedom to one, and eliminates terms that are not of the form $\langle\hat{R}_k^\dagger\hat{R}_k\rangle$ or $\langle\hat{R}_k\hat{R}_k^\dagger\rangle$. Thus

$$\begin{aligned}&\mathrm{Tr}_R\left\{\hat{H}_V\mathrm{e}^{-i\hat{H}_0\tau}\hat{H}_V\mathrm{e}^{i\hat{H}_0\tau}\hat{\rho}_S(t)\hat{\rho}_R\right\}\\ =\ &\hbar^2\sum_k|g_k|^2\left(\langle\hat{R}_k^\dagger\hat{R}_k\rangle\hat{\sigma}^{(-)}\hat{\sigma}^{(+)}\hat{\rho}_S\mathrm{e}^{-i(\omega_0-\bar{\omega}_k)\tau} + \langle\hat{R}_k\hat{R}_k^\dagger\rangle\hat{\sigma}^{(+)}\hat{\sigma}^{(-)}\hat{\rho}_S\mathrm{e}^{i(\omega_0-\bar{\omega}_k)\tau}\right).\end{aligned} \tag{4.10}$$

Since we are assuming a zero temperature vacuum reservoir, $\langle\hat{R}_k^\dagger\hat{R}_k\rangle = 0$, and $\langle\hat{R}_k\hat{R}_k^\dagger\rangle = 1$ for all modes k. Therefore,

$$-\int_0^\infty d\tau\mathrm{Tr}_R\left\{\hat{H}_V\mathrm{e}^{-i\hat{H}_0\tau}\hat{H}_V\mathrm{e}^{i\hat{H}_0\tau}\hat{\rho}_S(t)\hat{\rho}_R\right\} = -\hbar^2\sum_k|g_k|^2\hat{\sigma}^{(+)}\hat{\sigma}^{(-)}\hat{\rho}_S\int_0^\infty d\tau\mathrm{e}^{i(\omega_0-\bar{\omega}_k)\tau} \tag{4.11}$$

Assuming that the system is coupled to a dense collection of reservoir modes, we may replace the summation over the reservoir modes by an integral. Therefore

$$\begin{aligned}&-\hbar^2\sum_k|g_k|^2\hat{\sigma}^{(+)}\hat{\sigma}^{(-)}\hat{\rho}_S\int_0^\infty d\tau\mathrm{e}^{i(\omega_0-\bar{\omega}_k)\tau}\\ =\ &-\hbar^2\hat{\sigma}^{(+)}\hat{\sigma}^{(-)}\hat{\rho}_S\lim_{\varepsilon\to0^+}\int_0^\infty d\tau\int_0^\infty d\bar{\omega}\mathscr{D}(\bar{\omega})|g(\bar{\omega})|^2\mathrm{e}^{i(\omega_0-\bar{\omega})\tau-\varepsilon\tau}\end{aligned} \tag{4.12}$$

where $\mathscr{D}(\bar{\omega})$ is the density of states for the reservoir modes, $g(\bar{\omega})$ is the continuum counterpart of g_k, and the convergence factor $\varepsilon \to 0^+$ selects the appropriate handedness for the contour around the pole in the $\bar{\omega}$ complex plane [32].

Assuming that $\mathscr{D}(\bar{\omega})$ is slowly-varying about ω_0, and that the coupling can be expressed as $g(\bar{\omega}) = g(\omega_0)\theta(\omega_c - \bar{\omega})$ where θ is the Heaviside function, an assumption that asserts the Markov approximation, the integration of equation (4.12) yields

$$\begin{aligned} & -\hbar^2\hat{\sigma}^{(+)}\hat{\sigma}^{(-)}\hat{\rho}_S \lim_{\varepsilon\to 0^+}\int_0^\infty d\tau \int_0^\infty d\bar{\omega}\mathscr{D}(\bar{\omega})|g(\omega_0)|^2\theta(\omega_c-\bar{\omega})\mathrm{e}^{i(\omega_0-\bar{\omega})\tau-\varepsilon\tau} \\ = \quad & -\hbar^2\mathscr{D}(\omega_0)|g(\omega_0)|^2 \lim_{\varepsilon\to 0^+}\left\{\left[\arctan\left(\frac{\omega_c-\omega_0}{\varepsilon}\right)+\arctan\left(\frac{\omega_0}{\varepsilon}\right)\right]+\frac{i}{2}\ln\left(\frac{\omega_0^2+\varepsilon^2}{(\omega_0-\omega_c)^2+\varepsilon^2}\right)\right\}, \end{aligned} \tag{4.13}$$

where we have additionally assumed that the density of states is slowly-varying to derive the imaginary part. The limit of $\varepsilon \to 0^+$ implies

$$\begin{aligned} & -\hbar^2\hat{\sigma}^{(+)}\hat{\sigma}^{(-)}\hat{\rho}_S \lim_{\varepsilon\to 0^+}\int_0^\infty d\tau \int_0^\infty d\bar{\omega}\mathscr{D}(\bar{\omega})|g(\omega_0)|^2\theta(\omega_c-\bar{\omega})\mathrm{e}^{i(\omega_0-\bar{\omega})\tau-\varepsilon\tau} \\ = \quad & -\pi\hbar^2\mathscr{D}(\omega_0)|g(\omega_0)|^2\left(1+\frac{i}{\pi}\ln\left|\frac{\omega_0}{\omega_0-\omega_c}\right|\right). \end{aligned} \tag{4.14}$$

From this expression it is clear that taking the limit of ω_c to infinity would cause the imaginary component of the integral to diverge. This behavior is known as the ultraviolet divergence. There are rigorous treatments of this divergence, such as electron mass renormalization in the context of quantum electrodynamics [33]. If ω_c were to be taken to infinity, the divergence would arise directly from the erroneous assumption that the density of states and atom-reservoir coupling could be treated as constants for all frequencies from zero to infinity. Assuming that the system couples to a resonant vacuum mode in the exact same manner that it does to a vacuum mode that is infinitely higher in energy is clearly incorrect. In quantum optics, the cut-off is typically taken to be the frequency ω_c for which a photon would have a wavelength equal to the size of the atom. Under this assumption, the imaginary term leads to a small energetic shift, analogous to the Lamb shift [33, 34], and is generally neglected since it is orders of magnitude less than optical system frequencies. Alternatively, it can also be incorporated in the definition of the resonant frequency. Neglecting this small energetic shift, we get

$$-\hbar^2 \sum_k |g_k|^2 \hat{\sigma}^{(+)}\hat{\sigma}^{(-)}\hat{\rho}_S \int_0^\infty d\tau \mathrm{e}^{i(\omega_0-\bar{\omega}_k)\tau} = \pi\hbar^2 |g(\omega_0)|^2 \mathscr{D}(\omega_0)\hat{\sigma}^{(+)}\hat{\sigma}^{(-)}\hat{\rho}_S. \tag{4.15}$$

Similar mathematical manipulations on equation (4.4) yield the following result for the master equation of a two level atom coupled to a zero temperature vacuum:

$$\frac{d\hat{\rho}_S}{dt} = -\frac{i}{\hbar}\left[\hat{H}_S, \hat{\rho}_S(t)\right] - \frac{\Gamma}{2}\left(\hat{\sigma}^{(+)}\hat{\sigma}^{(-)}\hat{\rho}_S + \hat{\rho}_S\hat{\sigma}^{(+)}\hat{\sigma}^{(-)} - 2\hat{\sigma}^{(-)}\hat{\rho}_S\hat{\sigma}^{(+)}\right), \tag{4.16}$$

where $\Gamma = 2\pi|g(\omega_0)|^2\mathscr{D}(\omega_0)$ is the decay rate for the excited two level atom. This decay rate agrees with the expression calculated with Fermi's golden rule [65].

4.2 Sharp reservoirs: a non-Markovian situation

Suppose instead of an atom being coupled to a continuum of modes up to ω_c such that $\omega_c \gg \omega_0$, as illustrated in Figure 4.2(a), the atom is coupled to modes up to $\omega_c = \omega_0$ as in Figure 4.2(b). This reservoir model was analyzed in detail in Pepino *et al.* [66]. Mathematically, this can be done by including the Heaviside function in our definition of the coupling constant, density of states, or vacuum mode occupancy. Regardless of the choice taken, the modification would take the integral in equation (4.12) and augment its form to the following:

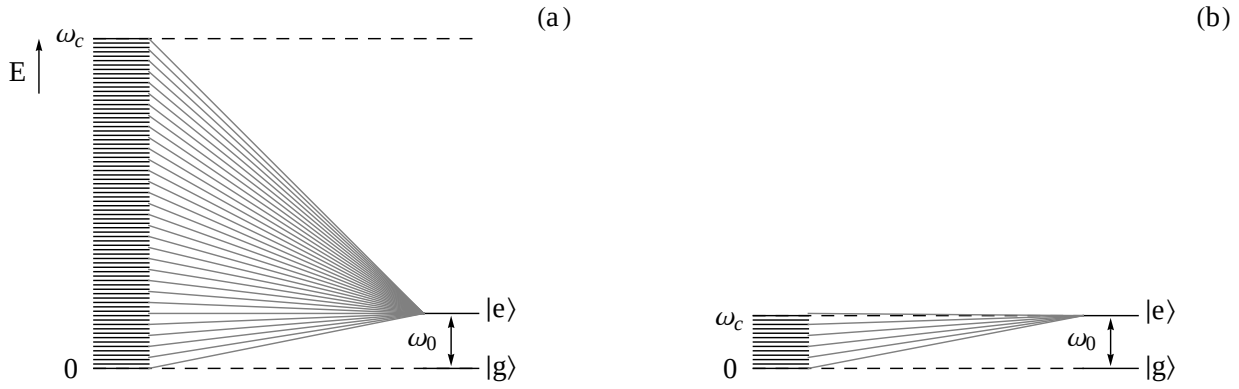

Figure 4.2: (a) A two-level atom coupled to a near-continuum of modes whose upper energy level $\omega_c \gg \omega_0$. (b) A two-level atom couple to an exotic reservoir whose maximum energy $\omega_c = \omega_0$. The latter reservoir model leads to divergences in the standard Born-Markov open quantum system treatment.

$$
\begin{aligned}
& -\hbar^2 \mathscr{D}(\omega_0)|g(\omega_0)|^2 \lim_{\varepsilon\to 0^+}\lim_{\omega_c\to\omega_0}\int_0^\infty d\tau \int_0^\infty d\bar{\omega}\theta(\omega_c-\bar{\omega})\mathscr{D}(\bar{\omega})|g(\bar{\omega})|^2 \mathrm{e}^{i(\omega_0-\bar{\omega})\tau-\varepsilon\tau} \\
= \quad & -\hbar^2 \mathscr{D}(\omega_0)|g(\omega_0)|^2 \lim_{\omega_c\to\omega_0}\left\{\frac{\pi}{2}+\frac{i}{2}\ln\left(\frac{\omega_0^2}{(\omega_0-\omega_c)^2}\right)\right\}. \qquad (4.17)
\end{aligned}
$$

Recall, in the previous model, the energy shift was a negligibly-small quantity. However, as ω_c approaches ω_0, the energy shift not only becomes non-negligible, it diverges! This infrared divergence occurs for all surviving integral terms in equation (4.4).

This result shows that we cannot simply employ the second-order Born-Markov approximations when the hard edge overlaps with system eigenenergies, as the resulting theory is mathematically undefined. The divergence is caused by a violation of our time scale assumption, where we have assumed $\tau_c \ll T_{sys}$. As we see in Section 4.3, the sharp cut-off must impart a correlation time on the system-reservoir interaction on the order of, or greater than, the system response time.

4.3 Fourth-order estimate of the full memory kernel

In this section we derive a higher-order treatment of the master equation formalism. A property of memory kernels that model relaxation processes is that they exhibit exponential decay [63]. Here, we estimate the all orders exponential decay by expanding the memory kernel of equation (3.44) to fourth-order in $\hat{\mathscr{L}}_V$. This order of expansion involves 256 possible terms. Here we focus on the fourth-order correction to the $\tilde{\sigma}^{(-)}(t)\tilde{\rho}_S(\tau)\tilde{\sigma}^{(+)}(\tau)$ term for two-level atom coupled to the zero-temperature vacuum, and expand the kernel about the divergence.

Transforming equation (3.44) into the interaction picture yields [67]

$$
\begin{aligned}
\frac{d}{dt}\tilde{\rho}_S &= -\int_0^t d\tau \langle \hat{\mathscr{L}}_V(t)\mathrm{e}^{-i\int_\tau^t d\tau' \hat{\mathbb{Q}}\hat{\mathscr{L}}_V(\tau')}\hat{\mathscr{L}}_V(\tau)\rangle\tilde{\rho}_S(\tau) \qquad (4.18) \\
&\simeq -\int_0^t d\tau \Bigg(\langle \hat{\mathscr{L}}_V(t)\hat{\mathscr{L}}_V(\tau)\rangle \\
&\quad -\int_\tau^t d\tau_1 \int_\tau^{\tau_1} d\tau_2 \langle \hat{\mathscr{L}}_V(t)\hat{\mathscr{L}}_V(\tau_1)\hat{\mathbb{Q}}\hat{\mathscr{L}}_V(\tau_2)\hat{\mathscr{L}}_V(\tau)\rangle \\
&\quad -\int_\tau^t d\tau_1 \int_\tau^{\tau_1} d\tau_2 \langle \hat{\mathscr{L}}_V(t)\hat{\mathscr{L}}_V(\tau_1)\rangle\langle \hat{\mathbb{Q}}\hat{\mathscr{L}}_V(\tau_2)\hat{\mathscr{L}}_V(\tau)\rangle \Bigg)\tilde{\rho}_S(\tau). \qquad (4.19)
\end{aligned}
$$

Expanding the second-order expectation value, and acting with the Liouvillian operators on $\tilde{\rho}_S(\tau)$, the zero-temperature reservoir assumption implies

$$\begin{aligned}\langle\hat{\mathscr{L}}_V(t)\hat{\mathscr{L}}_V(\tau)\rangle\tilde{\rho}_S(\tau) &= \sum_k |g_k|^2\Big(\langle\tilde{R}_k(t)\hat{R}_k^\dagger(\tau)\rangle\tilde{\sigma}^{(+)}(t)\tilde{\sigma}^{(-)}(\tau)\tilde{\rho}_S(\tau) \\ &\quad -\langle\tilde{R}_k(\tau)\hat{R}_k^\dagger(t)\rangle\tilde{\sigma}^{(-)}(t)\tilde{\rho}_S(\tau)\tilde{\sigma}^{(+)}(\tau) \\ &\quad -\langle\tilde{R}_k(t)\hat{R}_k^\dagger(\tau)\rangle\tilde{\sigma}^{(-)}(\tau)\tilde{\rho}_S(\tau)\tilde{\sigma}^{(+)}(t) \\ &\quad +\langle\tilde{R}_k(\tau)\hat{R}_k^\dagger(t)\rangle\tilde{\rho}_S(\tau)\tilde{\sigma}^{(+)}(\tau)\tilde{\sigma}^{(-)}(t)\Big) \qquad (4.20) \\ &= -\sum_k |g_k|^2\langle\tilde{R}_k(\tau)\hat{R}_k^\dagger(t)\rangle\tilde{\sigma}^{(-)}(t)\tilde{\rho}_S(\tau)\tilde{\sigma}^{(+)}(\tau)\pm\cdots, \qquad (4.21)\end{aligned}$$

where we will compare the matching fourth-order term to the second-order term of equation (4.21).

The fourth-order term in equation (4.19) can be expanded most simply by an application of Wick's theorem [67] along with the knowledge that the reservoir is in the zero-temperature vacuum state. Then, utilizing the fact that $\hat{\sigma}^{(-)}\cdot\hat{\sigma}^{(-)} = \hat{\sigma}^{(+)}\cdot\hat{\sigma}^{(+)} = 0$ leaves only four surviving terms. Of those four, only the following two are relevant for comparison with equation (4.21):

$$\begin{aligned}&-\int_\tau^t d\tau_1\int_\tau^{\tau_1} d\tau_2\langle\hat{\mathscr{L}}_V(t)\hat{\mathscr{L}}_V(\tau_1)\rangle\langle\hat{\mathbb{Q}}\hat{\mathscr{L}}_V(\tau_2)\hat{\mathscr{L}}_V(\tau)\rangle\Big)\tilde{\rho}_S(\tau) \\ &= \sum_l\sum_k |g_l|^2|g_k|^2\int_\tau^t d\tau_1\int_\tau^{\tau_1} d\tau_2\Big(\langle\hat{R}_l(\tau_1)\hat{R}_l^\dagger(\tau_2)\rangle\langle\tilde{R}_k(\tau)\hat{R}_k^\dagger(t)+\langle\hat{R}_l(\tau_2)\hat{R}_l^\dagger(t)\rangle\langle\tilde{R}_k(\tau_1)\hat{R}_k^\dagger(\tau)\rangle\Big) \\ &\quad\times\tilde{\sigma}^{(-)}(t)\tilde{\sigma}^{(+)}(\tau_1)\tilde{\sigma}^{(-)}(\tau_2)\tilde{\rho}_S(\tau)\tilde{\sigma}^{(+)}(\tau)\pm\cdots \qquad (4.22)\end{aligned}$$

Since

$$\begin{aligned}&\sum_l\sum_k |g_l|^2|g_k|^2\int_\tau^t d\tau_1\int_\tau^{\tau_1} d\tau_2\ \langle\hat{R}_l(\tau_2)\hat{R}_l^\dagger(t)\rangle\langle\tilde{R}_k(\tau_1)\hat{R}_k^\dagger(\tau)\rangle \\ &= \sum_l\sum_k |g_l|^2|g_k|^2\int_\tau^t d\tau_1\int_\tau^{\tau_1} d\tau_2\ \langle\hat{R}_l\hat{R}_l^\dagger\rangle\langle\tilde{R}_k\hat{R}_k^\dagger\rangle e^{i\omega_l(t-\tau_2)}e^{i\omega_k(\tau-\tau_1)} \\ &\simeq |g(\omega_0)|^4\pi^2\mathscr{D}(\omega_0)^2\int_{-\infty}^{\omega_0} d\omega_l\int_{-\infty}^{\omega_0} d\omega_k\int_\tau^t d\tau_1\int_\tau^{\tau_1} d\tau_2\ e^{i\omega_l(t-\tau_2)}e^{i\omega_k(\tau-\tau_1)} \\ &= |g(\omega_0)|^4\pi^2\mathscr{D}(\omega_0)^2\int_\tau^t d\tau_1\int_\tau^{\tau_1} d\tau_2\ \delta(t-\tau_2)\delta(\tau-\tau_1) \\ &= 0,\end{aligned}$$

equation (4.22) becomes

$$\pi\mathscr{D}(\omega_0)|g(\omega_0)|^2\sum_k|g_k|^2\int_\tau^t d\tau_1\int_\tau^{\tau_1}d\tau_2\Big[$$
$$\delta(\tau_2-\tau_1)\langle\tilde{R}_k(\tau)\hat{R}_k^\dagger(t)\rangle\tilde{\sigma}^{(-)}(t)\tilde{\sigma}^{(+)}(\tau_1)\tilde{\sigma}^{(-)}(\tau_2)\tilde{\rho}_S(\tau)\tilde{\sigma}^{(+)}(\tau)\Big]\pm\cdots$$
$$= \frac{\pi}{2}\mathscr{D}(\omega_0)|g(\omega_0)|^2\sum_k|g_k|^2(t-\tau)\langle\tilde{R}_k(\tau)\hat{R}_k^\dagger(t)\rangle\tilde{\sigma}^{(-)}(t)\hat{\sigma}^{(+)}\hat{\sigma}^{(-)}\tilde{\rho}_S(\tau)\tilde{\sigma}^{(+)}(\tau)\pm\cdots \quad (4.23)$$
$$= \frac{\pi}{2}\mathscr{D}(\omega_0)|g(\omega_0)|^2\sum_k|g_k|^2(t-\tau)\langle\tilde{R}_k(\tau)\hat{R}_k^\dagger(t)\rangle\tilde{\sigma}^{(-)}(t)\tilde{\rho}_S(\tau)\tilde{\sigma}^{(+)}(\tau)\pm\cdots$$
$$\equiv \eta\sum_k|g_k|^2(t-\tau)\langle\tilde{R}_k(\tau)\hat{R}_k^\dagger(t)\rangle\tilde{\sigma}^{(-)}(t)\tilde{\rho}_S(\tau)\tilde{\sigma}^{(+)}(\tau)\pm\cdots. \quad (4.24)$$

where we define

$$\eta=\frac{\pi}{2}\mathscr{D}(\omega_0)|g(\omega_0)|^2=\frac{\Gamma}{4}. \quad (4.25)$$

Here Γ, defined by equation (4.16), has already been introduced as the decay rate of the two level atom. The fact that $\langle\tilde{R}_k(\tau)\tilde{R}_k^\dagger(t)\rangle=\langle\tilde{R}_k(0)\tilde{R}_k^\dagger(t-\tau)\rangle$ means equation (4.19) can be simplified to

$$\frac{d}{dt}\tilde{\rho}_S = \int_0^t d\tau\left(\sum_k|g_k|^2\langle\tilde{R}_k(0)\tilde{R}_k^\dagger(t-\tau)\rangle\tilde{\sigma}^{(-)}(t-\tau)\tilde{\rho}_S(\tau)\tilde{\sigma}^{(+)}(0)\pm\cdots\right)\Big(1-\eta(t-\tau)\Big)$$
$$\simeq \int_0^t d\tau\left(\sum_k|g_k|^2\langle\tilde{R}_k(0)\tilde{R}_k^\dagger(t-\tau)\rangle\tilde{\sigma}^{(-)}(t-\tau)\tilde{\rho}_S(\tau)\tilde{\sigma}^{(+)}(0)\pm\cdots\right)\mathrm{e}^{-\eta(t-\tau)} \quad (4.26)$$

for $\eta t\ll 1$. Thus, the master equation in the interaction picture is

$$\frac{d}{dt}\tilde{\rho}_S = -\int_0^t d\tau\langle\hat{\mathscr{L}}_V(t)\mathrm{e}^{-i\int_\tau^t d\tau'\hat{\mathbb{Q}}\hat{\mathscr{L}}_V(\tau')}\hat{\mathscr{L}}_V(\tau)\rangle\tilde{\rho}_S(\tau) \quad (4.27)$$
$$\simeq -\int_0^t d\tau\langle\hat{\mathscr{L}}_V(0)\mathrm{e}^{-\eta(t-\tau)}\hat{\mathscr{L}}_V(t-\tau)\rangle\tilde{\rho}_S(\tau). \quad (4.28)$$

Since the transformation from the Schrödinger picture to the interaction picture is

$$\int_0^t\mathscr{R}(\tau)\hat{\rho}(t-\tau)d\tau\to\int_0^t\tilde{\mathscr{R}}(t-\tau)\tilde{\rho}(\tau)d\tau, \quad (4.29)$$

the master equation in the Schrödinger picture is given by

$$\frac{d}{dt}\hat{\rho}_S\simeq -i\hat{\mathscr{L}}_s\hat{\rho}_s-\int_0^t d\tau\langle\hat{\mathscr{L}}_V\mathrm{e}^{-i\hat{\mathscr{L}}_0\tau}\mathrm{e}^{-\eta\tau}\hat{\mathscr{L}}_V\rangle\hat{\rho}_S(t-\tau). \quad (4.30)$$

Physically, the new parameter η that we have introduced in this theory is the inverse of the finite correlation time that the system-reservoir interaction acquires when a sharp reservoir boundary overlaps with system eigenenergy differences. This accounts for the violation of the separation of

time scales assumption, since $\eta \sim \Gamma$ implies $\tau_c \sim T_{sys}$. Thus, the Markov approximation cannot be made in this case since the correlation function does not decay rapidly compared to the system time scale. If we are solely concerned with steady-state solutions of the master equation, long times t imply $\hat{\rho}_S(t-\tau) \simeq \hat{\rho}_S(t)$. Therefore, in this case $\hat{\rho}_s$ can be removed from the integral, whose upper limit goes to infinity:

$$\frac{d}{dt}\hat{\rho}_S \simeq -i\hat{\mathscr{L}}_s\hat{\rho}_s - \int_0^\infty d\tau \mathrm{e}^{-\eta\tau}\langle\hat{\mathscr{L}}_V \mathrm{e}^{-i\hat{H}_0\tau}\hat{\mathscr{L}}_V \mathrm{e}^{i\hat{H}_0\tau}\rangle\hat{\rho}_S(t). \tag{4.31}$$

In taking $t \to \infty$ we lose the ability to resolve the short-time characteristics of the evolution of the density operator. Since we will generally be concerned with the steady-state behavior of atomtronic systems in this thesis, this is a justified approximation. Equation (4.31) is the modified master equation we implement whenever there exists sharp reservoir boundaries that could overlap with system energy levels.

4.3.1 The physical interpretation of η

Here we compare the standard Born-Markov master equation to our non-Markovian model in order to illuminate the modification that η induces on a simple system. Consider a two-level atom with frequency ω_0 coupled to an exotic reservoir that is comprised solely of ground state two-level atoms with transition energies ranging from 0 to ω_μ, and excited two-level atoms with transition energies greater than ω_μ.

We can calculate the steady-state population as a function of the system frequency ω_0 by taking the trace of the product of the Born-Markov master equation with $\hat{\sigma}^{(+)}\hat{\sigma}^{(-)}$. Since $\partial_t\hat{\rho}_S = 0$, and $\mathrm{Tr}_S\{[\hat{H}_S, \hat{\rho}_S]\hat{\sigma}^{(+)}\hat{\sigma}^{(-)}\} = 0$, we get

$$0 = \mathrm{Tr}_S\left\{\lim_{\epsilon\to 0}\int_0^\infty d\tau \mathrm{e}^{-\epsilon\tau}\left[\hat{H}_V, \left[\hat{H}_V(-\tau), \hat{\rho}_S\right]\right]\hat{\sigma}^{(+)}\hat{\sigma}^{(-)}\right\}, \tag{4.32}$$

which yields a steady-state value for the average system excitation of

$$\langle\hat{\sigma}^{(+)}\hat{\sigma}^{(-)}\rangle = \theta(\omega_0 - \omega_\mu). \tag{4.33}$$

This step function about the reservoir boundary is what one might expect from such a model since, $\omega_0 < \omega_\mu$ couples the system solely to vacuum modes while $\omega_0 > \omega_\mu$ drives the system with the excited reservoir.

The limit $\epsilon \to 0$ is convergent in this case due to a cancellation of the imaginary terms that occur by taking the trace of $\hat{\rho}_S$ with the observable $\hat{\sigma}^{(+)}\hat{\sigma}^{(-)}$.

Employing our non-Markovian model to the same system,

$$0 = \mathrm{Tr}_S \left\{ \int_0^\infty d\tau \mathrm{e}^{-\eta\tau} \left[\hat{H}_V, \left[\hat{H}_V(-\tau), \hat{\rho}_S \right] \right] \hat{\sigma}^{(+)}\hat{\sigma}^{(-)} \right\}, \tag{4.34}$$

which yields a steady-state value for the average system excitation of

$$\langle \hat{\sigma}^{(+)}\hat{\sigma}^{(-)} \rangle = \frac{1}{2} - \frac{1}{\pi} \arctan\left(\frac{\omega_\mu - \omega_0}{\eta} \right). \tag{4.35}$$

This expression is very similar to the one obtained from the Born-Markov model. The only difference here is a population transition region broadened by η, as shown in Figure 4.3. Interestingly, in the case of a Fermi-Dirac reservoir, the finite correlation time acquired by the system-reservoir coupling is directly analogous to including a finite temperature in the reservoir structure.

This result also makes sense from a perturbative standpoint, where one would expect that a higher-order treatment of the memory kernel would mix the otherwise sharp distribution of the reservoir modes. Since $\eta = \Gamma/4 = |g(\omega_0)|^2 \mathscr{D}(\omega_0)\pi/2 = \pi|g(\omega_0)|^2/(2\Delta\omega)$, the broadening is directly

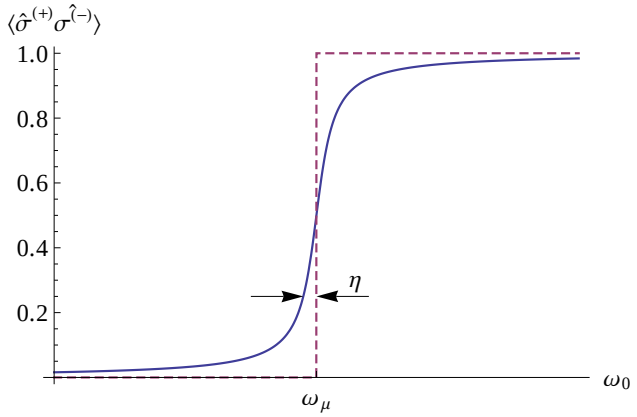

Figure 4.3: The analytic comparison of the Born-Markov master equation to our non-Markovian master equation applied to a two-level atom coupled to a reservoir with a sharp boundary.

proportional to the reservoir square of the coupling, and inversely proportional to the energetic spacing. This might have been anticipated since our perturbative expansion of the memory kernel was taken to second order.

4.4 Closed system model estimate for η

In this section we present a simple model calculation that clearly confirms our prediction of the higher-order behavior of the memory kernel for a structured reservoir with a hard edge. Here we test our estimation of η by performing full calculations on reasonably large, closed quantum systems. The closed system we consider is again a single excited two-level atom 'system', but this time coupled to N energetically equally-spaced ground state 'reservoir' two-level atoms as illustrated in Figure 4.4. We take the energy spacing of the reservoir modes to be $\Delta\omega$. The Hamiltonian that models this system is

$$\hat{H} = \hbar \left[\frac{1}{2}\omega_0 \hat{\sigma}_0^{(z)} + \frac{1}{2}\sum_{j=1}^{N} \omega_j \ \hat{\sigma}_j^{(z)} + g\left(\hat{\sigma}_j^{(+)}\hat{\sigma}_0^{(-)} + \hat{\sigma}_j^{(-)}\hat{\sigma}_0^{(+)}\right) \right], \tag{4.36}$$

where ω_0 and $\hat{\sigma}_0^{(z)}$ are the frequency and Pauli spin matrix of the system two level atom, $\omega_j = j\Delta\omega$ is the energy level of the jth 'vacuum mode' and g is the coupling of the jth mode to the system, taken to be uniform. Here $\omega_c = N\Delta\omega$, and the uniform spacing of the j modes implies that the

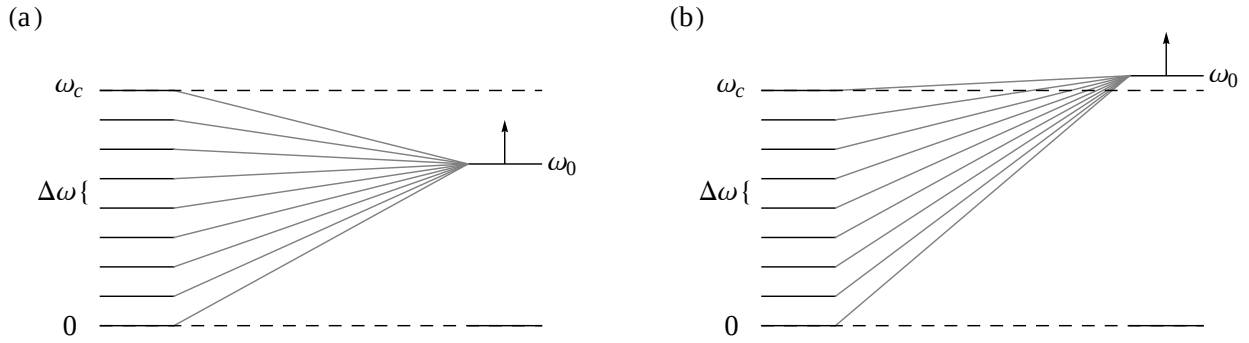

Figure 4.4: The illustration of a numerical experiment consisting of a large closed system consisting of a single two level atom coupled to a finite collection of equally-spaced reservoir modes. The population of the single two-level atom is recorded as its frequency ω_0 scans through the reservoir frequencies starting from (a) the middle where $\omega_0 < \omega_c$ to (b) $\omega_0 > \omega_c$.

density of states for the reservoir is $\mathscr{D}(\omega_0) = 1/\Delta\omega$.

Ideally, we would like to configure the reservoir with a sharp boundary ω_μ between excited and ground state two-level atoms to match the model described above. Unfortunately, the $N+1$ coupled atomic system has a Hilbert space with dimension 2^{N+1}, which grows exponentially, becoming numerically-unmanageable as a function of N very quickly. Instead, we consider conditions where the system is initially excited, and the reservoir solely consists of ground state two-level atoms with energies ranging from 0 to ω_c. This allows us two work in the single excitation manifold whose dimension is merely $N + 1$. In doing so, we are able to model much larger systems that, in turn, approximate system-reservoir dynamics more accurately. This model is sufficient for our comparison with the non-Markovian model but, the lack of an excited two-level atom drive with energies above ω_c, restricts the validity of the model to the regime where $\omega_0 \leq \omega_c$. The reservoir boundary ω_c in this case models the reservoir edge ω_μ, since $\hat{\sigma}_0^{(+)}|e\rangle = 0$, where $|e\rangle$ is the excited state of the atom.

In the limit where $\mathscr{D}(\omega_0) \ll 1/g$, the system effectively couples to a single mode, and Rabi flops between the system and reservoir modes. Therefore, in order to approximate system-reservoir behavior, we require $\mathscr{D}(\omega_0) > 1/g$, which guarantees that the system interacts with several modes of the reservoir. Since the major feature that the non-Markovian model added was a broadening of the system population transition as a function of the system frequency ω_0, here we record the average population $\bar{P}_0$ of this closed system as a function of $\omega_0 - \omega_c$. We then measure the width of the population transition as ω_0 approaches ω_c from below.

For fixed $\mathscr{D}(\omega_0)$ and g, we simulate the model described above by time evolving the excitation of the two-level atom system as a function of $\omega_c - \omega_0$. Since this is a closed quantum system, the excitation of the atom system undergoes collapses and revivals due to the fact that there is no true steady-state for the Hamiltonian system. We calculate the average excitation of the system in the region precisely between consecutive revivals. Obtaining a series of these average system excitations as a function of $\omega_c - \omega_0$, we can numerically construct the average population function $\bar{P}_0(\omega_c - \omega_0)$. The half width at half maximum of $\bar{P}_0(\omega_c - \omega_0)$ is determined from the fall-off of

the excitation as a function of $\omega_c - \omega_0$ about the 50% occupancy level. This broadened population transition as a function of frequency is then directly comparable to η.

Figure 4.5 demonstrates this process for the case where $\Delta\omega/\omega_c = 0.005$ and $g/\omega_c = 0.015$ are fixed. Figure 4.5(a) is a plot of the population of the system as a function of time where

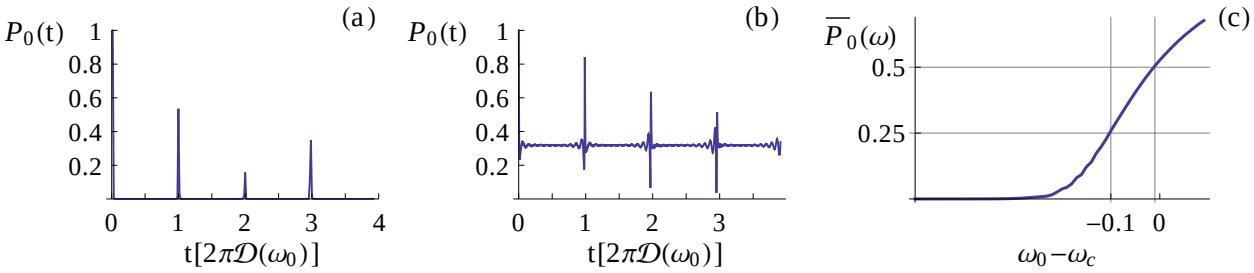

Figure 4.5: A demonstration of the calculation of a η/ω_c for a large closed quantum system. For fixed $\Delta\omega/\omega_c$ and g/ω_c, time evolution of this as a function of $\omega_0 - \omega_c$ exhibits collapses and revivals due to the fact that it is a closed quantum system. (a) The time evolution for $\omega_0 - \omega_c = -\omega_c$. (b) The time evolution for $\omega_0 \simeq \omega_c$. We record the collapsed population value as a function of $\omega_0 - \omega_c$, and then plot them (c). The half width at half maximum is the value η.

$\omega_0 \ll \omega_c$. For a given $\Delta\omega$, the revival time is approximately equal to $2\pi\mathscr{D}(\omega_0)$ as can be observed on the plot. The quasi-steady-state can thus be calculated by time-averaging about $\pi\mathscr{D}(\omega_0)$. The quasi-steady-state for this case is approximately zero, since the system frequency is covered above and below by vacuum modes. Figure 4.5(b) is a plot of the population of the system as a function of time where $\omega_0 < \omega_c$, but $\simeq 8\%$ of its value. Here the revival time is the same, since the density of states is unchanged, and the quasi-steady-state is now a nonzero value. Figure 4.5(c) is the function $\bar{P}_0(\omega_c - \omega_0)$ obtained from data obtained in the manner just described. This particular numerical experiment yields $\simeq 0.09$, where the theoretically-predicted broadening is $\eta \simeq 0.07$. The procedure is repeated for a variety of values of g and $\mathscr{D}(\omega_0)$. The resulting data is given in Table (4.4).

Since we are checking the claim that $\eta = g^2\mathscr{D}(\omega_0)\pi/2$, in Figure 4.6 we plot $\eta \times 2/(g\mathscr{D}(\omega_0)\pi)$ as a function of g. In doing so, if η accurately models the system broadening, the slope of this line should be $\simeq 1$. The top (blue), middle (red), and bottom (yellow) points and lines correspond to the data and linear fit for $\mathscr{D}(\omega_0)\omega_c = 100$, $\mathscr{D}(\omega_0)\omega_c = 200$, and $\mathscr{D}(\omega_0)\omega_c = 500$ respectively. The

$\mathscr{D}(\omega_0)\omega_c = 100$		$\mathscr{D}(\omega_0)\omega_c = 200$		$\mathscr{D}(\omega_0)\omega_c = 500$	
g/ω_c	η/ω_c	g/ω_c	η/ω_c	g/ω_c	η/ω_c
0.020	0.081	0.010	0.044	0.006	0.040
0.022	0.096	0.012	0.060	0.008	0.067
0.025	0.121	0.015	0.090	0.010	0.099
0.027	0.138	0.017	0.113	0.012	0.136
		0.020	0.148	0.014	0.176

Table 4.1: A table of half width at half maxima as a function of $\mathscr{D}(\omega_0)$ and g for a large-closed quantum system. The standard Born-Markov theory predicts that these values should be zero. We can check the validity of our non-Markovian theory against these values to see if it characterizes the broadening correctly.

linear fits for $\mathscr{D}(\omega_0)\omega_c = 100$, $\mathscr{D}(\omega_0)\omega_c = 200$, and $\mathscr{D}(\omega_0)\omega_c = 500$ are

$$\eta \times \frac{2}{\pi g \mathscr{D}(\omega_0)} \simeq 0.972\ g + \frac{0.6}{\mathscr{D}(\omega_0)}, \tag{4.37}$$

$$\eta \times \frac{2}{\pi g \mathscr{D}(\omega_0)} \simeq 0.972\ g + \frac{0.8}{\mathscr{D}(\omega_0)}, \tag{4.38}$$

$$\eta \times \frac{2}{\pi g \mathscr{D}(\omega_0)} \simeq 0.940\ g + \frac{1.5}{\mathscr{D}(\omega_0)}. \tag{4.39}$$

In order to make the closed system model comparable to the theory presented in Section 4.2, we require that $g \gg 1/\mathscr{D}(\omega_0)$, or equivalently $g^2\mathscr{D}(\omega_0) \gg g$. Under this condition, the nonzero

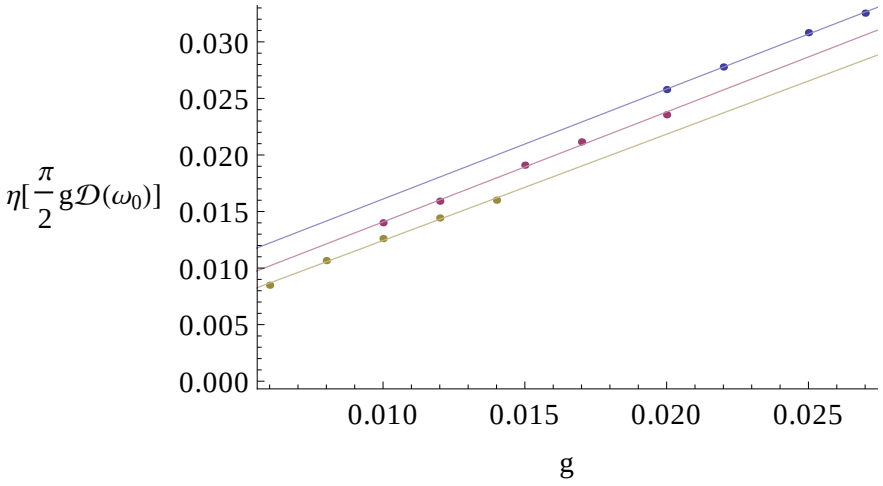

Figure 4.6: A plot of the data in Table 4.4 where the top (blue), middle (red), and bottom (yellow) lines correspond to $\mathscr{D}(\omega_0) = 100\omega_c$, $\mathscr{D}(\omega_0)\omega_c = 200$, and $\mathscr{D}(\omega_0)\omega_c = 500$ respectively. From these lines, the extrapolated equations, and given the fact that we require $g \gg \mathscr{D}(\omega_0)$, we confirm our previous definition of η.

intercept is negligible. From this large closed system model, we conclude that

$$\eta \simeq \frac{\pi}{2} g^2 \mathscr{D}(\omega_0), \tag{4.40}$$

which is in direct agreement with the non-Markovian correction calculated in Section 4.2.

4.5 Conclusion

In this chapter, we derived the decay of a two level atom that agreed with the decay obtained from Fermi's golden rule. After coupling the system to an exotic reservoir whose cut-off energetically matched the frequency of the atom, the standard Born-Markov master equation formalism acquired a diverging energy shift. This divergence was an artifact of the approximations that are typically made. By choosing the sharp reservoir boundary close to relevant system energies, we inadvertently contradicted the separation of time scales that we required in the original derivation of our coarse-grained master equation. This led to a violation of the Markov approximation.

To treat this problem correctly, we referred to the all-orders memory kernel form of the master equation. Observing the form of this expression and being aware of the long-time behavior of relaxation processes, we estimated the all-orders behavior by expanding the kernel to fourth-order, deriving an estimate for the decay of the kernel, which we referred to as $1/\eta$. Here we found that η was equal to one fourth of the decay rate of the two-level system coupled to the reservoir. The proximity of the T_{sys} and τ_c implied by $\eta \sim \Gamma$ indicates that this specific type of system-reservoir interaction is non-Markovian. The implication of the higher order correction in the formalism is that the sharp bare reservoir levels are broadened and mixed by their interaction with the system. In other words, the resolution of the levels of the reservoir get smeared by an amount $\simeq \eta$ due to their interaction with a common system. This is what one might expect from a perturbation theory standpoint. The resulting expression that we obtained was a solvable master equation with higher-order behavior accounted for. In its form, this master equation is incapable of resolving short times. Since we will be solely concerned with steady-state system behavior, the loss of the ability to model short times is not necessarily of major consequence.

We tested our all-orders approximate memory kernel model against a large, closed quantum system. Varying parameters such as the density of states and the couping strength of this closed system, we were able to verify that our model encapsulates the all-orders behavior of the large closed system quite well.

Chapter 5

Atomtronics with Atoms in Optical Lattices

The atomtronic systems we consider in this chapter involve bosonic atoms traversing optical lattice potentials. Here we employ a novel application of the master equation approach to open quantum systems where the reservoirs act as 'sources' and 'sinks'. We monitor the current response across the lattice as atoms move across from a high chemical potential reservoir to a low chemical potential reservoir. This concept is illustrated in Figure 5.1.

After quantifying our measure of atomic current, we examine the behavior of specific systems coupled to two different types of reservoirs: strongly-interacting and weakly-interacting bosonic reservoirs. In the limit of very strong atom-atom interactions, the zero-temperature bosons in the reservoir fermionize and map onto a zero-temperature, non-interacting fermion system with an equilibrium characterized by a Fermi-Dirac distribution with chemical potential μ_R that separates vac-

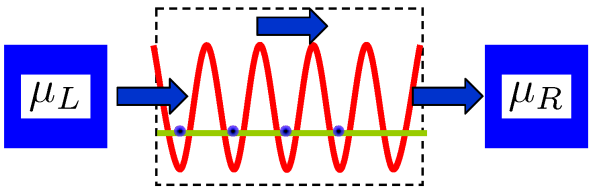

Figure 5.1: Illustration of an optical lattice coupled to two different reservoirs of ultracold atoms with chemical potentials μ_L and μ_R. As depicted in the figure, when $\mu_L > \mu_R$, a current of atoms in induced across the system from left to right.

uum states from occupied states. In the limit of weak atom-atom interactions, the zero-temperature atoms can Bose-condense, and the 'reservoir' becomes a superfluid that is the matter analog of a single coherent driving field. As we shall see, the strongly-interacting and weakly-interacting reservoirs lead to very different system responses. The systems and computational methods we develop in this section are also suitable for the generic study of transport properties of atoms through customized optical lattices.

In this chapter, we demonstrate theoretically a variety of highly customized optical lattices that mimic the behavior of a semiconductor diode, field-effect transistor (FET), and bipolar junction transistor (BJT) when driven by atomic reservoirs with chemical potential differences. We show that these fundamental electronic-like elements can be cascaded, leading to the the development of more complex logic components. The resulting atomtronics technology proposed in this work is intended to be a one-to-one analogy of traditional electronic systems.

5.1 Calculating atomic current through a custom optical lattice

Given a specific system and reservoir, we derive and solve the appropriate master equation for the evolution of the reduced system density operator $\hat{\rho}_S$. One $\hat{\rho}_S$ is known, the expectation value of any system observable can be obtained by taking the trace of the product of $\hat{\rho}_S$ with the observable in question. The observable that we are concerned with here is the atomic current that corresponds to atoms moving into or out of the system via the reservoir channels. In this section, we derive the operator whose expectation value is this current.

Consider a system coupled to many reservoirs. The modified master equation (4.31) for such a system-reservoir interaction is given by

$$\frac{d}{dt}\hat{\rho}_S = -\frac{i}{\hbar}\left[H_S, \hat{\rho}_S\right] - \frac{1}{\hbar^2}\mathrm{Tr}_R\left\{\sum_\kappa \int_0^\infty d\tau \mathrm{e}^{-\eta\tau}\left[\hat{V}_\kappa, \left[\hat{V}_\kappa(-\tau), \hat{\rho}_R\hat{\rho}_S\right]\right]\right\} \tag{5.1}$$

where,

$$\hat{V}_\kappa = \sum_j \hbar g_{\kappa,j}(\hat{a}_\kappa^\dagger \hat{R}_{\kappa,j} + \hat{a}_\kappa \hat{R}_{\kappa,j}^\dagger) \tag{5.2}$$

$$\equiv \hbar(\hat{a}_\kappa^\dagger \hat{\mathcal{G}}_\kappa + \hat{a}_\kappa \hat{\mathcal{G}}_\kappa^\dagger) \tag{5.3}$$

and $g_{\kappa,j}$ is the coupling constant for the reservoir mode j coupled to the lattice site κ, $\hat{a}_\kappa^\dagger$ creates a particle on system site κ, and $\hat{R}_{\kappa,j}$ annihilates a particle from the mode j of the reservoir that is connected to lattice site κ.

Here we examine how a particular reservoir coupled to lattice site q affects the population of system eigenstates $|\beta_n\rangle$; each $|\beta_n\rangle$ being an eigenstate in the n-particle manifold of the system. The evolution of the population of this state is given by

$$\begin{aligned}
\frac{d}{dt}\langle\beta_n|\hat{\rho}_S|\beta_n\rangle &= -\frac{i}{\hbar}\langle\beta_n|\left[H_S,\hat{\rho}_S\right]|\beta_n\rangle - \frac{1}{\hbar^2}\mathrm{Tr}_R\Bigg\{\sum_\kappa\int_0^\infty d\tau \mathrm{e}^{-\eta\tau}\langle\beta_n|\left[\hat{V}_\kappa,\left[\hat{V}_\kappa(-\tau),\hat{\rho}_R\hat{\rho}_S\right]\right]|\beta_n\rangle\Bigg\} \\
&= -\frac{1}{\hbar^2}\int_0^\infty d\tau \mathrm{e}^{-\eta\tau}\mathrm{Tr}_R\Bigg\{\langle\beta_n|\left[\hat{V}_q,\left[\hat{V}_q(-\tau),\hat{\rho}_R\hat{\rho}_S\right]\right]|\beta_n\rangle\Bigg\} \\
&\quad -\mathrm{Tr}_R\Bigg\{\sum_{\kappa\neq q}\int_0^\infty d\tau \mathrm{e}^{-\eta\tau}\langle\beta_n|\left[\hat{V}_\kappa,\left[\hat{V}_\kappa(-\tau),\hat{\rho}_R\hat{\rho}_S\right]\right]|\beta_n\rangle\Bigg\} \qquad (5.4)
\end{aligned}$$

where $[H_S,\hat{\rho}_S]=0$ since $|\beta_n\rangle$ is an eigenstate of H_S. Since we are interested in the influence on the population of state $|\beta_n\rangle$ solely due to the action of reservoir q, we focus our attention on the terms in equation (5.4) involving $\hat{V}_q$ alone. Expanding these terms, we get

$$\begin{aligned}
&-\frac{1}{\hbar^2}\int_0^\infty d\tau \mathrm{e}^{-\eta\tau}\mathrm{Tr}_R\Bigg\{\langle\beta_n|\left[\hat{V}_q,\left[\hat{V}_q(-\tau),\hat{\rho}_R\hat{\rho}_S\right]\right]|\beta_n\rangle\Bigg\} \\
&= \int_0^\infty d\tau \mathrm{e}^{-\eta\tau}\langle\beta_n|\Bigg[\Big(\hat{a}_q^\dagger(-\tau)\hat{\rho}_S\hat{a}_q\langle\hat{\mathcal{G}}_q^\dagger\hat{\mathcal{G}}_q(-\tau)\rangle + \hat{a}_q^\dagger\hat{\rho}_S\hat{a}_q(-\tau)\langle\hat{\mathcal{G}}_q^\dagger(-\tau)\hat{\mathcal{G}}_q\rangle\Big) \\
&\quad -\Big(\hat{a}_q\hat{a}_q^\dagger(-\tau)\hat{\rho}_S\langle\hat{\mathcal{G}}_q^\dagger\hat{\mathcal{G}}_q(-\tau) + \hat{\rho}_S\hat{a}_q(-\tau)a_q^\dagger\langle\hat{\mathcal{G}}_q^\dagger(-\tau)\hat{\mathcal{G}}_q\rangle\Big)\Bigg]|\beta_n\rangle \\
&\quad + \int_0^\infty d\tau \mathrm{e}^{-\eta\tau}\langle\beta_n|\Bigg[\Big(\hat{a}_q(-\tau)\hat{\rho}_S\hat{a}_q^\dagger\langle\hat{\mathcal{G}}_q\hat{\mathcal{G}}_q^\dagger(-\tau)\rangle + \hat{a}_q\hat{\rho}_S\hat{a}_q^\dagger(-\tau)\langle\hat{\mathcal{G}}_q(-\tau)\hat{\mathcal{G}}_q^\dagger\rangle\Big) \\
&\quad -\Big(\hat{a}_q^\dagger\hat{a}_q(-\tau)\hat{\rho}_S\langle\hat{\mathcal{G}}_q\hat{\mathcal{G}}_q^\dagger(-\tau) + \hat{\rho}_S\hat{a}_q^\dagger(-\tau)a_q\langle\hat{\mathcal{G}}_q(-\tau)\hat{\mathcal{G}}_q^\dagger\rangle\Big)\Bigg]|\beta_n\rangle \qquad (5.5)
\end{aligned}$$

where the first terms in the brackets (*i.e.* those proportional to $\langle\hat{\mathcal{G}}_q^\dagger\hat{\mathcal{G}}_q\rangle$) add atoms into the system, and the second terms in the brackets (*i.e.* those proportional to $\langle\hat{\mathcal{G}}_q\hat{\mathcal{G}}_q^\dagger\rangle$) remove atoms out of the system.

The positive terms on proportional to $\langle\hat{\mathcal{G}}_q^\dagger\hat{\mathcal{G}}_q\rangle$ in equation (5.5), responsible for supplying population to the $|\beta_n\rangle$ state, are proportional to $\langle\beta_n|\hat{a}_q^\dagger\hat{\rho}_S\hat{a}_q|\beta_n\rangle = \langle b_{n-1}|\hat{\rho}_S|b_{n-1}\rangle$, where $|b_{n-1}\rangle$ is a quantum state that belongs to the $(n-1)$-atom manifold. Therefore, as illustrated in Figure 5.2(a),

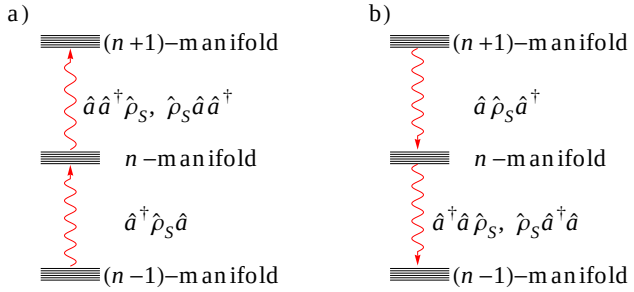

Figure 5.2: An analysis of how the terms in the master equation contribute to population in the n-particle manifold. (a) The action of a reservoir adding particles to the system. The operator $\hat{a}^\dagger\hat{\rho}_S\hat{a}$, linking manifolds n and $(n-1)$, increases the n-particle manifold, promoting atoms from the $(n-1)$ manifold. The number-conserving operators $\hat{a}\hat{a}^\dagger\hat{\rho}_S$ and $\hat{\rho}_S\hat{a}\hat{a}^\dagger$ decrease population in the n-particle manifold as the system is promoted to the $(n+1)$ manifold. (b) The action of a reservoir removing particles from the system. The operator $\hat{a}\hat{\rho}_S\hat{a}^\dagger$, linking manifolds n and $(n+1)$ increases population in the n-particle manifold as particles are removed from $(n+1)$. The number-conserving operators $\hat{a}^\dagger\hat{a}\hat{\rho}_S$ and $\hat{\rho}_S\hat{a}^\dagger\hat{a}$ decrease population from the n-particle manifold as the reservoir removes a particle.

the $|\beta_n\rangle$ state receives population from the manifold below it as a particle enters the system. The negative terms proportional to $\langle\hat{\mathcal{G}}_q^\dagger\hat{\mathcal{G}}_q\rangle$ in this equation, responsible for depleting population from the $|\beta_n\rangle$, are proportional to either $\langle\beta_n|\hat{a}_q\hat{a}_q^\dagger\hat{\rho}_S|\beta_n\rangle$ or $\langle\beta_n|\hat{\rho}_S\hat{a}_q\hat{a}_q^\dagger|\beta_n\rangle$. Since $\hat{a}_q\hat{a}_q^\dagger$ preserves particle number, these terms generate population loss out of the n-atom manifold: the $|\beta_n\rangle$ state loses population as the system is promoted to a state in the $(n+1)$-particle manifold as a particle is added to the system. This behavior is also illustrated in Figure 5.2(a).

In contrast, the other terms in equation (5.5) behave as follows. The positive terms proportional to $\langle\hat{\mathcal{G}}_q\hat{\mathcal{G}}_q^\dagger\rangle$, responsible for removing atoms from the system, are proportional to $\langle\beta_n|\hat{a}_q\hat{\rho}_S\hat{a}_q^\dagger|\beta_n\rangle = \langle b_{n+1}|\hat{\rho}_S|b_{n+1}\rangle$ where $|b_{n+1}\rangle$ belongs to the $(n+1)$-atom manifold. Thus, the state $|\beta_n\rangle$ receives population from above as particles leave the system. The negative terms proportional to $\langle\hat{\mathcal{G}}_q\hat{\mathcal{G}}_q^\dagger\rangle$, responsible for depleting population from $|\beta_n\rangle$, are proportional to either $\langle\beta_n|\hat{a}_q^\dagger\hat{a}_q\hat{\rho}_S|\beta_n\rangle$ or $\langle\beta_n|\hat{\rho}_S\hat{a}_q^\dagger\hat{a}_q|\beta_n\rangle$. Since $\hat{a}_q^\dagger\hat{a}_q$ preserves particle number, population is lost out of the $|\beta_n\rangle$ state, where it goes to a state in the $(n-1)$-manifold as a particle is removed from the system. These actions are illustrated in Figure 5.2(b).

To find the net current observable for the state $|\beta_n\rangle$, we take the sum of positive contributions

from the influx terms and the negative contributions from the outflux terms, *i.e.*

$$\begin{aligned}\langle \hat{J}_q(\beta_n)\rangle &= \int_0^\infty d\tau \mathrm{e}^{-\eta\tau}\Big[\langle\beta_n|\Big(\hat{a}_q^\dagger(-\tau)\hat{\rho}_S\hat{a}_q\langle\hat{\mathcal{G}}_q^\dagger\hat{\mathcal{G}}_q(-\tau)\rangle + \hat{a}_q^\dagger\hat{\rho}_S\hat{a}_q(-\tau)\langle\hat{\mathcal{G}}_q^\dagger(-\tau)\hat{\mathcal{G}}_q\rangle\Big)|\beta_n\rangle \\ &\quad -\langle\beta_n|\Big(\hat{a}_q^\dagger\hat{a}_q(-\tau)\hat{\rho}_S\langle\hat{\mathcal{G}}_q\hat{\mathcal{G}}_q^\dagger(-\tau) + \hat{\rho}_S\hat{a}_q(-\tau)a_q^\dagger\langle\hat{\mathcal{G}}_q^\dagger(-\tau)\hat{\mathcal{G}}_q\rangle\Big)|\beta_n\rangle\Big]. \qquad (5.6)\end{aligned}$$

Under this convention, a positive value for $\langle\hat{J}_q\rangle$ corresponds to current entering the system. Alternatively, we could have taken the sum of the negative contributions from the influx terms and positive contributions from the outflux terms. In which case, a positive value for $\langle\hat{J}_q\rangle$ would correspond to current exiting the system.

The total current into, or out of, the system lattice site q can be obtained by summing the net current of all of the eigenstates $|\beta_n\rangle$. This sum is equivalent to a trace over the system eigenstates. Using the cyclic property of the trace, we obtain

$$\begin{aligned}\langle\hat{J}_q\rangle &= \mathrm{Tr}_S\Big\{\Big[\int_0^\infty d\tau\mathrm{e}^{-\eta\tau}\Big(\hat{a}_q\hat{a}_q^\dagger(-\tau)\langle\hat{\mathcal{G}}_q^\dagger\hat{\mathcal{G}}_q(-\tau)\rangle + \hat{a}_q(-\tau)\hat{a}_q^\dagger\langle\hat{\mathcal{G}}_q^\dagger(-\tau)\hat{\mathcal{G}}_q\rangle|\rangle \\ &\quad -\hat{a}_q^\dagger\hat{a}_q(-\tau)\langle\hat{\mathcal{G}}_q\hat{\mathcal{G}}_q^\dagger(-\tau) + \hat{a}_q(-\tau)a_q^\dagger\langle\hat{\mathcal{G}}_q^\dagger(-\tau)\hat{\mathcal{G}}_q\rangle\Big)\Big]\hat{\rho}_S\Big\} \qquad (5.7) \\ &\equiv \mathrm{Tr}_S\Big\{\hat{J}_q\hat{\rho}_S\Big\} \qquad (5.8)\end{aligned}$$

where we identify $\hat{J}_q$ as the system current operator at the system-reservoir junction q. We use this current operator throughout the remainder of the thesis to analyze effective transport through our proposed devices.

5.2 A strongly-interacting boson reservoir model (fermionized bosons)

A zero temperature strongly-interacting boson reservoir is comprised of a near-continuum of occupied levels up to some energy ω_μ, above which the modes are assumed to be in vacuum. When ω_μ lies above a system energy difference, sufficient energy is available for the system to be excited. The sharpness in the number distribution of the zero temperature Fermi-Dirac distribution implies that we need to use the non-Markovian master equation (4.31), to model this particular system-reservoir interaction. In a manner analogous to Pauli blocking, the atom-atom repulsion of

the strongly-interacting reservoir model has the desirable feature that atoms that enter the system cannot go back. They are forced to exit the system through the reservoir channel corresponding to the lower chemical potential. This characteristic makes this reservoir model an ideal model to study transport properties of custom optical lattices. We use this model to construct the majority of our proposed atomtronic components. Here we derive the master equation for an optical lattice system whose site q is coupled to a single reservoir in detail. Additional reservoirs can be added by following the same steps outlined here.

The starting point for this derivation is equation (4.31). Expanding the Liouvillians, we get

$$\frac{d\hat{\rho}_S}{dt} = -\frac{i}{\hbar}[\hat{H}_S, \hat{\rho}_S] - \frac{1}{\hbar^2}\int_0^\infty d\tau \mathrm{e}^{-\eta\tau}\mathrm{Tr}_R\left\{\left[\hat{H}_V, \left[\hat{H}_V(-\tau), \hat{\rho}_R\hat{\rho}_S\right]\right]\right\} \tag{5.9}$$

where $\eta = \Gamma/4$, the system decay rate Γ is derived below, $\hat{\mathscr{L}}_V(-\tau) = \mathrm{e}^{-i\hat{H}_0\tau/\hbar}\hat{\mathscr{L}}_V\mathrm{e}^{i\hat{H}_0\tau/\hbar}$, $\hat{H}_0 = \hat{H}_S + \hat{H}_R$, and the averaging is performed over the reservoir degrees of freedom. For an N-site Bose-Hubbard system, the Hamiltonian is

$$\hat{H}_S = \sum_{j=1}^{N}\left(\hbar\omega_j\hat{a}_j^\dagger\hat{a}_j + \frac{U_j}{2}\hat{a}_j^\dagger\hat{a}_j^\dagger\hat{a}_j\hat{a}_j\right) + \sum_{j=1}^{N-1}J_j\left(\hat{a}_j^\dagger\hat{a}_{j+1} + \hat{a}_j\hat{a}_{j+1}^\dagger\right) \tag{5.10}$$

where ω_j and U_j are the oscillator frequency and on-site interaction energy for site j, and J_j is the tunneling energy between sites j and $j+1$. The reservoir consists of a near-continuum ensemble of non-interacting oscillators whose Hamiltonian is

$$\hat{H}_R = \sum_k \hbar\bar{\omega}_k\hat{R}_k^\dagger\hat{R}_k. \tag{5.11}$$

where $\bar{\omega}_k$ is the frequency of reservoir mode k. The zero temperature Fermi-Dirac distribution is characterized by a reservoir frequency $\bar{\omega}_\mu$ such that for $\bar{\omega}_k \leq \bar{\omega}_\mu$,

$$\langle\hat{R}_k^\dagger\hat{R}_k\rangle = 1 \qquad \langle\hat{R}_k\hat{R}_k^\dagger\rangle = 0 \tag{5.12}$$

and for $\bar{\omega}_k > \bar{\omega}_\mu$,

$$\langle\hat{R}_k^\dagger\hat{R}_k\rangle = 0 \qquad \langle\hat{R}_k\hat{R}_k^\dagger\rangle = 1. \tag{5.13}$$

The Hamiltonian that describes the system-reservoir interaction is

$$\hat{H}_V = \hbar\left(\sum_k g_{q,k}\hat{R}_k^\dagger\hat{a}_q + g_{q,k}^*\hat{R}_k\hat{a}_q^\dagger\right) \tag{5.14}$$

where $g_{q,k}$ is the complex coupling constant that couples the oscillator to the mode k of the reservoir that is coupled to the system site q. Expanding the commutators of equation (5.9), we get

$$\begin{aligned}\frac{d\hat{\rho}_S}{dt} &= -\frac{i}{\hbar}[\hat{H}_S,\hat{\rho}_S] - \frac{1}{\hbar^2}\int_0^\infty d\tau \mathrm{e}^{-\eta\tau}\mathrm{Tr}\Big\{\hat{H}_V\hat{H}_V(-\tau)\hat{\rho}_R\hat{\rho}_S - \hat{H}_V(-\tau)\hat{\rho}_R\hat{\rho}_S\hat{H}_V \\ &\quad -\hat{H}_V\hat{\rho}_R\hat{\rho}_S\hat{H}_V(-\tau) + \hat{\rho}_R\hat{\rho}_S\hat{H}_V(-\tau)\hat{H}_V\Big\}. \end{aligned} \tag{5.15}$$

Inserting equation (5.14) yields

$$\begin{aligned}\frac{d\hat{\rho}_S}{dt} &= -\frac{i}{\hbar}[\hat{H}_S,\hat{\rho}_S] - \int_0^\infty d\tau \mathrm{e}^{-\eta\tau}\mathrm{Tr}\Big\{\sum_k |g_{q,k}|^2\Big(\hat{R}_k^\dagger\hat{R}_k(-\tau)\hat{a}_q\hat{a}_q^\dagger(-\tau)\hat{\rho}_S\hat{\rho}_R \\ &\quad + \hat{R}_k\hat{R}_{q,k}^\dagger(-\tau)\hat{a}_q^\dagger\hat{a}_q(-\tau)\hat{\rho}_S\hat{\rho}_R + \hat{\rho}_S\hat{\rho}_R\hat{R}_k^\dagger(-\tau)\hat{R}_k\hat{a}_q(-\tau)\hat{a}_q^\dagger + \hat{\rho}_S\hat{\rho}_R\hat{R}_k(-\tau)\hat{R}_k^\dagger\hat{a}_q^\dagger(-\tau)\hat{a}_q \\ &\quad - \hat{R}_k^\dagger\hat{a}_q\hat{\rho}_S\hat{\rho}_R\hat{R}_k(-\tau)\hat{a}_q^\dagger(-\tau) - R_k\hat{a}_q^\dagger\hat{\rho}_S\hat{\rho}_R\hat{R}_k^\dagger(-\tau)\hat{a}_q(-\tau) - \hat{R}_k^\dagger(-\tau)\hat{a}_q(-\tau)\hat{\rho}_S\hat{\rho}_R\hat{R}_k\hat{a}_q^\dagger \\ &\quad - \hat{R}_k(-\tau)\hat{a}_q^\dagger(-\tau)\hat{\rho}_S\hat{\rho}_R\hat{R}_k^\dagger\hat{a}_q\Big)\Big\} \\ &= -i[\hat{H}_S,\hat{\rho}_S] - \int_0^\infty d\tau \mathrm{e}^{-\eta\tau}\sum_k |g_{q,k}|^2\Big(\langle\hat{R}_k^\dagger\hat{R}_k(-\tau)\rangle\Big[\hat{a}_q\hat{a}_q^\dagger(-\tau)\hat{\rho}_S - \hat{a}_q^\dagger(-\tau)\hat{\rho}_S\hat{a}_q\Big] \\ &\quad + \langle\hat{R}_k\hat{R}_k^\dagger(-\tau)\rangle\Big[\hat{a}_q^\dagger\hat{a}_q(-\tau)\hat{\rho}_S - \hat{a}_q(-\tau)\hat{\rho}_S\hat{a}_q^\dagger\Big] + \langle\hat{R}_k^\dagger(-\tau)\hat{R}_k\rangle\Big[\hat{\rho}_S\hat{a}_q(-\tau)\hat{a}_q^\dagger - \hat{a}_q^\dagger\hat{\rho}_S\hat{a}_q(-\tau)\Big] \\ &\quad + \langle\hat{R}_k(-\tau)\hat{R}_k^\dagger\rangle\Big[\hat{\rho}_S\hat{a}_q^\dagger(-\tau)\hat{a}_q - \hat{a}_q\hat{\rho}_S\hat{a}_q^\dagger(-\tau)\Big]\Big) \end{aligned} \tag{5.16}$$

where we have simplified the expression by taking advantage of the fact that the reservoir is diagonal in its energy eigenbasis, and then we have used the cyclic property of the trace operation.

Next we project this equation onto the system energy eigenbasis:

$$\begin{aligned}\frac{d}{dt}\hat{\sigma}_{ab} &= -i\omega_{ab}\hat{\sigma}_{ab} - \int_0^\infty d\tau \mathrm{e}^{-\eta\tau}\sum_k |g_{q,k}|^2\Big(\langle\hat{R}_k^\dagger\hat{R}_k\rangle\mathrm{e}^{i\bar{\omega}_k t}\Big[\hat{A}_{an}\hat{A}_{nm}^\dagger\mathrm{e}^{-i\omega_{nm}\tau}\hat{\sigma}_{mb} \\ &\quad - \hat{A}_{an}^\dagger\mathrm{e}^{-i\omega_{an}\tau}\hat{\sigma}_{nm}\hat{A}_{mb}\Big] + \langle\hat{R}_k\hat{R}_k^\dagger\rangle\mathrm{e}^{-i\bar{\omega}_k t}\Big[\hat{A}_{an}^\dagger\hat{A}_{nm}\mathrm{e}^{-i\omega_{nm}\tau}\hat{\sigma}_{mb} - \hat{A}_{an}\mathrm{e}^{-i\omega_{an}\tau}\hat{\sigma}_{nm}\hat{A}_{mb}^\dagger\Big] \\ &\quad + \langle\hat{R}_k^\dagger\hat{R}_k\rangle\mathrm{e}^{-i\bar{\omega}_k t}\Big[\hat{\sigma}_{an}\hat{A}_{nm}\mathrm{e}^{-i\omega_{nm}\tau}\hat{A}_{mb}^\dagger - \hat{A}_{an}^\dagger\hat{\sigma}_{nm}\hat{A}_{mb}\mathrm{e}^{-i\omega_{mb}\tau}\Big] \\ &\quad + \langle\hat{R}_k\hat{R}_k^\dagger\rangle\mathrm{e}^{i\bar{\omega}_k t}\Big[\hat{\sigma}_{an}\hat{A}_{nm}^\dagger\mathrm{e}^{-i\omega_{nm}\tau}\hat{A}_{mb} - \hat{A}_{an}\hat{\sigma}_{nm}\hat{A}_{mb}^\dagger\mathrm{e}^{-i\omega_{mb}\tau}\Big]\Big) \\ &= -i\omega_{ab}\hat{\sigma}_{ab} - \int_0^\infty d\tau \mathrm{e}^{-\eta\tau}\sum_k |g_{q,k}|^2\Big(\langle\hat{R}_k^\dagger\hat{R}_k\rangle\Big[\hat{A}_{an}\hat{A}_{nm}^\dagger\mathrm{e}^{-i(\omega_{nm}-\bar{\omega}_k)\tau}\hat{\sigma}_{mb} \\ &\quad - \hat{A}_{an}^\dagger\mathrm{e}^{-i(\omega_{an}-\hat{\omega}_k)\tau}\hat{\sigma}_{nm}\hat{A}_{mb} + \hat{\sigma}_{an}\hat{A}_{nm}\mathrm{e}^{-i(\omega_{nm}+\bar{\omega}_k)\tau}\hat{A}_{mb}^\dagger - \hat{A}_{an}^\dagger\hat{\sigma}_{nm}\hat{A}_{mb}\mathrm{e}^{-i(\omega_{mb}+\bar{\omega}_k)\tau}\Big] \\ &\quad + \langle\hat{R}_k\hat{R}_k^\dagger\rangle\Big[\hat{A}_{an}^\dagger\hat{A}_{nm}\mathrm{e}^{-i(\omega_{nm}+\bar{\omega}_k)\tau}\hat{\sigma}_{mb} - \hat{A}_{an}\mathrm{e}^{-i(\omega_{an}+\bar{\omega}_k)\tau}\hat{\sigma}_{nm}\hat{A}_{mb}^\dagger \\ &\quad + \hat{\sigma}_{an}\hat{A}_{nm}^\dagger\mathrm{e}^{-i(\omega_{nm}-\bar{\omega}_k)\tau}\hat{A}_{mb} - \hat{A}_{an}\hat{\sigma}_{nm}\hat{A}_{mb}^\dagger\mathrm{e}^{-i(\omega_{mb}-\bar{\omega}_k)\tau}\Big]\Big) \end{aligned} \tag{5.17}$$

where we have defined $\hat{\sigma}_{ab} = \langle a|\hat{\rho}_S|b\rangle$, $\hat{A}_{ab} = \langle a|\hat{a}_q|b\rangle$, and $\hat{A}^\dagger_{ab} = \langle a|a_q^\dagger|b\rangle$ to simplify the notation, and $\omega_{ab} = \omega_a - \omega_b$ is the frequency difference of states $|a\rangle$ and $|b\rangle$. Converting the sum over reservoir modes to an integral, and asserting the reservoir statistics defined in equation (5.13), we get

$$\begin{aligned}
\frac{d}{dt}\hat{\sigma}_{ab} &= -i\omega_{ab}\hat{\sigma}_{ab} - \int_0^\infty d\tau \mathrm{e}^{-\eta\tau}\int_0^{\bar{\omega}_\mu} d\bar{\omega}\mathscr{D}(\bar{\omega})|g_q(\bar{\omega})|^2\Big[\hat{A}_{an}\hat{A}^\dagger_{nm}\mathrm{e}^{-i(\omega_{nm}-\bar{\omega})\tau}\hat{\sigma}_{mb} \\
&\quad - \hat{A}^\dagger_{an}\mathrm{e}^{-i(\omega_{an}-\hat{\omega})\tau}\hat{\sigma}_{nm}\hat{A}_{mb} + \hat{\sigma}_{an}\hat{A}_{nm}\mathrm{e}^{-i(\omega_{nm}+\bar{\omega})\tau}\hat{A}^\dagger_{mb} - \hat{A}^\dagger_{an}\hat{\sigma}_{nm}\hat{A}_{mb}\mathrm{e}^{-i(\omega_{mb}+\bar{\omega})\tau}\Big] \\
&\quad - \int_0^\infty d\tau \mathrm{e}^{-\eta\tau}\int_{\bar{\omega}_\mu}^{\bar{\omega}_c} d\bar{\omega}\mathscr{D}(\bar{\omega})|g_q(\bar{\omega})|^2\Big[\hat{A}^\dagger_{an}\hat{A}_{nm}\mathrm{e}^{-i(\omega_{nm}+\bar{\omega})\tau}\hat{\sigma}_{mb} \\
&\quad - \hat{A}_{an}\mathrm{e}^{-i(\omega_{an}+\bar{\omega})\tau}\hat{\sigma}_{nm}\hat{A}^\dagger_{mb} + \hat{\sigma}_{an}\hat{A}^\dagger_{nm}\mathrm{e}^{-i(\omega_{nm}-\bar{\omega})\tau}\hat{A}_{mb} - \hat{A}_{an}\hat{\sigma}_{nm}\hat{A}^\dagger_{mb}\mathrm{e}^{-i(\omega_{mb}-\bar{\omega})\tau}\Big]
\end{aligned} \tag{5.18}$$

where $\mathscr{D}(\bar{\omega})$ is the density of reservoir modes and $g_q(\bar{\omega})$ is the continuous analog of $g_{q,k}$. The upper limit on the second $\bar{\omega}$ integral goes to $\bar{\omega}_c$ instead of to infinity to avoid the ultraviolet divergence as previously discussed in Section 4.1. If we assume that the density of states and coupling function are slowly-varying about ω_{nm}, we can define the n, m matrix elements of

$$\begin{aligned}
\left(G^{(\pm)}_{\text{in}}\right)_{nm} &= \int_0^\infty d\tau\int_0^{\bar{\omega}_\mu} d\bar{\omega}|g_q(\bar{\omega})|^2\mathscr{D}(\bar{\omega})\mathrm{e}^{-i(\omega_{nm}\pm\bar{\omega})\tau-\eta\tau} \\
&= \pm|g_q(\bar{\omega}_0)|^2\mathscr{D}(\bar{\omega}_0)\Bigg[\arctan\left(\frac{\omega_{nm}\pm\bar{\omega}_\mu}{\eta}\right) - \arctan\left(\frac{\omega_{nm}}{\eta}\right) \\
&\quad - \frac{i}{2}\ln\left(\frac{(\omega_{nm}\pm\bar{\omega}_\mu)^2+\eta^2}{\omega_{nm}^2+\eta^2}\right)\Bigg]
\end{aligned} \tag{5.19}$$

and

$$\begin{aligned}
\left(G^{(\pm)}_{\text{out}}\right)_{nm} &= \int_0^\infty d\tau\int_{\bar{\omega}_\mu}^{\bar{\omega}_c} d\bar{\omega}\mathscr{D}(\bar{\omega})\mathrm{e}^{-i(\omega_{nm}\pm\bar{\omega})\tau-\eta\tau} \\
&= \pm|g_q(\bar{\omega}_0)|^2\mathscr{D}(\bar{\omega}_0)\Bigg[\arctan\left(\frac{\bar{\omega}_c\pm\bar{\omega}_\mu}{\eta}\right) - \arctan\left(\frac{\omega_{nm}\pm\bar{\omega}_\mu}{\eta}\right) \\
&\quad - \frac{i}{2}\ln\left(\frac{(\bar{\omega}_c\pm\bar{\omega}_\mu)^2+\eta^2}{(\omega_{nm}\pm\bar{\omega}_\mu)^2+\eta^2}\right)\Bigg].
\end{aligned} \tag{5.20}$$

This implies

$$\begin{aligned}\frac{d}{dt}\hat{\sigma}_{ab} &= -i\omega_{ab}\hat{\sigma}_{ab} - \frac{\Gamma}{2\pi}\Big[\hat{A}_{an}\hat{A}^{\dagger}_{nm}\left(G^{(-)}_{\text{in}}\right)_{nm}\hat{\sigma}_{mb} - \hat{A}^{\dagger}_{an}\left(G^{(-)}_{\text{in}}\right)_{an}\hat{\sigma}_{nm}\hat{A}_{mb} \\ &\quad + \hat{\sigma}_{an}\hat{A}_{nm}\left(G^{(+)}_{\text{in}}\right)_{nm}\hat{A}^{\dagger}_{mb} - \hat{A}^{\dagger}_{an}\hat{\sigma}_{nm}\hat{A}_{mb}\left(G^{(+)}_{\text{in}}\right)_{mb}\Big] \\ &\quad - \frac{\Gamma}{2\pi}\Big[\hat{A}^{\dagger}_{an}\hat{A}_{nm}\left(G^{(+)}_{\text{out}}\right)_{nm}\hat{\sigma}_{mb} - \hat{A}_{an}\left(G^{(+)}_{\text{out}}\right)_{an}\hat{\sigma}_{nm}\hat{A}^{\dagger}_{mb} \\ &\quad + \hat{\sigma}_{an}\hat{A}^{\dagger}_{nm}\left(G^{(-)}_{\text{out}}\right)_{nm}\hat{A}_{mb} - \hat{A}_{an}\hat{\sigma}_{nm}\hat{A}^{\dagger}_{mb}\left(G^{(-)}_{\text{out}}\right)_{mb}\Big] \end{aligned} \tag{5.21}$$

where the decay rate, or linewidth, $\Gamma = 2\pi|g_q(\bar{\omega}_0)|^2\mathscr{D}(\bar{\omega}_0)$ is equal to what one acquires from Fermi's golden rule.

This is the complete master equation for a Bose-Hubbard system that has site q coupled to a reservoir characterized by $\bar{\omega}_\mu$. In atomtronics applications, we require at least two reservoirs to drive current through the system in steady-state. Other reservoirs can be added in a similar manner to equation (5.21) where they may be characterized by their own system-reservoir decay rate and chemical potential.

5.2.1 The atomtronic wire

Here we begin the analysis of atomtronics components by considering the atomtronics counterpart to a simple circuit of a battery connected to a resistive wire. As seen in Figure 5.3, the analogy of a wire is an energetically-flat optical lattice, with uniform tunneling and interaction energies ($\epsilon_j \equiv \epsilon$, $U_j \equiv U$, and $J_{jk} \equiv J$ for all neighboring sites). For this system, and all atomtronics systems discussed in this thesis, we assume $U \gg J$. The corresponding Bose-Hubbard model for

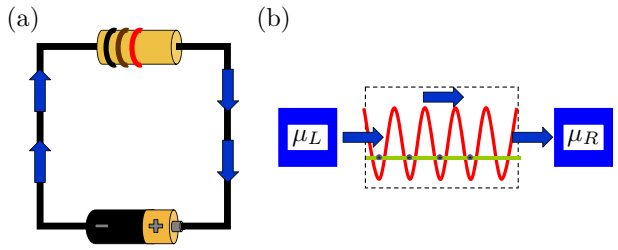

Figure 5.3: Illustration of the analogy between (a) the electronic circuit of a wire (with some inherent resistance) connected to a battery and (b) its atomtronic counterpart.

this N-site system is

$$\hat{H}_S = \sum_{j=1}^{N} \left(\hbar\omega \hat{a}_j^\dagger \hat{a}_j + \frac{U}{2} \hat{a}_j^\dagger \hat{a}_j^\dagger \hat{a}_j \hat{a}_j \right) + J \sum_{j=1}^{N-1} \left(\hat{a}_j^\dagger \hat{a}_{j+1} + \hat{a}_j \hat{a}_{j+1}^\dagger \right). \tag{5.22}$$

where $\hbar\omega = \epsilon$. For this system, we assume weak reservoir coupling and calculate the atomic current as a function of chemical potential difference. This numerical experiment is carried out by initially setting both left and right chemical potentials (μ_L and μ_R) to zero, and then raising μ_L so that an atomic current response is induced across the system from left to right. Using the analysis outlined in Appendix A, solve for $\hat{\rho}_S$ in steady-state. We then compute the current $\langle J_R \rangle$ out of the right side of the system. This data is presented in Figure 5.4. Here we see that the current increases with the chemical potential difference, but in quantized steps that correspond directly to the left chemical potential overcoming multiples of the on-site interaction energy. This is the energy needed to increase the number of atoms on the left site by one. A closer examination of the numerical simulation implemented in Figure 5.4 reveals two subtle features. Moving from left to right across graph in Figure 5.4, the first current jump occurs at $(\mu_L - \epsilon)/U = 0$, and the current increases in two steps. One might have expected to observe a single jump, since the condition to put a particle in the lattice is $\mu_L \geq \epsilon$. This is a result of the fact that the degeneracy of the Fock states in the one-particle manifold is split by $2J$ in the system state eigenbasis due to tunneling.

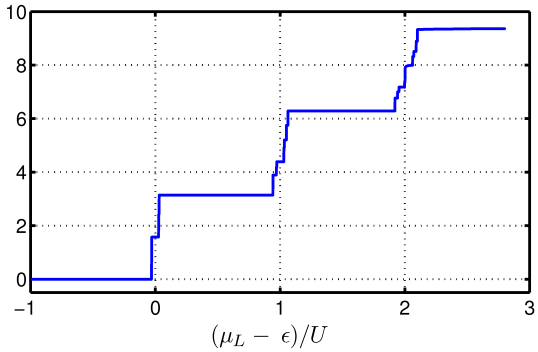

Figure 5.4: Current of the atomtronic wire (in units of Γ_0), in the case of weak coupling to the reservoirs, as a function of the left chemical potential. The current monotonically increases in quantized jumps as the on-site interaction energy to put on an additional particle is overcome. The parameters used to model the atomtronic wire in this simulation are $\epsilon/U = 3$, $J/U = 3 \times 10^{-2}$, and $\hbar\Gamma_0/U = 10^{-6}$.

In addition, the jump in current is broadened slightly by both the nonzero η and by the system-reservoir coupling. This broadening, which makes the jump in current a smooth transition rather than a discontinuous step is even more apparent in the atomtronic devices presented below, where the system reservoir-coupling is taken to be orders of magnitude larger. Although the exact details for the second and third jumps are more complicated, the reasoning is the same: the eigenenergies are split by approximately $2J$, and the overall jump is smoothed out by η. These general properties hold for many of the numerical experiments that follow.

5.2.2 The atomtronic diode

A diode is a device with an approximately unidirectional current characteristic. The basic behavior is that a voltage bias across the diode yields a current in one direction, but if the voltage bias is reversed the current response is negligible. Such behavior can be realized in an optical lattice by creating an energy shift in half of the lattice with respect to the other as we now show. We find that the diode characteristic persists as the number of lattice sites is increased so we may anticipate the result to hold in the mesoscopic limit. For simplicity, here we illustrate the idea of the atomtronic diode in a double well lattice system. For the simulations for the rest of this chapter, we assume $J/U = 3 \times 10^{-2}$, $\hbar\Gamma_0/U = 10^{-2}$.

In the Fock basis for a two site system, there exist three states in the two-particle manifold: $|20\rangle$, $|11\rangle$, and $|02\rangle$, where $|nm\rangle$ refers to n particles on the left site and m particles on the right. The external energies of the two sites (ϵ_1 and ϵ_2) can be chosen so that the eigenstates $|20\rangle$ and $|11\rangle$ are approximately degenerate, leaving both states far detuned from $|02\rangle$. This configuration of the site energies is given by $\epsilon_1 = \epsilon$ and $\epsilon_2 = \epsilon_1 + U$. We refer to this as the "resonance condition". The corresponding Hamiltonian for this two-site system is

$$\hat{H}_S = \hbar\omega_1 \hat{a}_1^\dagger \hat{a}_1 + (\hbar\omega_1 + U)\, \hat{a}_2^\dagger \hat{a}_2 + \frac{U}{2}\left(\hat{a}_1^\dagger \hat{a}_1^\dagger \hat{a}_1 \hat{a}_1 + \hat{a}_2^\dagger \hat{a}_2^\dagger \hat{a}_2 \hat{a}_2\right) + J\left(\hat{a}_1^\dagger \hat{a}_2 + \hat{a}_1 \hat{a}_2^\dagger\right) \tag{5.23}$$

Figure 5.5 illustrates how the resonance condition generates reverse-bias and forward-bias behavior in a two-site optical lattice. As seen in Figure 5.5(a), if one holds the left reservoir

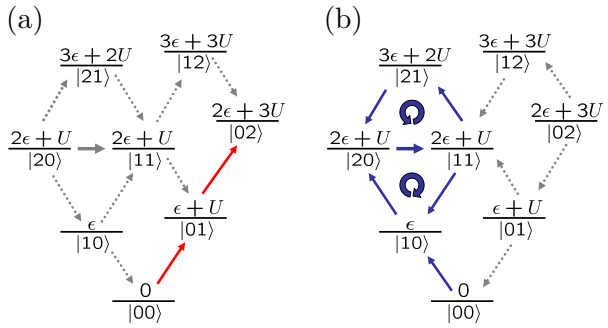

Figure 5.5: (a) Energy schematic of the reverse bias dynamics of the two site atomtronic diode. The red arrows represent the system transitions from an initially empty system. The gray (dotted) arrows represent all other possible transitions. Regardless of which state the system starts in, it evolves almost entirely to the $|02\rangle$ state. (b) Energy schematic of the forward-bias dynamics of the two-site atomtronic diode. Blue arrows illustrate transitions into current-bearing cycles, while gray (dotted) arrows represent all other possible transitions.

chemical potential at $\mu_L = 0$ and raises the right reservoir chemical potential μ_R, the system will undergo a transition from $|00\rangle$ to $|01\rangle$. The states $|01\rangle$ and $|10\rangle$ are separated in energy by U. As a result, most of the population remains in the $|01\rangle$ state. Increasing μ_R above the point where the transition from $|01\rangle$ to $|02\rangle$ is allowed, the system remains almost completely settled in the $|02\rangle$ state.

As seen in the Figure 5.5(b), if one holds $\mu_R = 0$ and raises μ_L, the system first undergoes a transition from $|00\rangle$ to $|10\rangle$. However, increasing μ_L so the system evolves to $|20\rangle$ leads to a very different situation than in the above case: since $|20\rangle$ is resonant with $|11\rangle$, both states are simultaneously populated. Since $\mu_R = 0$ takes all particles out of the site on the right, the system can make a transition from $|11\rangle$ back to $|10\rangle$. The combined effect of setting μ_L and μ_R to these values is to force the system to undergo a closed cycle of transitions between $|10\rangle$, $|20\rangle$ and $|11\rangle$. The result is a net atomic transport (or current flow) across the system. A second contributor to the net current through the system is the fact that μ_L allows transitions from $|11\rangle$ to $|21\rangle$. Thus, an additional current-generating cycle exists: $|11\rangle$ to $|21\rangle$ to $|20\rangle$ and back to $|11\rangle$. Both cycles contribute positively to a net current flow across the system.

For systems consisting of N lattice sites, the diode configuration is composed of two con-

nected, energetically-flat lattices whose energy separation is $\Delta\epsilon = U$. The basic dynamical response seen for two sites holds also for larger systems due to the fact that the flat lattice allows for effective transport. This is because adding a particle to the left site of the left half of the lattice is energetically degenerate with adding a particle to any sites up to, and including, the left site of the junction. Therefore, there exist current cycles initially generated from the degenerate $|222...2\rangle \otimes |0...000\rangle$ to $|222...1\rangle \otimes |1...000\rangle$ transition. Going the other direction, one can, in principle, go to $|0...000\rangle \otimes |222...2\rangle$ but, as is seen for the double well model, conditions are not energetically favorable, and atomic transport across the junction is greatly suppressed. Figure 5.6 is a schematic of a four-site atomtronic diode in the forward-biased direction.

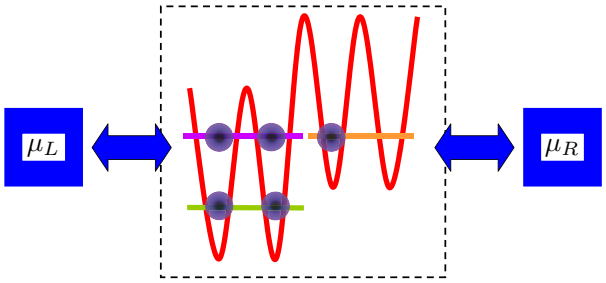

Figure 5.6: Schematic of the four-site optical lattice atomtronic diode.

In support of the fact that the dynamics of the diode are qualitatively-independent of the overall size of the lattice, we model a four-site diode here. The Hamiltonian for this system is

$$\begin{aligned}\hat{H}_S &= \hbar\omega_1\left(\hat{a}_1^\dagger\hat{a}_1 + \hat{a}_2^\dagger\hat{a}_2\right) + (\hbar\omega_1 + U)\left(\hat{a}_3^\dagger\hat{a}_3 + \hat{a}_4^\dagger\hat{a}_4\right) \\ &\quad + \frac{U}{2}\sum_{j=1}^{4}\hat{a}_j^\dagger\hat{a}_j^\dagger\hat{a}_j\hat{a}_j + J\sum_{j=1}^{3}\left(\hat{a}_j^\dagger\hat{a}_{j+1} + \hat{a}_j\hat{a}_{j+1}^\dagger\right). \end{aligned} \tag{5.24}$$

Figures 5.7(a-b) and Figures 5.7(c-d) are numerical simulations of the current responses of the two site diode Hamiltonian, and four site diode Hamiltonian, respectively. The general features of both diodes are qualitatively identical.

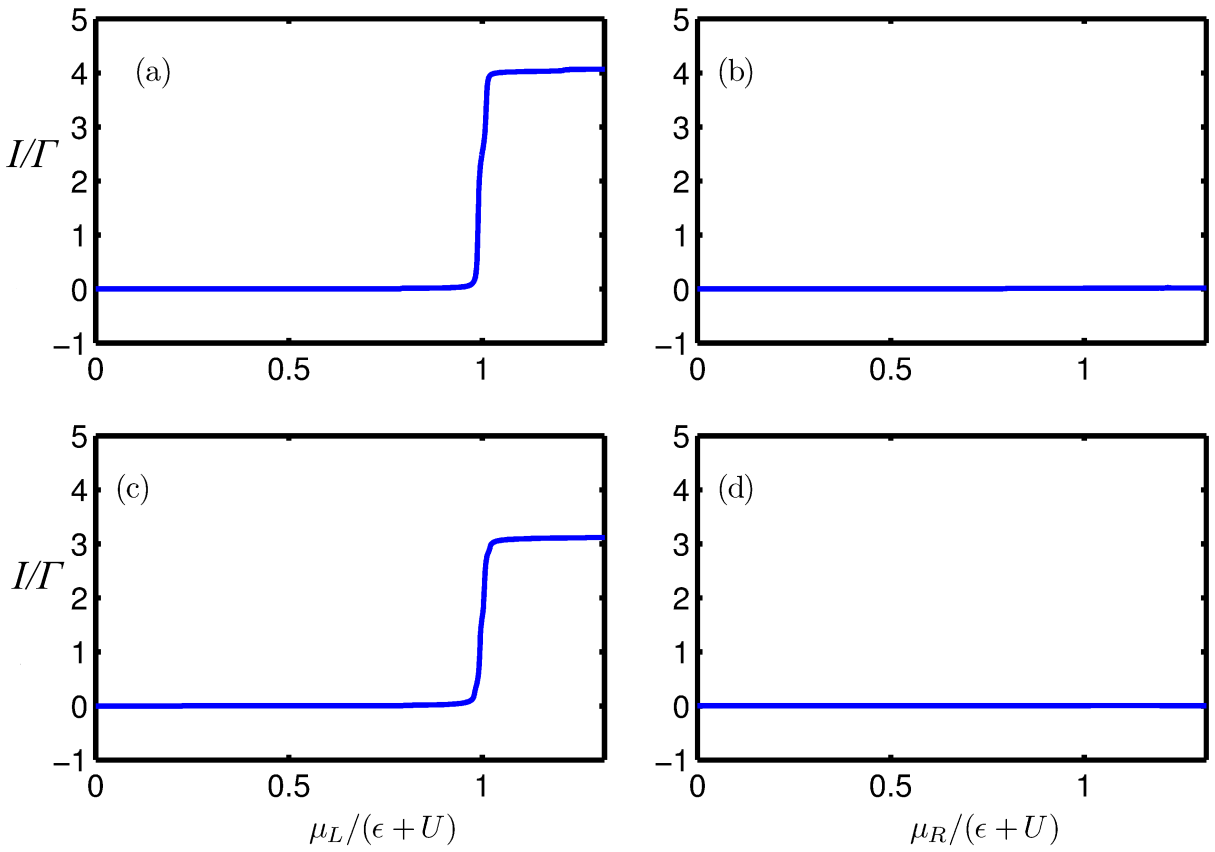

Figure 5.7: Current responses (in units of Γ_0) of (a) forward-bias two site diode, (c) the four site diode as a function of μ_L (with $\mu_R = 0$); current response of (b) the reverse-bias two site diode and (d) four site diode as a function of μ_R (with $\mu_L = 0$). The chemical potentials of all figures are normalized to the resonance condition, and the currents normalized to Γ_0.

5.2.2.1 Noise analysis of the atomtronic diode

Given the current characteristics of the diode, one might ask how much does the signal fluctuate about its steady-state value. Quantifying the signal-to-noise ratio (SNR) is an important measure of the functionality of any device. A time-averaged SNR can be obtained by constructing the power noise density function, convolving it with a filter, and then integrating over all frequencies. For the current operator $\hat{J}_q$, the corresponding $S_0(\omega)$ is

$$S_0(\omega) = \lim_{T\to\infty} \frac{1}{T} \left| \int_0^T \langle \hat{J}_q(t) \rangle \mathrm{e}^{-i\omega t} dt \right|^2 , \tag{5.25}$$

Given a system steady-state time t_0, the Wiener-Khintchine theorem can be stated as

$$S_0(\omega) = \mathrm{Re}\left\{\frac{2}{\pi}\int_0^\infty d\tau \mathrm{e}^{-i\omega\tau}\langle \hat{J}_q(t_0+\tau)\hat{J}_q(t_0)\rangle\right\}. \tag{5.26}$$

since the function is $\langle \hat{J}_q(t_0+\tau)\hat{J}_q(t_0)\rangle$ is a real-valued function [68].

Propagation of $\langle \hat{J}_q(t_0+\tau)\hat{J}_q(t_0)\rangle$ becomes tractable under the quantum regression theorem, which asserts that this correlation function evolves under the same equation of motion as $\hat{\rho}_S(t)$. We can confirm this by considering the correlation function for the full system and reservoir problem. In this case,

$$\langle \hat{J}_q(t_0+\tau)\hat{J}_q(t_0)\rangle = \mathrm{Tr}_{SR}\left\{\left(\mathrm{e}^{i\hat{H}(t_0+\tau)/\hbar}\hat{J}_q\mathrm{e}^{-i\hat{H}(t_0+\tau)/\hbar}\right)\left(\mathrm{e}^{i\hat{H}t_0/\hbar}\hat{J}_q\mathrm{e}^{-i\hat{H}t_0/\hbar}\right)\left(\mathrm{e}^{-i\hat{H}t_0/\hbar}\hat{\rho}\mathrm{e}^{i\hat{H}t_0/\hbar}\right)\right\} \tag{5.27}$$

where $\hat{H} = \hat{H}_S + \hat{H}_R + \hat{H}_V$, $\hat{\rho}(t_0)$ is in steady-state and the trace is over the system and reservoir degrees of freedom. The cyclic property of the trace implies

$$\begin{aligned}
\langle \hat{J}_q(t_0+\tau)\hat{J}_q(t_0)\rangle &= \mathrm{Tr}_{SR}\left\{\hat{J}_q\mathrm{e}^{-i\hat{H}\tau/\hbar}\hat{J}_q\left(\mathrm{e}^{-i\hat{H}2t_0/\hbar}\hat{\rho}\mathrm{e}^{i\hat{H}2t_0/\hbar}\right)\mathrm{e}^{i\hat{H}\tau/\hbar}\right\} \\
&= \mathrm{Tr}_{SR}\left\{\hat{J}_q\mathrm{e}^{-i\hat{H}\tau/\hbar}\left[\hat{J}_q\hat{\rho}(t_0)\right]\mathrm{e}^{i\hat{H}\tau/\hbar}\right\} \\
&= \mathrm{Tr}_S\left\{\hat{J}_q\ \mathrm{Tr}_R\left\{\mathrm{e}^{-i\hat{H}\tau/\hbar}\left[\hat{J}_q\hat{\rho}(t_0)\right]\mathrm{e}^{i\hat{H}\tau/\hbar}\right\}\right\}
\end{aligned} \tag{5.28}$$

where we have used $\hat{\rho}(2t_0) = \hat{\rho}(t_0)$ since $\hat{\rho}$ is in steady-state, and the fact that $\hat{J}_q$ is a system observable. The evolution of the full density operator is

$$\hat{\rho}(\tau) = \mathrm{e}^{-i\hat{H}\tau/\hbar}\hat{\rho}\mathrm{e}^{i\hat{H}\tau/\hbar}, \tag{5.29}$$

implying that the evolution of the reduced density operator is

$$\hat{\rho}_S(\tau) = \mathrm{Tr}_R\left\{\mathrm{e}^{-i\hat{H}\tau/\hbar}\hat{\rho}\mathrm{e}^{i\hat{H}\tau/\hbar}\right\}. \tag{5.30}$$

Comparing equation (5.28) with equation (5.30), we see that $\hat{\rho}_S$ and $\left[\hat{J}_q\hat{\rho}(t_0)\right]$ evolve in the exact same manner. Since $\hat{\rho}_S$ evolves under the master equation, it follows that $\left[\hat{J}_q\hat{\rho}(t_0)\right]$ evolves under the master equation as well.

In the Liouville representation, we can express the equation of motion for $\left[\hat{J}_q\hat{\rho}_S(t_0)\right]$ as

$$\frac{d}{dt}\left[\hat{J}_q\hat{\rho}(t_0)\right] = \hat{\mathscr{L}}_{\mathrm{MEq}}\left[\hat{J}_q\hat{\rho}_S(t_0)\right](t) \tag{5.31}$$

where $\hat{\mathscr{L}}_{\mathrm{MEq}}$ is the super operator that defines the master equation for $\hat{\rho}_S$. This equation can be Laplace transformed into

$$\left[\hat{J}_q\hat{\rho}_S(t_0)\right](s) = (s\hat{\mathbb{1}} - \hat{\mathscr{L}}_{\mathrm{MEq}})^{-1}\left[\hat{J}_q\hat{\rho}_S(t_0)\right](t_0) \tag{5.32}$$

From Equation (5.26), taking $s \to i\omega$ in Equation (5.32) implies

$$\begin{aligned} S_0(\omega) &= \mathrm{Re}\left\{\frac{2}{\pi}\int_0^\infty d\tau \mathrm{e}^{-i\omega\tau}\langle\hat{J}_q(t_0+\tau)\hat{J}_q(t_0)\rangle\right\} \\ &= \mathrm{Re}\left\{\frac{2}{\pi}\int_0^\infty d\tau \mathrm{e}^{-i\omega\tau}\mathrm{Tr}_S\left\{\hat{J}_q[\hat{J}_q\hat{\rho}_S(t_0)](\tau)\right\}\right\} \\ &= \mathrm{Re}\left\{\frac{2}{\pi}\,\mathrm{Tr}_S\left\{\hat{J}_q\left(i\omega\hat{\mathbb{1}} - \hat{\mathscr{L}}_{\mathrm{MEq}}\right)^{-1}[\hat{J}_q\hat{\rho}_S(t_0)](t_0)\right\}\right\}. \end{aligned} \tag{5.33}$$

We simulate time-averaging by convolving this expression with an exponential filter

$$F(t) = \frac{1}{T}\mathrm{e}^{-t/T} \tag{5.34}$$

where T is the time the current measurement is averaged over. The convolution theorem then implies

$$S(T,\omega) = \mathrm{Re}\left\{S_0(\omega)\frac{1}{1+i\omega T}\right\}. \tag{5.35}$$

Since $S_0(\omega)$ is a real-valued function due to the fact that the correlation function is both real and symmetric,

$$S(T,\omega) = S_0(\omega)\frac{1}{1+(\omega T)^2}. \tag{5.36}$$

In this convention,

$$\langle\hat{J}_q^2\rangle = \int_0^\infty S_0(\omega)d\omega. \tag{5.37}$$

Therefore the time-averaged SNR is

$$\mathcal{R}_{SN}(T) = \frac{\langle\hat{J}_q\rangle}{\sqrt{\int_0^\infty S(T,\omega)d\omega - \langle\hat{J}\rangle^2}}. \tag{5.38}$$

where $\langle \hat{J}_q \rangle$ is the expectation value of current. For values of $1/T$ that are small compared to appreciable changes of $S_0(\omega)$,

$$\begin{aligned} \mathcal{R}_{SN}(T) &= \frac{\langle \hat{J}_q \rangle}{\sqrt{\int_0^\infty S(T,\omega) d\omega}} \\ &\simeq \sqrt{\frac{1}{S_0(0)}} \frac{\langle \hat{J}_q \rangle}{\sqrt{\int_0^\infty \frac{1}{1+(\omega T)^2}}} \\ &= \frac{\langle \hat{J} \rangle}{\sqrt{\mathrm{Re}\left\{ \lim_{\omega \to 0} \mathrm{Tr}_S \{ \hat{J} (i\omega \hat{\mathbb{1}} - \hat{\mathscr{L}}_{MEq})(\hat{J}\hat{\rho}_S) \} \right\}}} \sqrt{T} \end{aligned} \tag{5.39}$$

Typical optical lattice experiments can achieve an on-site interaction energy $U/\hbar \sim 1$ kHz. For the parameters used for the diode, we find

$$\mathcal{R}_{SN} \simeq 8.9 \sqrt{\mathrm{Hz}} \sqrt{T}. \tag{5.40}$$

Therefore, a signal-to-noise ratio of ~ 10 can be achieved by averaging the atomic current for 1 second. Gillen has reported having atoms trapped in Markus Greiner's customized optical lattice experiments for up to 17 seconds [25], which would seem to make the proposed diode system experimentally accessible. We note this ratio is certainly parameter-sensitive, and could perhaps be improved upon in a different regime.

5.2.3 The atomtronic field-effect transistor

A field-effect transistor (FET) is a device that allows an externally-applied field to control the amount of current that flows through the device. This characteristic allows the FET to be utilized as a voltage-to-current amplifier. Since the diode is optimized when the resonance condition is imposed on the optical lattice, small deviations from the resonance condition lead to large changes in the maximum current propagating across the lattice. These changes in the relative zero-point energies can be brought on by changes in an external field that is applied to the lattice. This is precisely the behavior of a FET where a current is controlled by an applied voltage. In Figure 5.8, we plot several current results for the forward-bias configuration as the separation in the external energy of the second site is raised past the resonance condition by fractions of J, the smallest

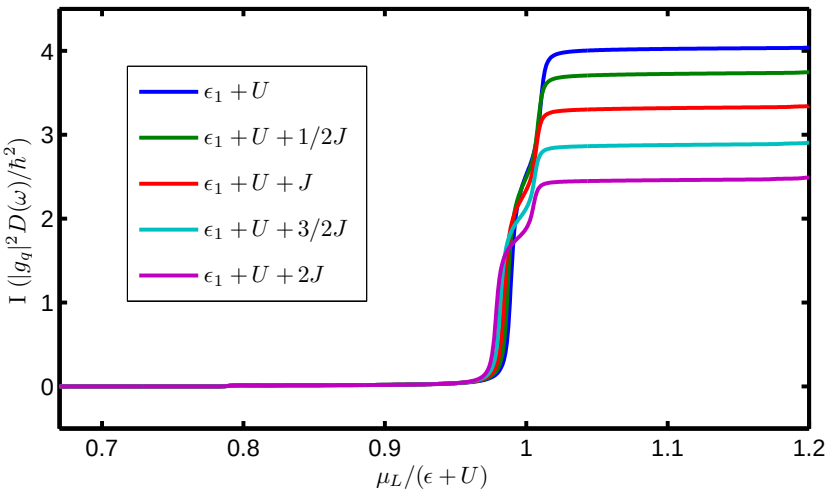

Figure 5.8: Current response of the atomtronic FET as a function of the chemical potential: small changes in ϵ_2 lead to appreciable changes in the current response. That is, as the system is detuned from its resonance condition, there is a fall off of the net current value across the device. The legend in this figure indicates the colored curves that correspond to particular values of ϵ_2.

system parameter in the model. In doing so, we successfully recover the FET-like behavior where small changes in an external field lead to appreciable changes in the current response of the device.

Along this line of reasoning, external fields can also be used to switch the atomic current completely off by either shifting the sites well out of resonance or by exchanging their value, changing the lattice from the forward-bias configuration to the reverse-bias. Such a switch might be useful if one desired a control of the atomic transport that was function of time.

5.2.4 The atomtronic bipolar junction transistor

A bipolar junction transistor (BJT) is a three terminal device in which the overall current across the emitter and collector is controlled by a much weaker current via the base. Two practical applications of the BJT are signal amplification and switching (on and off) of the emitter current.

Realization of BJT-like behavior in atomtronic systems requires at least three sites connected

to three different reservoirs. If the atomtronic diode is considered to be an atomtronic p-n junction, one might guess that the atomtronic n-p-n transistor would entail raising the external energy of the left and right (collector and emitter) sites higher than the middle (base) site by the on-site interaction energy. This configuration is illustrated in Figure 5.9(a). The reason this configuration yields BJT-like behavior is due to the approximate degeneracy between the Fock states $|110\rangle$, $|020\rangle$, and $|011\rangle$.

We implement numerical simulations of this lattice configuration by fixing a chemical potential difference across the lattice. The left reservoir chemical potential μ_L is set to maintain one particle on the left site and the chemical potential of the right reservoir μ_R is set to zero. The atomic current is measured as a function of μ_M.

When there are no atoms on the middle site, the configuration of the reservoirs pump the system into the $|100\rangle$ Fock state (as seen in Figure 5.9(b)). The $|100\rangle$ and the $|001\rangle$ states are degenerate with each other, but the system must undergo a second-order, off-resonant transition via the $|010\rangle$ state in order to transition from $|100\rangle$ to $|001\rangle$. Such transitions are suppressed by

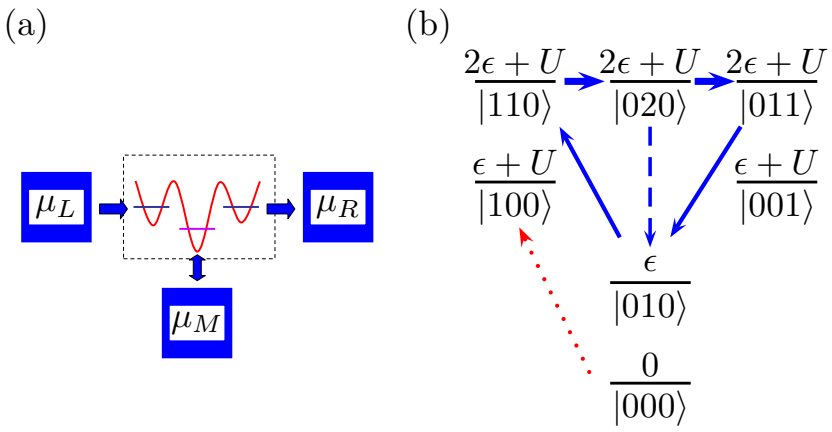

Figure 5.9: (a) An illustration of the BJT lattice-reservoir system. (b) The energy schematic of the three-site optical lattice under the extended resonance condition. Here the left reservoir is set to maintain an occupancy of one atom on the left site and the right is set to remove all atoms. If the middle reservoir is set to remove all particles, then the system evolves to the $|100\rangle$ state (red dotted arrow). If the middle reservoir is set to maintain an occupancy of one atom on the middle site, then the degeneracy between states $|110\rangle$, $|020\rangle$, and $|011\rangle$ allows current to traverse the system.

a factor of $(J/U)^2$ and thus become less likely as the energy difference between $|100\rangle$ and $|010\rangle$ increases. Thus, when the middle reservoir is set to maintain zero atoms on the middle site, the net current out of what would correspond to the emitter lead of a conventional transistor is minimal.

When the middle reservoir's chemical potential is increased to allow a single atom into the middle site of the system, the degeneracy between the $|110\rangle$, $|020\rangle$, and $|011\rangle$ states is accessed, which allows atoms to travel across the system. One issue with this configuration is the following: in order to get to $|011\rangle$, the system has to make a transition through the $|020\rangle$ state. Since the middle reservoir is set to maintain an occupancy of one, but not two, atoms on the middle site, one of the atoms can be lost to the middle reservoir, leading to a loss of emitter current out of the base. If the couplings of all three reservoirs to the system are equal, then the result is the current measured passing through the base turns out to be greater than the current measured out of the emitter. Thus, the system represents an inefficient transistor realization. On the other hand, if the middle reservoir were to be coupled weakly compared to the other reservoirs, then current predominantly leaves the system via the emitter, which is the desired behavior.

Figure 5.10(a) is a numerical simulation of the current out of the emitter and the base as a function of the base chemical potential. The coupling strength of the base connected to the reservoir is one fifth the collector and emitter reservoir coupling. It should be noted that the region where the proposed atomtronic transistor mimics the electronic BJT is limited to the transition region, or current jump. One can increase the length of this region by increasing the overall system-reservoir coupling strength. Figure 5.10(b) shows that the gain of this device is fairly linear.

5.2.5 Discrete atomtronics logic

Integrated circuits are designed with a very large number of transistor elements to perform a desired function. The demonstrated ability to realize atomtronic diodes and transistors thus motivates the question as to whether higher functionality can be realized with these ultracold atomic systems. Here we look at the most fundamental of these, the atomtronic AND logic gate.

A traditional logic element is a device with a given number of inputs and outputs, composed

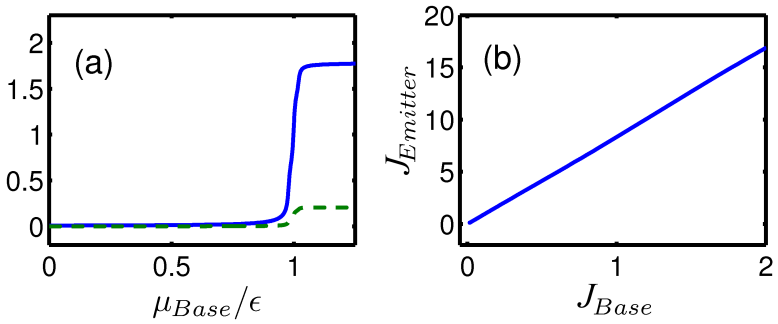

Figure 5.10: Characteristics of the atomtronic BJT. (a) For a fixed collector-emitter voltage bias, the current response measured through the base leg (green, dashed curve) and the emitter leg (blue curve) are plotted as a function of the base chemical potential. (b) The current out of the emitter is plotted vs. the current out of the base. Here a large linear gain is observed.

of switches, that generates a series of logical responses. Such logical behavior can be expressed in a truth table composed of 1's and 0's ('ons' and 'offs'). Logic elements are the fundamental building blocks of computing and discrete electronics. In Table 5.1(a) the truth table for the AND logic gate is given as an example. The next level of complexity in emulating electronic systems is to create logic elements from the atomtronic components.

An AND gate is a device with two inputs (A and B), and one output (O). As illustrated in Table 5.1(a), the device characteristic of the AND gate is that O remains off unless both A and B are on. In electronics, such a device can be constructed by connecting two transistors in series (as illustrated in Figure 5.11(a)). By direct analogy, the atomtronic AND gate can be constructed by connecting two atomtronic BJTs in series as illustrated in Figure 5.11(b).

When constructing practical logic circuits, the logical values of the 1s and 0s are mapped to a given energetic range. The data in Table 5.1(b) has been generated in a numerical experiment of the optical lattice configuration depicted in Figure 5.11(b). For this particular experiment, the maximal current out of the device is at least a factor of 6 greater than any other measured current. Thus a discernible difference between 'on' and 'off' is observed and the output currents reproduce the AND gate truth table to reasonable fidelity. Such a difference can also be enhanced by increasing the on-site interaction energy U of the lattice.

(a)

AND Gate		
A	B	O
0	0	0
1	0	0
0	1	0
1	1	1

(b)

Atomtronic AND Gate Simulation		
A	B	O
0	0	0.00
3.2	0	0.01
0	3.2	0.16
3.2	3.2	1.00

Table 5.1: AND gate truth table where the two inputs are labeled by A and B, the output labeled by O, and the 1 or 0 entries represent 'on' and 'off'. (a) Truth table describing the device characteristics. (b) Numerical simulation of the atomtronic AND gate normalized to the maximal output current 'O'. Here, the inputs A and B are the respective chemical potentials measured with respect to the on-site interaction energy (μ_A/U μ_B/U) and the output is the atomic current normalized by the maximum output current (I/I_{max}). In practice, the logical 'ins' and 'outs' are mapped to physical currents by setting threshold ranges. Since the maximal output current is larger than all other output values by at least a factor of 6, we can conclude that there exists logic gate behavior in this optical lattice setup.

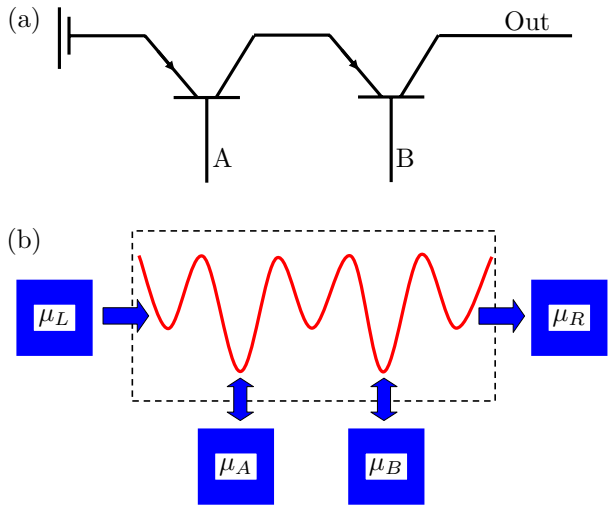

Figure 5.11: (a) Electronic schematic for the AND logic gate, a device constructed by cascading two transistors in series. (b) Atomtronics AND schematic. The atomtronic AND logic gate is constructed exactly like its electronic counterpart, *i.e.* by cascading two transistors in series. A chemical potential bias $\mu_L - \mu_R$ across the device attempts to drive a current across the device. No substantial current is observed, however, unless both μ_A and μ_B supply atoms onto the base terminals of their respective transistors.

5.3 Weakly-interacting boson reservoir model (BEC reservoir)

Up to this point, our reservoir models have all been of the strongly-interacting type. However, in this section we consider the driving mechanism for the system to be a near-zero temperature weakly-interacting trapped Bose gas. In other words, we take the reservoir drive to be a Bose-Einstein Condensate (BEC) in a superfluid state. Here, we develop the theory, and examine the current characteristics, for a one-dimensional lattice driven by a BEC on one end, while coupled to the zero-temperature vacuum on the other as depicted in Figure 5.12.

In contrast to the Fermi-Dirac type drive that we've used previously, the BEC drives the system with a monochromatic coherent frequency. This causes the system to exhibit resonant current responses as the BEC energy scans past the system energies. Additionally, once the BEC drive deposits an atom into the system, it cannot block the atom from going back in the same way as was observed for the Fermi-Dirac reservoir. For these reasons, one may anticipate that the overall measured current that flows through the system will be less.

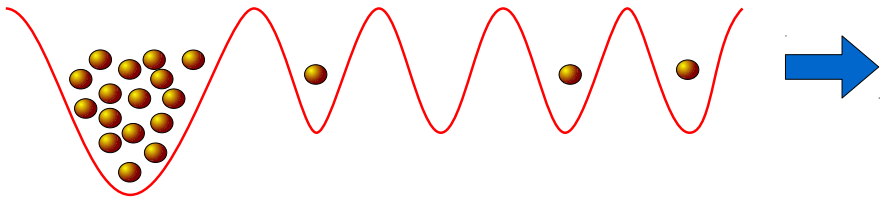

Figure 5.12: An illustration of an atomtronic wire coupled to a BEC drive as well as the vacuum.

5.3.1 The BEC reservoir model

We model the non-interacting BEC as a classical drive, since its interaction with the system is coherent, and we treat it as part of the closed system. The system Hamiltonian is comprised of a Bose-Hubbard lattice model whose site q is coherently driven by the BEC. Under the rotating wave approximation, this is given by

$$\hat{H}_S = \hbar\Omega_B \left(\hat{a}_q^\dagger \mathrm{e}^{-i\omega_B t} + \hat{a}_q \mathrm{e}^{i\omega_B t}\right) + \sum_j \hbar\omega_j \hat{a}_j^\dagger \hat{a} + \frac{U}{2}\hat{a}_j^\dagger \hat{a}_j^\dagger \hat{a}_j \hat{a}_j - J\left(\hat{a}_j^\dagger \hat{a}_{j+1} + \hat{a}_j \hat{a}_{j+1}^\dagger\right) \tag{5.41}$$

where Ω_B and $\hbar\omega_B$ are the coupling strength and ground state energy of the BEC coupled to the system, ω_j is the trap frequency of lattice site j, and U and J are the the on-site interaction and tunneling energies, and are assumed here to be uniform and real.

The time-dependence of $\hat{H}_S$ can be eliminated by transforming to an interaction picture that rotates with the BEC frequency ω_B yielding

$$\tilde{H}_s = \hbar\Omega_B \left(\hat{a}_q^\dagger + \hat{a}_q\right) + \sum_j \left(\hbar\omega_j - \omega_B\right) \hat{a}_j^\dagger \hat{a} + \frac{U}{2}\hat{a}_j^\dagger \hat{a}_j^\dagger \hat{a}_j \hat{a}_j - J\left(\hat{a}_j^\dagger \hat{a}_{j+1} + \hat{a}_j \hat{a}_{j+1}^\dagger\right). \tag{5.42}$$

When the lattice site l is coupled to the zero temperature vacuum, the master equation for this open quantum system becomes

$$\frac{d\hat{\rho}_S}{dt} = -\frac{i}{\hbar}[\tilde{H}_S, \hat{\rho}_S] - \frac{\Gamma_0}{2}\left(\hat{a}_l^\dagger \hat{a}_l \hat{\rho}_S + \hat{\rho}_S \hat{a}_l^\dagger \hat{a}_l - 2\hat{a}_l \hat{\rho}_S \hat{a}_l^\dagger\right) \tag{5.43}$$

where Γ_0 is the standard system-reservoir decay rate.

5.3.2 The BEC-driven atomtronic diode

Here we use Equation (5.43) to examine the current characteristics of an optical lattice in the diode configuration. Assuming $\hbar\omega_2 = \hbar\omega_1 + U$, coupling the BEC to site 1 and the vacuum to site 2 would drive the system in the forward-bias direction. Conversely, coupling the BEC and vacuum modes to 2 and 1 respectively drives the system in the reverse-bias direction. Taking $\hbar\Omega_B/U = 0.4$, $J/U = 3 \times 10^{-2}$, and $\hbar\Gamma_0/U = 10^{-2}$, we plot the expectation value of the forward-bias current, the reverse-bias current, and the current asymmetry as a function of the BEC frequency in Figure 5.13.

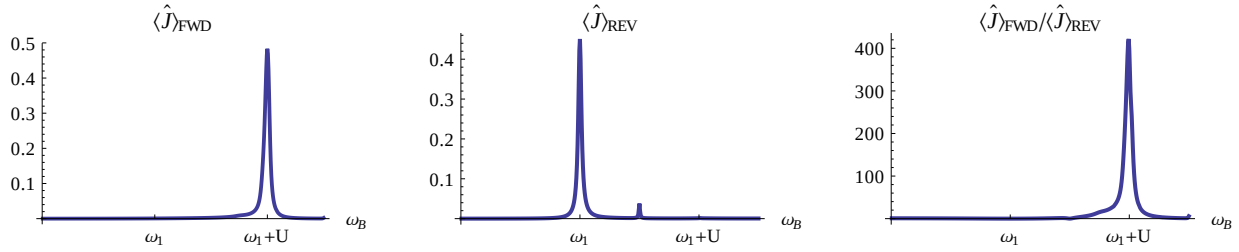

Figure 5.13: The current response of the BEC-driven diode in the (a) forward-bias configuration and (b) reverse-bias configuration (in arbitrary units). (c) The asymmetric current response of the system.

We first note the resonant nature of the current response in the forward-bias direction, where the maximal current peaks at the resonance condition $\bar{\omega}_B = \hbar\omega_1 + U$. The reverse-bias current has a resonant peak at $\omega_B = \omega_1$. This is a second-order, off-resonant process since the BEC in this case is resonant with the first site frequency. For the chosen parameter set, we achieve a maximum asymmetric current response of $\langle\hat{J}\rangle_{\rm FWD}/\langle\hat{J}\rangle_{\rm REV} \simeq 420$. An analysis of the Fock state populations for the forward-bias and reverse-bias system driven by a BEC characterized by a frequency $\hbar\omega_B = \hbar\omega_1 + U$ also confirms that the dynamics are in general agreement with the given physical interpretation.

Performing the same signal-to-noise ratio implemented in Section 5.2.2.1, and assuming $U/\hbar \sim 10^3$ Hz, we obtain

$$R_{\rm SN}(t) \simeq 18\sqrt{\rm Hz}\sqrt{t} \tag{5.44}$$

for the long-time-averaged behavior. This implies that a signal-to-noise ratio of 10 can be achieved by time-averaging for $\simeq$ 300 ms, and a ratio of 18 by time-averaging for one second. Since the upper limit on the lifetime of a BEC experiment is on the order of a second, we anticipate that the diode behavior should be observable and resolvable in an experiment.

5.4 Conclusion

In this chapter, we applied the mathematical tools that we developed in the previous chapters to fabricate theoretically optical lattice atomtronics systems in an open quantum system setting. In this novel approach to atomtronics, the coupling of multiple reservoirs with different chemical potentials induced an atomic current across the optical lattice in question. After deriving the system current operator, we introduced a strongly-interacting boson reservoir model. With this model, we studied a variety of highly-customized optical lattices. In doing so, we were able to recover the electronic-like behavior of a semiconductor diode, FET, and BJT in these systems. A SNR analysis was performed for the atomtronic diode using the quantum regression theorem where we concluded that an SNR of ~ 10 should be achievable by time-averaging the current for about one second. This implied that the functionality of the diode should be observable given the current state of experiments in this field. Afterwords, we demonstrated that these components could be used to build basic logic structures such as the AND gate.

We then implemented a weakly-interacting boson reservoir model, where the optical lattice is driven by a coherent BEC. The resonant nature of the BEC interacting with the system led to resonant responses in the current dynamics. Applying this reservoir model to the atomtronic diode, we were able to recover an asymmetric response. However, the resonant response was a sharp feature peaked about the resonance condition. The SNR of the BEC-driven diode at its maximal current response was larger by a factor of two when compared to the strongly-interacting reservoir model.

Chapter 6

Time-Dependent Open Quantum Systems

In the previous chapter, we demonstrated how the steady-state behavior of diodes and transistors can be realized utilizing atoms in optical lattices. Following the development of traditional electronics, we were able to recover elementary logic gates from the atomtronic transistors. We illustrated the AND gate in the last chapter. By similar simulations, we have also verified the behavior of the NOT, OR and NAND gates in optical lattice systems. From an electronics standpoint, the verification of these devices ends the discussion of steady-state, or combinatorial, logic behavior since, in principle, any universal computation can be constructed out of NAND and NOR gates alone. The next level of complexity in electronic circuitry involves the sequential logic components. These are pulse-driven devices that add the potential for memory and storage of information.

Similar to the NAND and NOR gates in combinatorial logic, an SR flip-flop is a fundamental building block for all sequential logic circuits. This device can be utilized as a memory element, where a bit of information can be stored or cleared. It is a four port device with inputs S, R and outputs Q, $\bar{Q}$. This device is a pulse-driven, as opposed to a steady-state, device. Its basic function is to set a signal Q by sending an electronic pulse through the S channel. This stored signal can then be reset by sending an electronic pulse through R, which changes the signal from Q to $\bar{Q}$. The truth table for a set-reset device is provided in Table 6.1. The functionality of this device crucially relies on the hysteresis behavior that when both S and R are on at the same time, the final state remains as it was before and is thus nondeterministic. That is, $S = 1$, $R = 1$ has two valid solutions where the state can either be Q or $\bar{Q}$. The specific solution depends on the condition of the system

SR Flip Flop Truth Table					
State	S	R	Q	$\bar{Q}$	Action
Set	1	0	1	0	Set
	1	1	1	0	No change
Reset	0	1	0	1	Reset
	1	1	0	1	No change
Invalid	0	0	$\times$	$\times$	$\times$

Table 6.1: The truth table for the SR flip-flop. This device, which exhibits a bistability for $s = 1$ and $R = 1$, is capable of storing state information.

before S and R were simultaneously on. The overview of the SR flip-flop makes clear important role that bistabilities play in the functionality of this class of devices. Investigating the bistable behavior of a cross-coupled transistor circuit reveals that the atomtronic analogs of this class of devices require effective atomic transport across off-resonant system junctions.

In this chapter, after discussing basic atomtronic bistable circuitry, we conclude our open quantum system treatment of atomtronics in optical lattices by demonstrating how effective atomic transport can be achieved across energy-shifted lattices by modulating the barrier in between sites. This topic makes extensive use of the time-dependent master equation formalism described in Section 3.4.

6.1 Bistable circuitry

In order to understand and develop a synchronous device that functions like a flip-flop, we first need to consider the role that bistabilities play in atomtronic circuits. In this section, we initiate the study of bistable atomtronic circuitry. The goal of this work is to ultimately construct and simulate the SR flip-flop.

The bistable circuit we study here is a cross-coupled transistor circuit illustrated in Figure 6.1(a). This circuit is a two input, two output device. When current simultaneously drives both inputs, the system responds with one of two steady-state solutions: the current is measured either through output A, or output B. The atomtronics analog to this bistable circuit is illustrated in

Figure 6.1(b) where two driven atomtronic transistors are cross-coupled. A topologically-equivalent, simpler version of this bistable circuit is illustrated in Figure 6.1(c).

There is an overarching theme that goes along with all of the atomtronics components that we have developed thus far, but also encompasses the devices under consideration: atomic transport can either be facilitated, or halted, by the strategic placement of energetic resonances and mismatches. Immediately from this diagram we see a significant problem in the direct realization of this device using the same general approach as before, since it requires atomic transport by hopping between sites that are not degenerate in energy. It appears that our immediate problem in developing the flip-flop, and thus the problem of understanding the functionality of bistable circuits

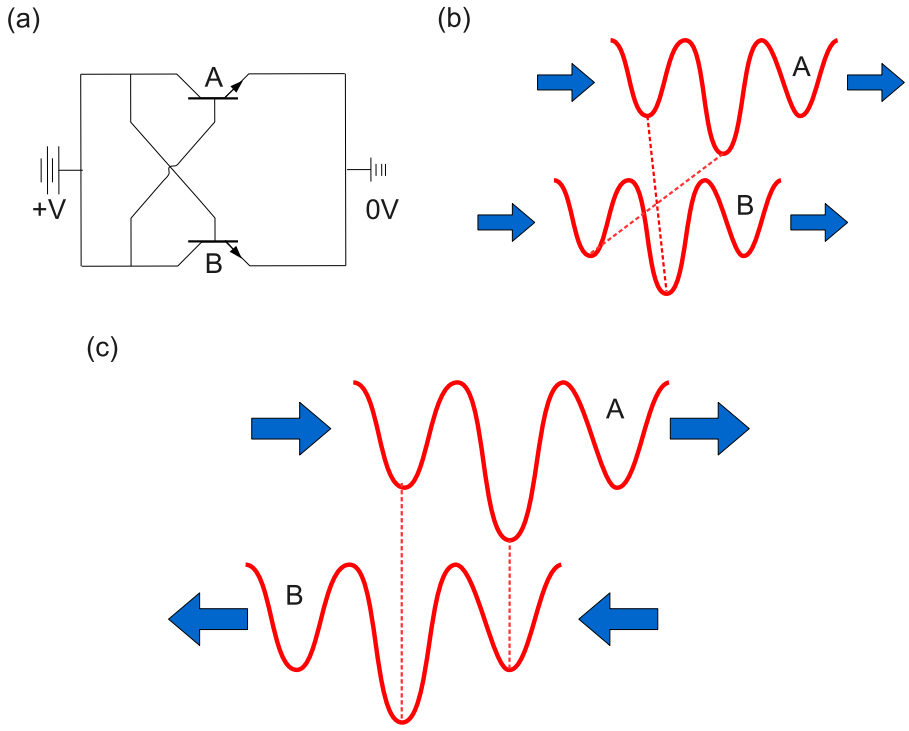

Figure 6.1: (a) Electronic schematic of a simple bistable circuit composed of two cross-coupled transistors. If the cross couplings are highly resistive (not shown here), then when current is introduced into the circuit, it either flows through transistor A or transistor B. (b) The equivalent atomtronics circuit bistable. Here, the dotted lines represent couplings between the two transistors. These couplings join together sites that are off-resonant. (c) A simpler, topologically-equivalent bistable circuit to that of (b).

is to resolve the question as to how one may obtain effective transport across non-resonant lattice sites. In the following section, we show that effective atomic transport across an energetically-offset lattice can be enhanced by modulating the tunneling barrier at the offset frequency difference.

6.2 Transport enhancement via tunneling barrier modulation

We can understand how atomic current can be enhanced across an off-resonant lattice by studying a simple double well system with infinite on-site repulsion. Infinite repulsion allows us to make the two-state approximation for the lattice site occupancy.

For a fixed complex tunneling rate J, a double well system exhibits a maximal current response when the site energies are the same, *i.e.* $\epsilon_1 = \epsilon_2 = \epsilon$. The Hamiltonian for this isolated quantum system is

$$\hat{H}_0 = \epsilon \hat{a}_1^\dagger \hat{a}_1 + \epsilon \hat{a}_2^\dagger \hat{a}_2 + J \hat{a}_1^\dagger \hat{a}_2 + J^* \hat{a}_1 \hat{a}_2^\dagger. \tag{6.1}$$

For a system with a frequency difference Δ between the two sites, the Hamiltonian is

$$\hat{H}_1 = \epsilon \hat{a}_1^\dagger \hat{a}_1 + (\epsilon + \hbar\Delta) \hat{a}_2^\dagger \hat{a}_2 + J \hat{a}_1^\dagger \hat{a}_2 + J^* \hat{a}_1 \hat{a}_2^\dagger. \tag{6.2}$$

If we transform this Hamiltonian into an interaction picture that rotates with $\hbar\Delta \hat{a}_2^\dagger \hat{a}_2$, then the interaction picture Hamiltonian is

$$\tilde{H}_1 = \epsilon \hat{a}_1^\dagger \hat{a}_1 + \epsilon \hat{a}_2^\dagger \hat{a}_2 + J \mathrm{e}^{-i\Delta t} \hat{a}_1^\dagger \hat{a}_2 + J^* \mathrm{e}^{i\Delta t} \hat{a}_1 \hat{a}_2^\dagger. \tag{6.3}$$

Now, if $J \to J\mathrm{e}^{i\Delta t}$, then

$$\tilde{H}_1 = \epsilon \hat{a}_1^\dagger \hat{a}_1 + \epsilon \hat{a}_2^\dagger \hat{a}_2 + J \hat{a}_1^\dagger \hat{a}_2 + J^* \hat{a}_1 \hat{a}_2^\dagger. \tag{6.4}$$

That is, modulating the tunneling rate J at the gap frequency Δ, makes $\tilde{H}_1 = \hat{H}_0$. Thus the effective transport of the gapped system will exhibit the same current response of the energetically-flat system if the barrier modulates at the gap frequency.

To verify this claim that modulating the barrier does, in fact, create the desired effect in an open quantum system setting, we derive the corresponding time-dependent master equation. We consider a reservoir which does not have any discontinuities that directly overlap with system

energy differences. In doing so, the standard Born-Markov rules apply. Recalling from Section 3.4 that the time-dependent master equation is

$$\begin{aligned}\frac{d\hat{\rho}_S}{dt} &= -i\hat{\mathscr{L}}_S(t)\hat{\rho}_S - \frac{1}{\hbar^2}\mathrm{Tr}_R\Bigg\{\int_0^\infty d\tau \\ &\quad\times\left[\hat{H}_V,\left[\mathrm{e}^{i\mathrm{T}\int_t^{t-\tau}\hat{H}_S(t_1)dt_1/\hbar}\mathrm{e}^{-i\hat{H}_R\tau/\hbar}\hat{H}_V\mathrm{e}^{-i\mathrm{T}\int_t^{t-\tau}\hat{H}_S(t_1)dt_1/\hbar}\mathrm{e}^{-i\hat{H}_R\tau/\hbar},\hat{\rho}_R\hat{\rho}_S(t)\right]\right]\Bigg\}.\end{aligned} \tag{6.5}$$

Due to the fact that the mathematical operations on all of the terms in the memory kernel are the same, and the similarity of these operations to those performed in Section 5.2, we go through a single term here at an accelerated pace.

Assuming the interaction Hamiltonian that couples a reservoir to system lattice site q is

$$\hat{H}_V = \hbar\sum_k(g_k\hat{a}_q^\dagger\hat{R}_k + g_k^*\hat{a}_q\hat{R}_k^\dagger), \tag{6.6}$$

we examine the term,

$$\int_0^\infty d\tau\mathrm{Tr}_R\left\{\sum_k|g_k|^2\hat{R}_k^\dagger\mathrm{e}^{-i\hat{H}_R\tau/\hbar}\hat{R}_k\mathrm{e}^{i\hat{H}_R\tau/\hbar}\hat{\rho}_R\right\}\hat{a}_q\mathrm{e}^{i\mathrm{T}\int_t^{t-\tau}\hat{H}_S(t_1)dt_1/\hbar}\hat{a}_q^\dagger\mathrm{e}^{-i\mathrm{T}\int_t^{t-\tau}\hat{H}_S(t_1)dt_1/\hbar}\hat{\rho}_s. \tag{6.7}$$

Momentarily shifting our focus to the trace,

$$\begin{aligned}
\mathrm{Tr}_R\left\{\sum_k |g_k|^2 \hat{R}_k^\dagger \mathrm{e}^{-i\hat{H}_R\tau/\hbar}\hat{R}_k \mathrm{e}^{i\hat{H}_R\tau/\hbar}\hat{\rho}_R\right\} &= \sum_k |g_k|^2 \langle \hat{R}_k^\dagger \hat{R}_k \mathrm{e}^{-i\hat{H}_R\tau/\hbar}\hat{R}_k \mathrm{e}^{i\hat{H}_R\tau/\hbar}\rangle \\
&= \sum_k |g_k|^2 \langle \hat{R}_k^\dagger \hat{R}_k\rangle \mathrm{e}^{i\bar{\omega}_k\tau} \\
&\simeq \lim_{\epsilon\longrightarrow 0} |g(\bar{\omega}_0)|^2 \mathscr{D}(\bar{\omega}_0)\int_0^\infty \mathrm{e}^{i\bar{\omega}\tau-\epsilon\tau}d\bar{\omega} \\
&= 2\pi|g(\bar{\omega}_0)|^2\mathscr{D}(\bar{\omega}_0)\delta(\tau) \\
&= \Gamma\delta(\tau) \qquad (6.8)
\end{aligned}$$

where $\mathscr{D}(\bar{\omega}_0)$ is the density of states and $|g(\bar{\omega}_0)|$ is the system-reservoir coupling. Both are taken to be constant about the system transition frequencies. Here we have taken ω_μ to be much larger than the system transition frequencies. Putting this back in equation (6.7), we get

$$\begin{aligned}
\Gamma\int_0^\infty d\tau\delta(\tau)\hat{a}_q \mathrm{e}^{i\mathrm{T}\int_t^{t-\tau}\hat{H}_S(t_1)dt_1}\hat{a}_q^\dagger \mathrm{e}^{-i\mathrm{T}\int_t^{t-\tau}\hat{H}_S(t_1)dt_1}\hat{\rho}_s &= \frac{\Gamma}{2}\hat{a}_q \mathrm{e}^{i\mathrm{T}\int_t^{t}\hat{H}_S(t_1)dt_1}\hat{a}_q^\dagger \mathrm{e}^{-i\mathrm{T}\int_t^{t}\hat{H}_S(t_1)dt_1}\hat{\rho}_s \\
&= \frac{\Gamma}{2}\hat{a}_q\hat{a}_q^\dagger\hat{\rho}_s. \qquad (6.9)
\end{aligned}$$

That is, under the Markov approximation, the time-ordered unitary operators become unity. This is due to the fact that in the Markovian limit, the memory kernel is effectively delta-correlated. Thus, it is guaranteed to decay on a much more rapid timescale than the system. As a result, despite the fact that there is a time-dependence in the system Hamiltonian, the memory kernel remains time-independent. Thus, the master equation for a time-dependent two-site lattice, where site 1 is being driven by an atomic reservoir and site 2 is coupled to the zero temperature vacuum is

$$\frac{d\hat{\rho}_S}{dt} = -\frac{i}{\hbar}[\hat{H}_S(t),\hat{\rho}_S] - \frac{\Gamma_1}{2}(\hat{a}_1\hat{a}_1^\dagger\hat{\rho}_S + \hat{\rho}_S\hat{a}_1\hat{a}_1^\dagger - 2\hat{a}_1^\dagger\hat{\rho}_S\hat{a}_1) - \frac{\Gamma_2}{2}(\hat{a}_2^\dagger\hat{a}_2\hat{\rho}_S + \hat{\rho}_S\hat{a}_2^\dagger\hat{a}_2 - 2\hat{a}_2\hat{\rho}_S\hat{a}_2^\dagger) \quad (6.10)$$

where

$$\frac{\hat{H}_S(t)}{\hbar} = \omega_1\hat{a}_1^\dagger\hat{a}_1 + \omega_2\hat{a}_2^\dagger\hat{a}_2 + J\mathrm{e}^{i\delta t}\hat{a}_1^\dagger\hat{a}_2 + J\mathrm{e}^{i\delta t}\hat{a}_1\hat{a}_2^\dagger. \qquad (6.11)$$

We solve equation (6.10) numerically, propagating $\hat{\rho}_S(t)$ as a function of time. To show that the full solutions are, in fact, identical, we plot the populations of the four states of the system ($|00\rangle$, $|01\rangle$, $|10\rangle$, and $|11\rangle$) as a function of time. Figures 6.2(a-c) are plots of the populations

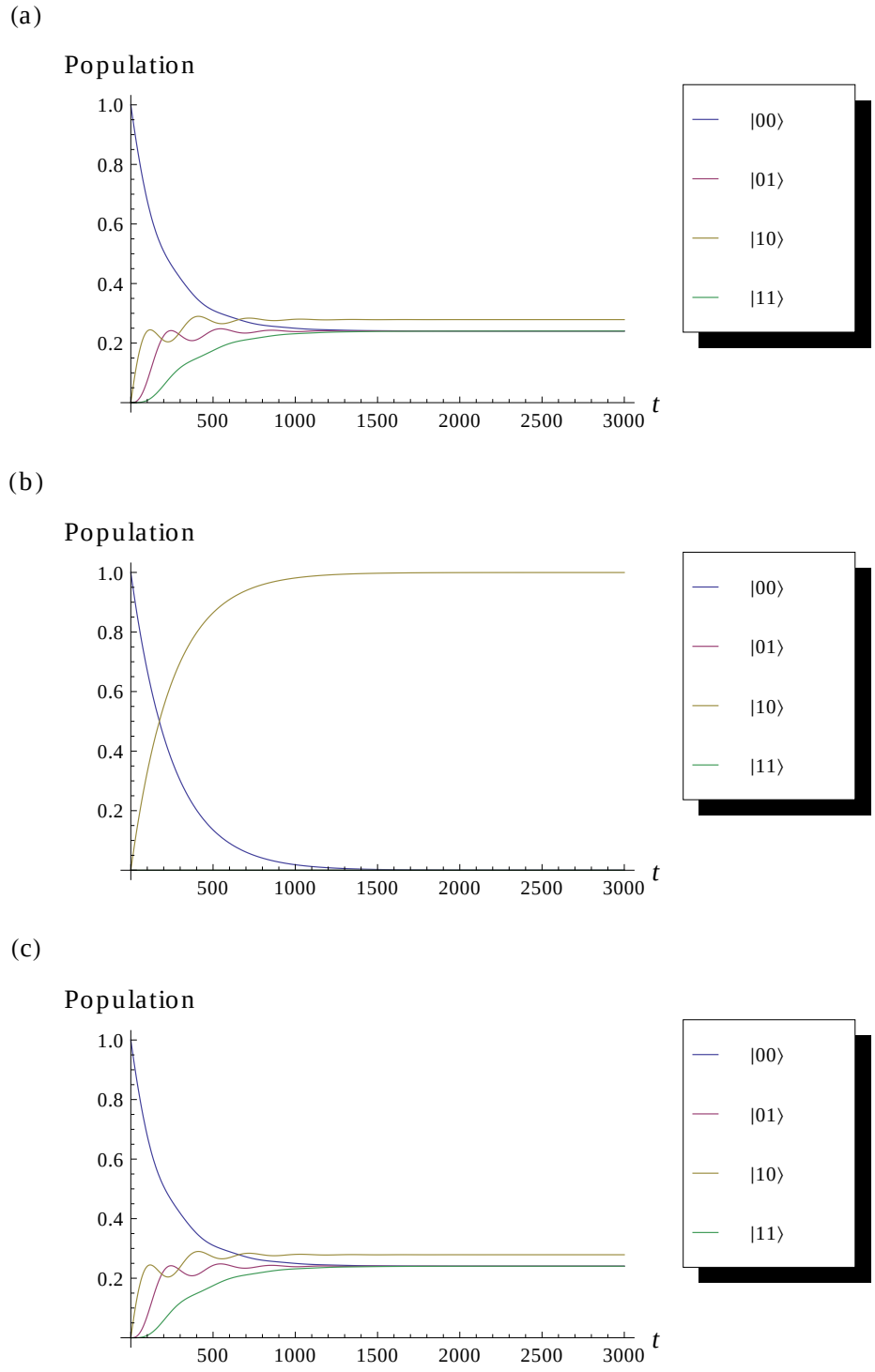

Figure 6.2: Numerical verification that oscillating an off resonant junction at the gap frequency enhances the effective transport. (a) Population as a function of time for a flat, two-site lattice. (b) Population as a function of time for a two-site lattice with zero-point frequencies ω_1 and $\omega_2 + \Delta$. (c) Population as a function of time for the two-site lattice defined in (b), but with a tunneling rate that oscillates at frequency Δ. The evolution of the gapped, oscillatory system (c) is identical to the evolution of the flat, stationary lattice (a). As a result, current flows through the systems modeled in (a) and (c) in the exact same manner.

of the system's four Fock states as a function of time (in arbitrary units). Figure 6.2(a) tracks the populations for the case where $\omega_1 = \omega_2$ with $\delta = 0$, *i.e.* the resonant lattice with constant J. The system starts in the initial Fock state $|00\rangle$ and decays to a specific mixture of all four states. The current is proportional to the average number of atoms on the right lattice site. Here $\langle N_2 \rangle \simeq 0.48$. Figure 6.2(b) are plots of the system populations given $\omega_2 = \omega_2 + \Delta$ with $\delta = 0$ (the off-resonant lattice with constant J) starting with the same initial condition. Here the system relaxes predominantly to the $|10\rangle$ state. The average number occupancy $\langle N_2 \rangle \simeq 0.0002$ confirms that atomic transport across is significantly reduced in the off-resonant lattice system. Figure 6.2(c) are plots of the system Fock states given $\omega_2 = \omega_1 + \Delta$ with $\delta = \Delta$ (the off-resonant lattice, gap-modulated J). Here the evolutions of the populations are identical to the evolutions in Figure 6.2(a). As a result, $\langle N_2 \rangle$ calculated here is identical to $\langle N_2 \rangle$ when $\Delta = \delta = 0$.

Therefore, we conclude that effective transport can be achieved through intra-system off-resonant junctions by modulating the corresponding barrier at the gap frequency.

6.3 Conclusion

In this chapter we reviewed classical sequential logic behavior and discussed the importance of bistabilities in these systems. Realizing such behavior in an optical lattice requires effective transport across off-resonant junctions. Using the time-dependent master equation formalism, we demonstrated how modulating the tunneling barrier at a frequency corresponding to the energy difference allows for effective transport in a well system with an energy gap.

Chapter 7

Atomtronics with Photons in Optical Cavities

Now we discuss the possible realization of atomtronics components in an entirely different physical system—photons in nonlinear cavities. This nonlinear optical system, illustrated in Figure 7.1, has a few significant advantages over the neutral atom counterpart. First, a 'current' signal comprised of photons tunneling through nonlinear cavity networks can be many orders of magnitude faster than an atomic current tunneling through optical lattice barriers [69]. The faster dynamics allow for a respectable signal-to-noise ratio to be achieved in a much shorter time interval. Second, the site-by-site optical lattice systems proposed in the previous two chapters are difficult to realize experimentally; at the moment, there are only a handful of labs in the world that are able to precisely construct and manipulate the lattices needed to realize the proposed devices. In contrast, coupled cavity arrays could potentially be easier to independently fabricate. Finally, from a practical device standpoint, photons can travel through optical networks with less dissipation, scattering, and thermal loss than is possible with their electronic counterparts. Consequently, these

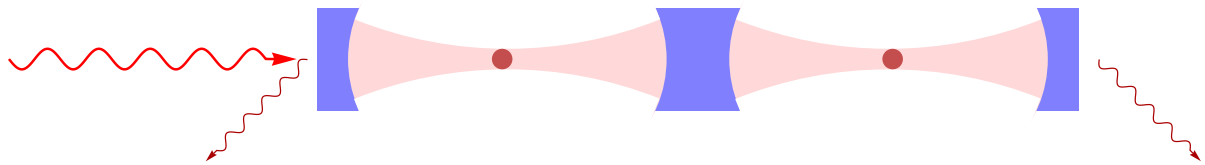

Figure 7.1: Illustration of a driven nonlinear coupled cavity array coupled to the environment at both ends.

devices could potentially find application in optical computing and signal processing.

As demonstrated in Section 2.2.4, recovering the dynamics of the atomtronic systems in an optical framework is possible when a $\chi^{(3)}$ nonlinear material is introduced to the cavities. In a second quantized form, the nonlinear cavity network represents an alternative realization of the Bose-Hubbard model. With that in mind, and derived from our results for the atomtronic systems, these systems will only recover the desired current dynamics if they are capable of physically supporting the parameter regime where $U \gg J, \hbar\Gamma$.

We begin this chapter by presenting our model system driven by a continuous wave (CW) laser, as well as a stochastic pulse laser. The system responses to these two driving mechanisms are then explored through numerical experiments. From these experiments, we locate parameter regimes where the system exhibits large asymmetric current responses. Afterwords, we review possible experimental implementations of the atomtronics diode in coupled high Q etalon cavities, toroidal microcavities, and photonic bandgap nanocavities.

7.1 Driving the few-photon optical diode

If the coupled cavity system is driven by a continuous wave (CW) laser, the driving field can be treated classically. For driving frequency ω_L, and under the rotating wave approximation, the Hamiltonian for a system whose cavity q is coherently driven is

$$\hat{H}_S = \sum_j^N \hbar\omega_j \hat{a}_j^\dagger \hat{a}_j + \frac{U_j}{2}\hat{a}_j^\dagger \hat{a}_j^\dagger \hat{a}_j \hat{a}_j + \sum_{\langle j,k\rangle} J_{jk}\hat{a}_j^\dagger \hat{a}_k + J_{jk}^* \hat{a}_j \hat{a}_k^\dagger + \hbar\Omega_L \left(\hat{a}_q^\dagger \mathrm{e}^{-i\omega_L t} + \hat{a}_q \mathrm{e}^{i\omega_L t}\right), \tag{7.1}$$

Transforming into an interaction picture that rotates with the driving field, a transformation defined by the unitary operator

$$\hat{U}(t) = \mathrm{e}^{-i\sum_j \omega_L \hat{a}_j^\dagger \hat{a}_j t} \tag{7.2}$$

yields

$$\tilde{H}_S = \sum_j^N \hbar(\omega_j - \omega_L)\hat{a}_j^\dagger \hat{a}_j + \frac{U_j}{2}\hat{a}_j^\dagger \hat{a}_j^\dagger \hat{a}_j \hat{a}_j + \sum_{\langle j,k\rangle} J_{jk}\hat{a}_j^\dagger \hat{a}_k + J_{jk}^* \hat{a}_j \hat{a}_k^\dagger + \hbar\Omega_L \left(\hat{a}_q^\dagger + \hat{a}_q\right), \tag{7.3}$$

which is a simpler equation to solve numerically.

In addition to the continuous wave laser drive, a system under the influence of a series of random laser pulses can be modeled by substituting

$$\Omega_L \rightarrow \Omega_L(t) = \Omega_0 \sum_j \theta(t-t_j)\mathrm{e}^{-\xi(t-t_j)} \tag{7.4}$$

where ξ is the uniform pulse width, Ω_0 is the pulse strength, $\theta(t-t_j)$ is the Heaviside function centered at t_j, and the pulses are assumed have a Poissonian spectrum with pulse number density $N/T = \lambda$, where T defines the time-averaging of the classical correlation function. For this stochastic drive, the classical field-field correlation function is

$$\begin{aligned}\langle E^*(\tau)E(0)\rangle &= \frac{1}{T}\int_0^T dt E^*(\tau+t)E(t) \\ &\propto \Omega_0^2\frac{1}{T}\sum_{j,k}^{N}\int_0^T dt\theta(t+\tau-t_j)\theta(t-t_k).\end{aligned} \tag{7.5}$$

Assuming that $\xi \gg \lambda$,

$$\begin{aligned}\langle E^*(\tau)E(0)\rangle &\propto \theta(t-t_k)\mathrm{e}^{-\xi(\tau+2t-t_j-t_k)} \\ &= \Omega_0^2\frac{1}{T}\sum_{k=1}^{N}\mathrm{e}^{-\xi\tau}\int_0^{T-t_k} dt\mathrm{e}^{-2\xi t} \\ &= \Omega_0^2\frac{1}{T}\frac{1}{2\xi}\sum_{k=1}^{N}\mathrm{e}^{-\xi\tau}\left[1-\mathrm{e}^{-2\xi(T-t_k)}\right]\end{aligned} \tag{7.6}$$

In the limit that $T \rightarrow \infty$,

$$\langle E^*(\tau)E(0)\rangle \propto \frac{\Omega_0^2\lambda}{2\xi}\mathrm{e}^{-\xi\tau}. \tag{7.7}$$

This also happens to be the classical correlation function for coherent drives undergoing phase diffusion [51] as well as other stationary Markov processes such as Gaussian amplitude fluctuations [70]. Thus, the stochastic pulse drive model encompasses the physics of a larger class of driving fields.

7.2 Theoretical prediction of the photon diode

From equation (7.3), the forward-biased coherently driven system Hamiltonian for the optical diode is

$$\begin{aligned}\tilde{H}_S &= \hbar(\omega_1-\omega_L)\hat{a}_1^\dagger\hat{a}_1 + (\hbar\omega_1+U-\hbar\omega_L)\hat{a}_2^\dagger\hat{a}_2 + \frac{U}{2}\left(\hat{a}_1^\dagger\hat{a}_1^\dagger\hat{a}_1\hat{a}_1 + \hat{a}_2^\dagger\hat{a}_2^\dagger\hat{a}_2\hat{a}_2\right) \\ &\quad + J\left(\hat{a}_1^\dagger\hat{a}_2 + \hat{a}_1\hat{a}_2^\dagger\right) + \hbar\Omega_L\left(\hat{a}_1^\dagger + \hat{a}_1\right),\end{aligned} \tag{7.8}$$

where ω_1 is the frequency of cavity 1, $\omega_2 = \omega_1 + U/\hbar$ is the frequency of cavity 2, U is the effective photon-photon interaction energy, taken to be the same for the two cavities, J is the tunneling rate between cavities and Ω_L is the Rabi frequency of the laser driving cavity 1. The reverse bias Hamiltonian is the same, except with the laser coupled to cavity 2, *i.e.*

$$\begin{aligned}\tilde{H}_S &= \hbar(\omega_1 - \omega_L)\hat{a}_1^\dagger\hat{a}_1 + (\hbar\omega_1 + U - \hbar\omega_L)\hat{a}_2^\dagger\hat{a}_2 + \frac{U}{2}\left(\hat{a}_1^\dagger\hat{a}_1^\dagger\hat{a}_1\hat{a}_1 + \hat{a}_2^\dagger\hat{a}_2^\dagger\hat{a}_2\hat{a}_2\right) \\ &\quad + J\left(\hat{a}_1^\dagger\hat{a}_2 + \hat{a}_1\hat{a}_2^\dagger\right) + \hbar\Omega_L\left(\hat{a}_2^\dagger + \hat{a}_2\right). \end{aligned} \tag{7.9}$$

We use the Fock state notation $|n, m\rangle$ to denote n photons in the left cavity and m photons in the right, so that the analysis runs parallel to our previous discussions of the atomtronic diode.

In our model, we couple both ends of the cavity array to a broad continuum of zero-temperature vacuum modes. Since there are no discontinuities in the reservoir structure, we can employ the standard Born-Markov result. The equation of motion for the reduced density operator of the system is then

$$\frac{d\hat{\rho}_S}{dt} = -\frac{i}{\hbar}\left[\tilde{H}_S, \hat{\rho}_S\right] - \frac{\Gamma_1}{2}\left(\hat{a}_1^\dagger\hat{a}_1\hat{\rho}_S + \hat{\rho}_s\hat{a}_1^\dagger\hat{a}_1 - 2\hat{a}_1^\dagger\hat{\rho}_S\hat{a}_1\right) - \frac{\Gamma_2}{2}\left(\hat{a}_2^\dagger\hat{a}_2\hat{\rho}_S + \hat{\rho}_s\hat{a}_2^\dagger\hat{a}_2 - 2\hat{a}_2^\dagger\hat{\rho}_S\hat{a}_2\right) \tag{7.10}$$

where $\Gamma_{1,2}$ are the decay rates out of cavities 1 and 2.

Below we present simulations of this Hamiltonian. We calculate the occupancy of site 2 for the forward-bias and reverse-bias driven Hamiltonians as a function of the drive frequency and amplitude. It is sufficient to calculate the occupancy of site 2 in order to characterize the system's current response since the current out of the system is directly proportional to this value. The ratio of forward-bias to reverse-bias site occupancies is then equal to the system's asymmetric current response. For the constant drive we perform the steady-state analysis laid out in appendix A. The asymmetry turns out to be fairly sensitive to both the drive frequency and strength. Therefore, in order to find the maximum asymmetric device response, we generate a surface plot of the system's response as a function of the driving laser's frequency and strength.

The data for the first numerical experiment in this series is displayed in Figure 7.2 and uses parameters $\hbar\Gamma_1 = \hbar\Gamma_2 = J = 10^{-2}U$, which satisfy $U \gg J, \hbar\Gamma$. Figure 7.2(a) shows the system's

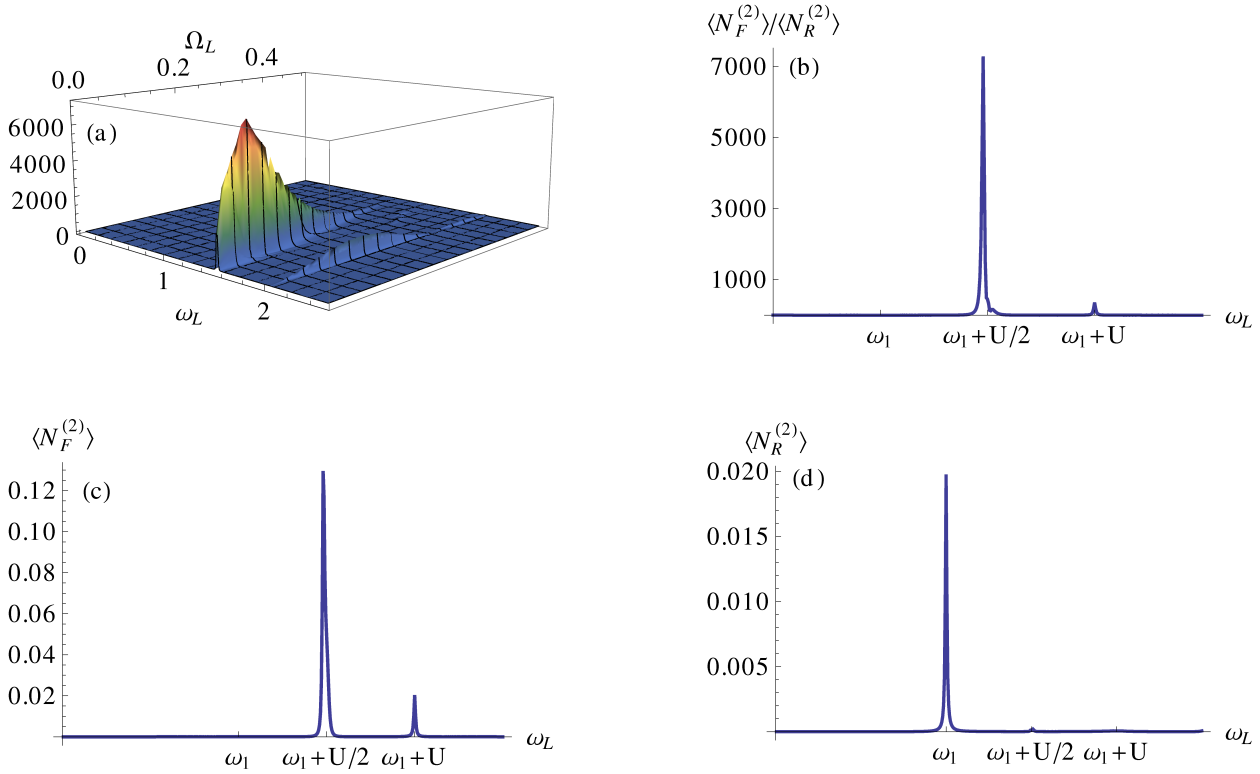

Figure 7.2: Here we find the maximum asymmetric current response for the few-photon optical diode under a CW laser drive assuming $\hbar\Gamma_1 = \hbar\Gamma_2 = J = 10^{-2}U$. (a) A surface plot of the current asymmetry as a function of ω_L and Ω. The current response is nonlinear with respect to both parameters, but the surface plot allows us to find a parameter set that generates an asymmetric current response of over 7000 for these parameters. Using the optimal choice of ω_c, we plot (b) the asymmetric response as a function of ω_L, the average number occupancy of site 2 in the (c) forward-bias direction and (d) reverse-bias direction.

asymmetric response as a function of the drive strength and frequency. This graph shows a nonlinear response of the $\langle N_2\rangle$ as a function of both ω_L, and Ω_L. Figures 7.2(b-d) show the asymmetric, forward-bias, and reverse-bias responses as a function of drive frequency for $\Omega_L \simeq 0.07U/\hbar$, the value of the drive strength that yields the maximal asymmetry. An interesting feature in Figures 7.2(b-c) is the location of the resonance response.

There is a dwarfed peak at $\omega = \omega_1 + U/\hbar$. This peak is small due to the fact that the drive is solely resonant with the $|1,0\rangle \rightarrow |2,0\rangle$ transition. If the system is initially empty however, the $|0,0\rangle \rightarrow |1,0\rangle$ transition is necessarily off-resonant to the drive field. An analysis of the Fock state population reveals that for $\Omega_L = \omega_1 + U/\hbar$, there is virtually no population in the $|2,0\rangle$, and $|1,1\rangle$

sites; the population is mainly found in the $|0,0\rangle$ and $|0,1\rangle$ states. This implies that the asymmetric response for this driving frequency is actually due to a second-order, off-resonant transition where the drive field finds itself resonant with the $|0,1\rangle$ state.

There is a comparably much larger response that occurs at $\omega_L = \omega_1 + U/(2\hbar)$. This is exactly half the energy needed for two photons to excite the system. When the system is driven at this two-photon transition, the Fock state analysis confirms that the system is being excited into the two-photon manifold with nonnegligible occupancies of states $|2,0\rangle$ and $|1,1\rangle$. Thus the asymmetric current characteristic in this case is due to a similar mechanism to that responsible for the atomtronic diode to operate. The maximal asymmetric response observed in this system is

$$\frac{\langle \hat{I}_{FWD} \rangle}{\langle \hat{I}_{REV} \rangle} \simeq 7.2 \times 10^3. \tag{7.11}$$

This value improves as U is increased and J is decreased, since both actions suppress second order tunneling events.

For the next numerical experiment presented in Figure 7.3, we use the parameters $\hbar\Gamma_1 = \hbar\Gamma_2 = 5 \times 10^{-2}U$, and $J = 10^{-2}U$. As seen in these plots, the greater cavity decay rate (or smaller cavity finesse) yields similar features, with an asymmetric value of

$$\frac{\langle \hat{I}_{FWD} \rangle}{\langle \hat{I}_{REV} \rangle} \simeq 4.5 \times 10^2, \tag{7.12}$$

i.e. more than an order of magnitude less. The reduction in overall cavity finesse can be interpreted to cause more photons to leak out of cavity 1 before they have the opportunity to tunnel into cavity 2, from where they can be lost and contribute to the photon current. Thus the current value that we measure here is less in magnitude than the earlier case.

Finally, we investigate the system's response to a pulse drive. The results are illustrated in Figure 7.4 where we drive the system with a single pulse. As discussed in Section 7.1, this result models a low density chain of pulses, but could equally well represent a drive of constant intensity with phase diffusion, as well as a drive with amplitude fluctuations. Here the parameters we use are $\hbar\Gamma_1 = \hbar\Gamma_2 = J = 10^{-2}U$, with the pulse width $\hbar\eta = 2 \times 10^{-2}U$. Since the parameters are the

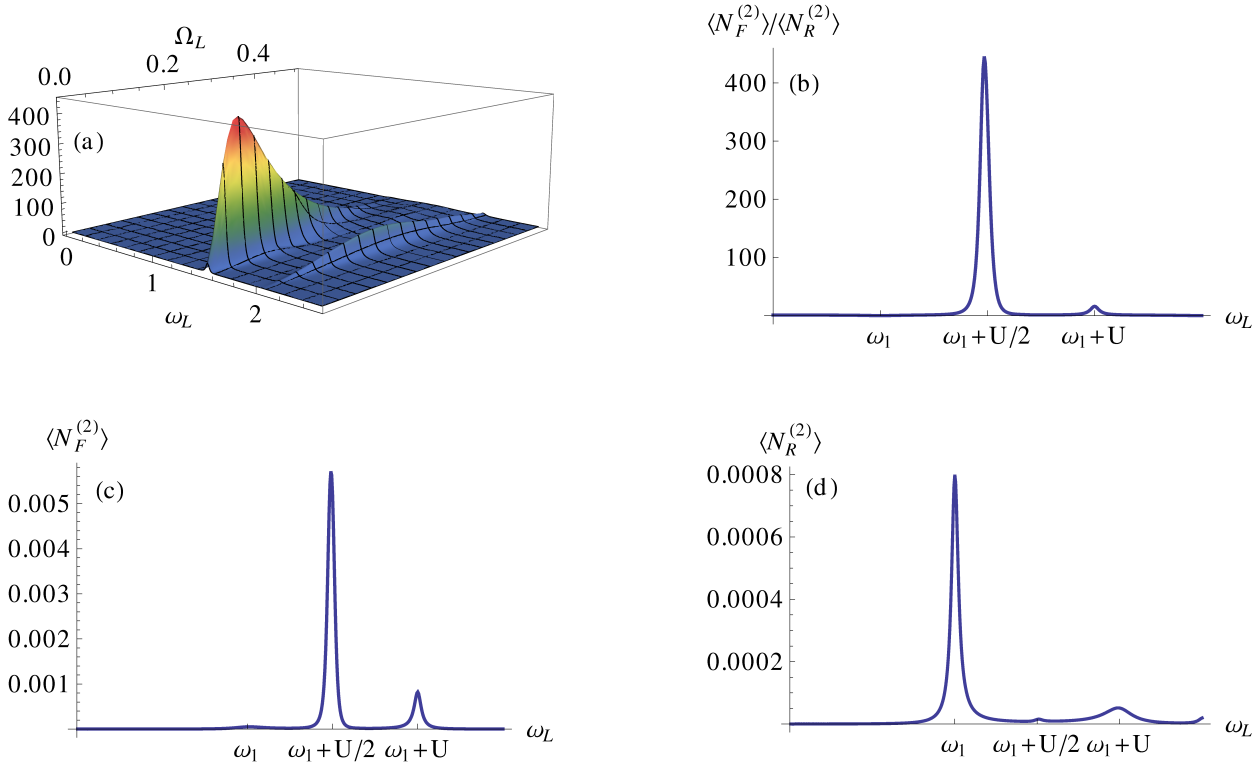

Figure 7.3: Here we find the maximum asymmetric current response for the few-photon optical diode under a CW laser drive assuming $\hbar\Gamma_1 = \hbar\Gamma_2 = 5U10^{-2}$, and $J = U10^{-2}$. (a) A surface plot of the current asymmetry as a function of ω_L and Ω. The current response is nonlinear with respect to both parameters, but the surface plot allows us to find a parameter set that generates an asymmetric current response is reduced from 7000 to ~ 450 due to the larger cavity decay rate. Using the optimal choice of ω_c, we plot (b) the asymmetric response as a function of ω_L, the average number occupancy of site 2 in the (c) forward-bias direction and (d) reverse-bias direction.

same as in the first numerical experiment, these results can be compared to those in the first set. As can be seen in Figure 7.4, the main effect of the pulse drive is a broadening of the response $\sim \xi$ at the expense of the overall magnitude of the asymmetry. Here the maximal current asymmetry is

$$\frac{\langle \hat{I}_{FWD}\rangle}{\langle \hat{I}_{REV}\rangle} \simeq 3 \times 10^3, \tag{7.13}$$

which is approximately half the value seen for the continuous laser drive earlier.

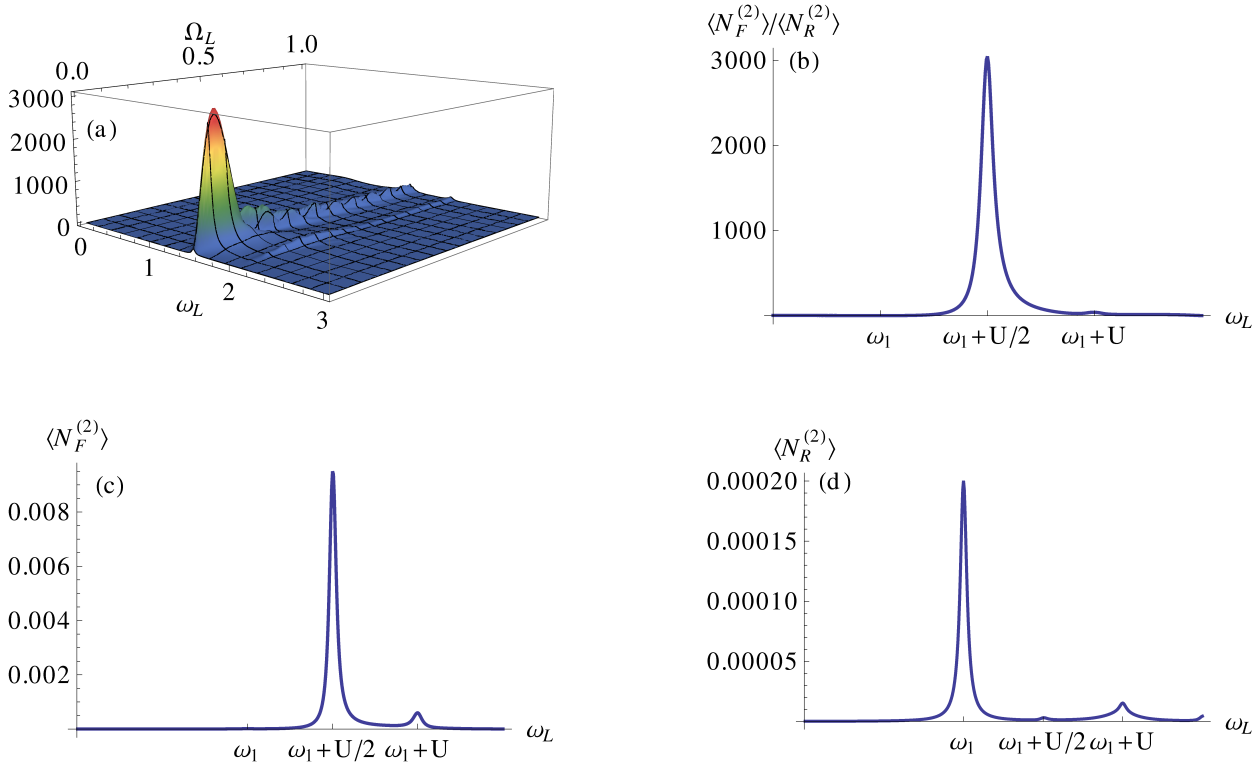

Figure 7.4: Here we find the maximum asymmetric current response for the few-photon optical diode under a pulsed laser drive assuming $\hbar\Gamma_1 = \hbar\Gamma_2 = J = U10^{-2}$. (a) A surface plot of the current asymmetry as a function of ω_L and Ω. The current response is nonlinear with respect to both parameters, but the surface plot allows us to find a parameter set that generates an asymmetric current response of $\simeq 3000$. Using the optimal choice of ω_c, we plot (b) the asymmetric response as a function of ω_L, the average number occupancy of site 2 in the (c) forward-bias direction and (d) reverse-bias direction.

7.3 Exploring experimental realizations of the photon diode

In this section we investigate specific possible realizations of our photon diode. We first consider experiments that involve single to many EIT atoms coupled to high finesse etalon cavities. Afterwords, we examine systems comprised of single EIT atoms coupled to toroidal microcavities. Finally, we conclude this section with a discussion of single quantum dot-doped photonic band-gap nanocavities. The advantages and shortcomings of each of these systems is discussed.

7.3.1 Single atom EIT cavity QED as a few photon diode

We can determine whether or not it is possible to realize the few-photon optical diode in an etalon cavity QED experiment involving a single EIT atom by checking if such systems support the parameter regime $J, \hbar\Gamma \ll U$. Here we take optimistic cavity QED parameters from Kampschulte *et al.* [71], where the cavity has a mode waist of $\mathrm{w}_0 = 23$ μm, a length of $l = 150$ μm, a finesse of $\mathcal{F} = 1.2 \times 10^6$, we also take (g, Γ, γ)=$2\pi(120, 40, 2.6)$ MHz, where g is the atom-field coupling, Γ is the decay rate of the cavity and γ is the decay rate of the atom.

From equation (2.88), the EIT generated Kerr nonlinearity is

$$U = -\hbar \frac{g_{24}^2}{\Delta} \left(\frac{g_{13}}{\Omega_c} \right)^2 . \tag{7.14}$$

Taking $(g_{13}/\Omega_c)^2 = 0.1$, which satisfies the validity conditions in equation (2.87) and assuming $\Delta \sim 10^9$ Hz, which is an approximate value for experiments using alkali atoms [55] , we see that

$$\frac{U}{\hbar} \simeq -\frac{g_{24}^2}{\Delta} 10^{-1} \sim 1\mathrm{MHz}. \tag{7.15}$$

Since this implies $\hbar\Gamma/U \sim 40$, which is far from $\hbar\Gamma \ll U$, it seems like the diode cannot be realized in such a cavity QED system. Reducing the length of the cavity may help, since it leads to a greater atom-cavity coupling term. Here we look at the ratio Γ/U in greater detail to see if that is the case. We first note that

$$\Gamma = \frac{\omega_{ax}}{\mathcal{F}} = \frac{2\pi c}{\lambda_{ax}\mathcal{F}} \sim \frac{2\pi c}{l\mathcal{F}} \tag{7.16}$$

where c is the speed of light, λ_{ax} is the wavelength of the axial mode and l is the length of the cavity. Noting that

$$\frac{|U|}{\hbar} \simeq 10^{-1} \frac{g_{24}^2}{\Delta} = \frac{\mu_{24}^2 \omega_0}{2\pi\epsilon_0 \hbar V \Delta} 10^{-1} \simeq \frac{\mu_{24}^2 \omega_0}{2\pi\epsilon_0 \hbar l \mathrm{w}_0^2 \Delta} 10^{-1}, \tag{7.17}$$

where μ_{24} is the dipole moment of the $|2\rangle \rightarrow |4\rangle$ transition,$V = l\mathrm{w}_0^2$ is the effective mode volume of the cavity ϵ_0 is the permittivity of free space, and ω_0 is the frequency resonant with the $|1\rangle \rightarrow |3\rangle$ atomic transition (in rad/sec). Therefore

$$\frac{\hbar\Gamma}{U} \sim (40\pi^2 \hbar c \epsilon_0) \left(\frac{\Delta}{\mu_{24}^2 \omega_0} \right) \left(\frac{\mathrm{w}_0^2}{\mathcal{F}} \right). \tag{7.18}$$

From this expression, we conclude that the ratio is independent in the length of the cavity. Setting the atomic parameters aside, this ratio can be reduced by decreasing the mode waist of the cavity, and increasing the cavity finesse. However, for $\Delta \sim 10^9$ Hz, $\mu_{24} \sim 10^{-29}$ Cm, and $\omega_0 \sim 2\pi \times 10^{14}$ Hz, and $w_0 \sim 10^{-5}$ m, we would need $\mathcal{F} \sim 10^{10}$ in order to achieve a ratio of $\hbar\Gamma/U \sim 10^{-2}$. Such a finesse lies well beyond what is experimentally obtainable in modern state-of-the-art experiments.

7.3.1.1 Many atom EIT cavity QED as a few photon diode

It was originally proposed by Imamoğlu *et al.* that adding more identically prepared EIT atoms to the cavity would linearly increase the magnitude of U. If this was true, than an arbitrarily large Kerr nonlinearity could be achieved in the cavity [55]. This is, however, not the case if one is concerned with working in the few-photon regime. As pointed out by others [53, 54, 56], and explained later by Fleischhaur, Imamoğlu, and Marangos [48], in the few-photon regime, the system undergoes a collective enhancement. This enhancement modifies the validity condition from $|g_{13}|/|\Omega_c| \ll 1$ to $\sqrt{N}|g_{13}|/|\Omega_c| \ll 1$ where N is the number of atoms. This new validity condition places an upper bound on the overall magnitude of the nonlinearity. The argument provided in reference [48] basically goes as follows. The non-interacting effective Hamiltonian for the N-atom system is

$$\begin{aligned}\tilde{H}_{\text{eff}}^{(N)} &= \hbar\Bigg[\sum_{j=1}^{N}\delta\hat{\sigma}_{22}^{(j)} + (\delta - i\gamma_3)\hat{\sigma}_{33}^{(j)} + (2\delta + \Delta - i\frac{\gamma_{42}}{2})\hat{\sigma}_{44}^{(j)} + g_{13}(\hat{a}^\dagger\hat{\sigma}_{13}^{(j)} + \hat{a}\hat{\sigma}_{31}^{(j)}) \\ &\quad + g_{24}(\hat{a}^\dagger\hat{\sigma}_{24}^{(j)} + \hat{a}\hat{\sigma}_{42}^{(j)}) + \Omega_c(\hat{\sigma}_{32}^{(j)} + \hat{\sigma}_{23}^{(j)})\Bigg] \qquad (7.19)\end{aligned}$$

where $\hat{\sigma}_{nm}^{(j)}$ is the atomic operator for atom j, and we have assumed all of the atoms to be coupled to the cavity in exactly the same way. This is the Tavis-Cummings Hamiltonian. Assuming that there is only one photon in the cavity, the N-atom ground state

$$|\mathbf{1}^N\rangle \equiv |1, 1, ..., 1\rangle \qquad (7.20)$$

couples only to the following symmetric states via the N-atom Hamiltonian:

$$|\mathbf{1}^{N-1}\mathbf{2}\rangle \equiv \frac{1}{\sqrt{N}}\sum_{j=1}^{N}|1,...,2_j,...,1\rangle \tag{7.21}$$

$$|\mathbf{1}^{N-1}\mathbf{3}\rangle \equiv \frac{1}{\sqrt{N}}\sum_{j=1}^{N}|1,...,3_j,...,1\rangle. \tag{7.22}$$

Taking matrix elements of the N-atom Hamiltonian we get

$$\langle\mathbf{1}^{N}|\tilde{H}_{\text{eff}}^{(N)}|\mathbf{1}^{N-1}\mathbf{3}\rangle = \hbar\sqrt{N}g_{13} \tag{7.23}$$

$$\langle\mathbf{1}^{N-1}\mathbf{2}|\tilde{H}_{\text{eff}}^{(N)}|\mathbf{1}^{N-1}\mathbf{3}\rangle = \hbar\Omega_c. \tag{7.24}$$

Thus, following the procedure outlined in Section 2.3.1 were we look for steady-state solutions of the N-atom system in the 1-photon manifold of the cavity:

$$|\Psi^{(N)}\rangle_1 = |n=1\rangle|\mathbf{1}^{N}\rangle + c_2|n=0\rangle|\mathbf{1}^{N-1}\mathbf{2}\rangle + c_3|n=0\rangle|\mathbf{1}^{N-1}\mathbf{3}\rangle, \tag{7.25}$$

we conclude that

$$\begin{aligned}\hat{H}_{\chi^{(3)}} &\simeq -\hbar N\frac{g_{13}^2 g_{24}^2}{\Omega_c^2\Delta}\hat{a}^\dagger\hat{a}^\dagger\hat{a}\hat{a} \\ &\equiv U\hat{a}^\dagger\hat{a}^\dagger\hat{a}\hat{a},\end{aligned} \tag{7.26}$$

but under the restriction that

$$\left(\frac{\sqrt{N}g_{13}}{\Omega_c}\right)^2 \ll 1. \tag{7.27}$$

Therefore, the overall magnitude of $\chi^{(3)}$ cannot be enhanced if we work in this approximation, while simultaneously restricting ourselves to few photon cavity QED. The few photon regime is of particular interest for realizing our atomtronic components in this new system.

There is an additional, possibly helpful, effect that occurs for many-atom cavity QED systems. As originally pointed out independently by Müller *et al.* [72] and Lukin *et al.* [73], the many atom EIT media leads to a reduction in the cavity linewidth. Since we require $U \gg \hbar\Gamma, J$ and, recalling from Section 2.2.3 that $J \sim \hbar\Gamma$, the reduction in the linewidth Γ might help us achieve this parameter hierarchy in this EIT cavity QED system.

Recall from equation (2.16) and equation (2.21) that

$$\frac{I_c}{I_i} = \frac{\frac{T}{(1-R)^2}}{1+\frac{4\mathcal{F}^2}{\pi^2}\sin^2\left(\frac{\varphi}{2}\right)} \tag{7.28}$$

implies that the linewidth can be determined from

$$\frac{\pi}{\mathcal{F}} \simeq \varphi. \tag{7.29}$$

For an index of refraction $n = 1$, we found

$$\Gamma_0 = \frac{\omega_{ax}}{\mathcal{F}}. \tag{7.30}$$

From equation (2.71) $|\delta| \ll |\Omega_c|, |\gamma|$ implies

$$\chi^{(1)}(\delta\omega) = N\frac{1}{\omega_0}\left(\frac{g_{13}}{\Omega_c}\right)^2 \delta\omega \tag{7.31}$$

where ω_0 is the cavity resonance. Thus, the index of refraction

$$n = (1+\chi^{(1)})^{1/2} \simeq 1 + \frac{1}{2}\chi^{(1)} = 1 + \frac{N}{2}\frac{1}{\omega_0}\left(\frac{g_{13}}{\Omega_c}\right)^2 \delta\omega \equiv 1 + \frac{D}{\omega_0}\delta\omega \tag{7.32}$$

where, from our EIT validity condition,

$$D = \frac{N}{2}\left(\frac{g_{13}}{\Omega_c}\right)^2 \ll 1. \tag{7.33}$$

For this index of refraction,

$$\begin{aligned}
\frac{\pi}{\mathcal{F}} &\simeq \phi = 2\pi\frac{\omega}{\omega_{ax}}n \simeq 2\pi\frac{\omega_0+\delta\omega_{1/2}}{\omega_{ax}}\left(1+\frac{1}{\omega_0}D\delta\omega_{1/2}\right) \\
&= \frac{2\pi}{\omega_{ax}}\left(\omega_0 + D\delta\omega_{1/2} + \delta\omega_{1/2} + \frac{D}{\omega_0}(\delta\omega_{1/2})^2\right) \qquad (7.34) \\
&\simeq \frac{2\pi}{\omega_{ax}}\delta\omega_{1/2}\omega_{ax}\,(1+D) \qquad (7.35)
\end{aligned}$$

where we have taken ω_0 to be a harmonic of ω_{ax}. The first and fourth terms of equation (7.34) are neglected because the first was equal to a phase shift of 2π and the fourth term is much smaller than the rest due to the optical frequency in the denominator. Expressing this new linewidth $\Gamma = 2\delta\omega_{1/2}$ in terms of the empty cavity line with Γ_0 we get

$$\Gamma = \frac{\Gamma_0}{1+D}. \tag{7.36}$$

We conclude that there is a narrowing of the cavity linewidth. However, since we must be in the few-photon regime for the atomtronic components to function, the linewidth narrowing is

negligible since the magnitude of D is restricted by equation (7.33). Note that, since the Finesse is solely related to the reflectivity of the cavity, the axial mode spacing gets reduced by a factor of $1/(1+D)$ as well.

From the fact that the Kerr nonlinearity obtains only a limited enhancement from the inclusion of several atoms in the cavity, and the fact that the linewidth does not get significantly reduced in the few photon regime, we conclude that etalon cavity QED systems are probably not suitable for the experimental realization of the few photon optical diode.

7.3.2 Toroidal microcavities as a few photon diode

In the context of realizing the few photon diode, coupled toroidal microcavities have a major advantage over their etalon counterpart: the cavities are coupled together via evanescent coupling with a tapered fiber. As a result, the effective cavity-cavity coupling rate can be easily tuned by changing the relative distance between the cavity and the fiber.

Recently Aoki *et al.* have observed strong coupling between single atoms and these microcavities [40], thus EIT atoms could provide these cavities with a Kerr nonlinearity. Here we examine the suitability of toroidal cavities for the realization of the few photon diode by using the theoretical estimates provided by Spillane *et al.* [42]. The analysis they provide is for toroidal cavities that are driven by a laser with wavelength $\lambda = 852$ nm, which is the relevant transition for strong-coupling cesium, and is a relevant transition for EIT. We assume a toroidal cavity with principal diameter of 20 μm, and minor diameter of 1 μm. According to Spillane, this cavity can have an effective mode volume of $V = 50\ \mu\text{m}^3$, a quality factor $Q = 10^{10}$, and it is possible to acquire an atom-cavity coupling rate of $g \simeq 420$ MHz. Since the corresponding driving frequency is $\nu_0 \simeq 3.5 \times 10^{14}$ Hz, this cavity has a linewidth of $\Gamma \simeq 3.5 \times 10^4$ Hz, which is quite narrow compared to the best high finesse etalon cavity linewidth achievable. For a single atom interacting with the cavity, recall that

$$U = -\hbar \frac{g_{24}^2}{\Delta} \left(\frac{g_{13}}{\Omega_c} \right)^2 . \tag{7.37}$$

Assuming $\Delta = -1.5 \times 10^9\ \text{s}^{-1}$ [75], and taking $(g_{13}/\Omega_c)^2 = 0.1$, and assuming $g_{24} = g_{13}$, we get a

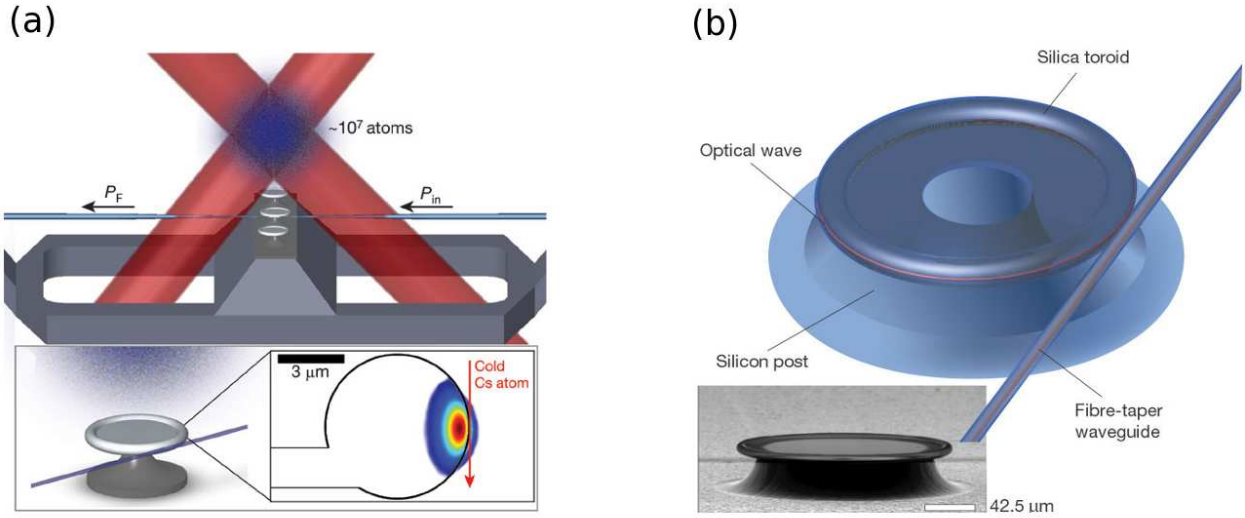

Figure 7.5: (a) An illustration of an experiment involving the coupling of a microtoroid to a single atom. Reprinted with permission from reference [40]. (b) An illustration of a silica toroid coupled to a tapered fiber waveguide as well as an image of an actual toroidal cavity. Reprinted with permission from reference [74].

nonlinear interaction of $U \simeq 1.8 \times 10^7$. Therefore,

$$\frac{\Gamma}{U} < 0.002. \tag{7.38}$$

Using this ratio in our simulation of the asymmetric current response for the few photon diode, we obtain current asymmetries greater than 3×10^5.

The fact that the tapered fiber coupled cavities make J a tunable parameter, it is possible for the system to be in the regime where $J \ll U$ as well. This puts toroidal cavities coupled to cesium atoms well within the required parameter regime to realize the few photon diode.

It should be noted that state-of-the-art experiments have fallen appreciably short of the projected values used above. For pure silica toroids, $Q \sim 10^8$ is closer to the current experimental upper bound than 10^{10}. Since the ratio Γ/U is proportional to $1/Q$, this seems to pose a problem

for immediate realization of the diode. However, Hartmann and coworkers [76] have suggested an alternative three-level, standard lambda scheme where the atoms are prepared in an antisymmetric metastable state. These single atoms have roughly the same nonlinear response as Imamoğlu's four-level scheme, but the multiple-atom situation is predicted to be quite different. Brandão, Hartmann and Plenio [77] claim that, unlike the four-level scheme where collective enhancement prevented the number of atoms from increasing the magnitude of the nonlinearity for the four-level atom, their scheme experiences appreciable enhancement with the number of atoms. Their prediction is that many-atom cavities can experience at least a two order of magnitude improvement over the equivalent four-level scheme. Therefore, a loss in currently achievable Q could be compensated by a gain in $\chi^{(3)}$ from an alternative three-level scheme.

7.3.3 Photonic band-gap cavities as a few photon diode

Photonic crystals are constructed out of dielectric semiconductor slabs, where a periodic array of holes are 'drilled' into the dielectric material allowing only a specific mode of light to propagate through it. Cavities, even arrays of cavities, on the order of one micron or smaller can be formed in these materials by surrounding unperforated slabs of dielectric in the crystal with lattice 'defect' holes. Due to their size, these cavities are called nanocavities.

This system is another potential candidate for realization of the few photon diode for the following reasons: First, cavity arrays can be constructed and individually-tailored without much difficulty. Post-fabrication cavity mode tuning is even possible [44] for these systems. Second, for a fixed cavity mode and Q, the photon tunneling rate J is tunable as it is related to the spatial separation of adjacent cavities [80]. Third, EIT atoms have been successfully embedded in rare-earth crystals, where they have maintained their EIT characteristics [45]. As an alternative to an EIT-generated Kerr nonlinearity, quantum dots can be embedded in the nanocavity. They can significantly increase the Kerr nonlinear response [81] of the cavity. Fourth, the effective mode volumes of these cavities can be ~ 0.03 μm. This leads to a dramatic enhancement of the coupling of the EIT atom or quantum dot to the cavity. Finally, quality factors have been observed to be

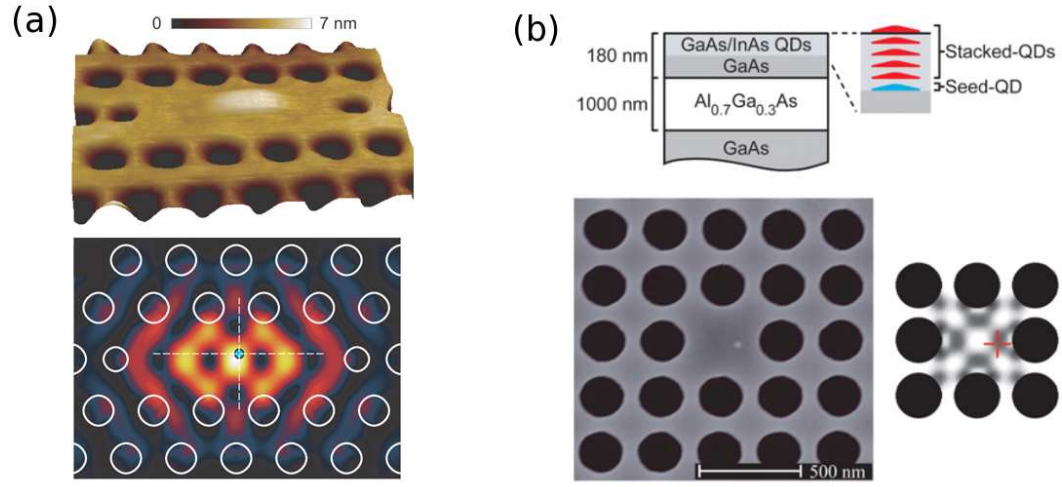

Figure 7.6: (a) (Top) Actual image of a $\sim$ 1 μm nanocavity housing a single quantum dot. (a)(Bottom) Calculation of the electromagnetic mode inside the cavity and its overlap with the quantum dot. Reprinted with permission from [78]. (b)(Top) The composition of a the quantum dot. (b)(Bottom left) Actual image of a $\sim$ 0.5 μm nanocavity. (b)(Bottom right) Calculation of the electromagnetic mode inside the cavity and its overlap with the quantum dot. Reprinted with permission from reference [79]

$\sim 1.4 \times 10^5$ for GaAs-based microcavities [82], and even larger for Si cavities, whose theoretical upper limit was reported to be$\sim 7 \times 10^7$ [83]. These observed and projected Q values do not reach the level achieved by toroidal cavities, but the enhanced atom/dot-cavity coupling can make up for the loss in Q.

7.3.3.1 The giant Kerr EIT nanocavity

Here we compare Imamoğlu's giant Kerr nonlinearity scheme for the etalon cavity to the same system in a nanocavity. Assuming a reasonable, but optimistic value of $Q \sim 10^6$, the wavelength of light of the cavity resonance $\lambda = 850$ nm, and a mode volume of the nanocavity that is $V = \lambda^3$,

we obtain a cavity linewidth $\Gamma \sim 3.5 \times 10^8$ Hz and a nonlinear interaction $U \sim 9 \times 10^8$ Hz leading to a ratio of $\Gamma/U \sim 0.4$. This ratio is much better than it was for the etalon cavity, but still at least an order of magnitude away from putting the system in a parameter regime where it can act as a few photon diode.

7.3.3.2 The quantum dot Kerr nanocavity

For the quantum dot-doped nanocavity, we carry out a semiclassical analysis using the parameters from Fushman *et al.* [81]. In their article, a quantum dot was strongly-coupled to a silicon-based two-dimensional nanocavity. This system, with a resonant wavelength of $\lambda \sim 10^{-6}$ m and $Q = 10^4$ achieved a $\chi^{(3)} = 2.4 \times 10^{-10}$ ($\mathrm{m}^2/\mathrm{Volt}^2$).

The quantum dot decay rate was reported to be on the order 10^2 less in magnitude, which makes it irrelevant for this analysis. The interaction energy (in units of Hz) generated by this Kerr nonlinearity is

$$U_{\mathrm{Kerr}} = \frac{1}{2\pi\hbar}\int \epsilon_0 \chi^{(3)} E^4 dV_{\mathrm{QD}} = \frac{V_{\mathrm{QD}}}{2\pi\hbar}\epsilon_0 \chi^{(3)} E^4 \tag{7.39}$$

where $V_{\mathrm{QD}} = 10^{-3}V$ is the assumed volume of the quantum dot, and V is the volume of the cavity. If we assume that $V = \lambda^3$, using equation (2.25), we get

$$U = \frac{\chi^{(3)} 2\pi c^2}{\epsilon_0 \lambda^5} 10^{-3}. \tag{7.40}$$

where c is the speed of light.

The decay rate of this system (in Hz) is

$$\Gamma = \frac{c}{\lambda Q}. \tag{7.41}$$

Therefore,

$$\frac{\Gamma}{U} = \frac{\epsilon_0}{2\pi\hbar c}\frac{\lambda^4}{Q}\frac{1}{\chi^{(3)}} 10^{-3} \sim 0.02. \tag{7.42}$$

These results indicate that it appears that quantum dot nanocrystal cavities should also be able to function as a few photon diode device.

7.4 Conclusion

In this chapter, with the observation that coupled nonlinear cavity arrays can also be modeled by the Bose-Hubbard model, we demonstrated how a few photon diode can be realized. We performed theoretical analyses showing that, under a variety of qualitatively-different driving fields, there exist parameter regimes where a two coupled cavity system exhibits a large asymmetry in its photon current response. Following this, we examined three different systems in which the few photon diode might be realized: high-finesse coupled etalon cavities, toroidal microcavities and photon bandgap nanocavity systems. After determining that realization of the few photon diode in an etalon cavity experiment was unlikely, we demonstrated that there is a strong possibility that it can be realized in both toroidal cavities with EIT-generated Kerr interactions, as well as a quantum dot-doped nanocavity.

Chapter 8

Conclusion

In this thesis, an open quantum system theory to study transport properties of atoms in optical lattices, and photons in nonlinear cavities has been constructed.

In the field of open quantum systems, it is typically uncommon to come across system-reservoir interactions where the spectral properties of the reservoir vary so strongly that they play an important role in the problem. Since we chose to model fermionized boson reservoirs, which early on yielded unphysical-diverging energy shifts, it was necessary for us to derive a non-Markovian master equation treatment from first principles in order to formulate a satisfactory theory.

After confirming that our theory correctly modeled the behavior of these exotic system-reservoir interactions for certain situations in which comparison with exact results was possible, we applied the approach to generate a complete analogy of boson reservoir-driven optical lattices with semiconductor electronic systems. The theories describing weakly-interacting and strongly-interacting boson reservoir sources were described, and the device behavior of a diode, FET, BJT, and AND gate were demonstrated theoretically.

In the context of understanding and developing an atom-optical analog of a fundamental sequential logic gate known as a SR flip-flop, a time-dependent system analysis was performed to confirm that effective transport across off-resonant lattice junctions could be achieved by modulating the tunneling barrier at the corresponding junction gap frequency.

Finally, the principles developed with ultracold atoms in optical lattices were applied to nonlinear cavity QED environments. In these systems we discovered a parameter regime that is

capable of realizing a few photon optical diode. An analysis of contemporary cavity QED systems revealed that such a parameter regime lay within a region that is accessible experimentally.

8.1 Future work and outlook

Our work towards developing sequential atomtronic behavior has established the foundation, concepts, and ideas of sequential logic. This is thus just the starting point from which a next generation research program could be launched. The next step would likely involve the theoretical modeling of the bistable BJT circuit in Section 6.1. The difficulty that must be overcome is the existance of two off-resonant couplings, whose energetic gaps are not equal to each other. As we have seen several times in this thesis, a single frequency can always be rotated out of the system Hamiltonian making it effectively a time-independent problem. In general, for two unequal frequencies, new theoretical techniques, such as an extension of Floquet theory, must be utilized in the analysis.

The work presented here could be extended to study fundamental transport properties across custom lattice structures, as well as to control the dynamics of such transport. Experimental techniques are advancing rapidly in this field and it is important that the fundamental theoretical framework advances at an equal pace in order that the dynamics and observables can be modeled and understood. The rich potential for novel quantum signal processing with atoms, with their comparatively complex internal level structure (when compared to electronics), and strongly interacting photons, which can rapidly transition through components generating comparatively minimal heat, motivates future work in these areas.

Bibliography

[1] W. D. Phillips. Nobel lecture: Laser cooling and trapping of neutral atoms. Rev. Mod. Phys., 70:721, 1998.

[2] C. E. Wieman, D. E. Pritchard, and D. J. Wineland. Atom cooling, trapping, and quantum manipulation. Rev. Mod. Phys., 71:S253, 1999.

[3] M. H. Anderson, J. R. Ensher, M. R. Matthews, C. E. Wieman, and E. A. Cornell. Observation of bose-einstein condensation in a dilute atomic vapor. Science, 269:198, 1995.

[4] M. Greiner, C. A. Regal, and D. S. Jin. Emergence of a molecular bose–einstein condensate from a fermi gas. Nature, 1, 2003.

[5] O. Morsch and M. Oberthaler. Dynamics of bose-einstein condensates in optical lattices. Rev. Mod. Phys., 78:179, 2006.

[6] M. P. A. Fisher, P. B. Weichman, G. Grinstein, and D. S. Fisher. Boson localization and the superfluid-insulator transition. Phys. Rev. B, 40:546, 1989.

[7] M. Greiner, O. Mandel, T. Esslinger, T. W. Hänsch, and I. Bloch. Quantum phase transition from a superfluid to a mott insulator in a gas of ultracold atoms. Nature, 415:39, 2002.

[8] A. Micheli, A. J. Daley, D. Jaksch, and P. Zoller. Single atom transistor in a 1d optical lattice. Phy. Rev. Lett., 93:140408, 2004.

[9] J. A. Stickney, D. Z. Anderson, and A. A. Zozulya. Transistorlike behavior of a bose-einstein condensate in a triple-well potential. Phys. Rev. A, 75:013608, 2007.

[10] D. M. Cardamone, C. A. Stafford, and S. Mazumdar. Controlling quantum transport through a single molecule. Nano Lett., 6:2422, 2006.

[11] C. A. Stafford, D. M. Cardamone, and S. Mazumdar. The quantum interference effect transistor. Nanotechnology, 18:424014, 2007.

[12] M. Theis, G. Thalhammer, K. Winkler, M. Hellwig, G. Ruff, and R. Grimm. Tuning the scattering length with an optically induced feshbach resonance. Phys. Rev. Lett., 93:123001, 2004.

[13] S. Inouye, M. R. Andrews, J. Stenger, H. J. Miesner, D. M. Stamper-Kurn, and W. Ketterle. Observation of feshbach resonances in a bose-einstein condensate. Nature, 392:151, 1998.

[14] S. Inouye, J. Goldwin, M. L. Olsen, C. Ticknor, J. L. Bohn, and D. S. Jin. Observation of heteronuclear feshbach resonances in a mixture of bosons and fermions. Phys. Rev. Lett., 93:183201, 2004.

[15] C. A. Stan, M. W. Zwierlein, C. H. Schunck, S. M. F. Raupach, and W. Ketterle. Obersveration of feshbach resonances between two different atomic species. Phys. Rev. Lett., 93:143001, October 2004.

[16] W. S. Bakr, J. I. Gillen, A. Peng, S. Fölling, and M. Greiner. A quantum gas microscope for detecting single atoms in a Hubbard-regime optical lattice. Nature, 462:74, 2009.

[17] O. Mandel, M. Greiner, A. Widera, T. Rom, T. W. Hänsch, and I. Bloch. Controlled collisions for mulit-particle entanglement of optically trapped atoms. Nature, 425:937, 2003.

[18] N. Strohmaier, Y. Takasu, K. Gunter, R. Jordens, M. Kohl, H. Moritz, and T. Esslinger. Interaction-controlled transport of an ultracold Fermi gas. Phys. Rev. Lett., 99:220601, 2007.

[19] K. Henderson, H. Kelkar, B. Gutiérrez-Medina, T. C. Li, and M. G. Raizen. Experimental Study of the Role of Atomic Interactions on Quantum Transport. Phys. Rev. Lett., 96:150401, 2006.

[20] J. H. Denschlag, J. E. Simsarian, H. Haeffner, C. McKenzie, A. Browaeys, D. Cho, K. Helmerson, S. L. Rolston, and W. D. Phillips. A Bose-Einstein condensate in an optical lattice. J. Phys. B, 35:3095, 2002.

[21] M. Greiner. Ultracold Quantum Gases in Three-Dimensional Optical Lattice Potentials. PhD thesis, Ludwig-Maximilians-Universität München, 2003.

[22] D. Jaksch, C. Bruder, J. I. Cirac, C. W. Gardiner, and P. Zoller. Cold bosonic atoms in optical lattices. Phys. Rev. Lett., 81:3108, 1998.

[23] A. Klein and D. Jaksch. Simulating high-temperature superconductivity model hamiltonians with atoms in optical lattices. Phys. Rev. A, 73:053613, 2006.

[24] B. Paredes, A. Widera, V. Murg, O. Mandel, S. Fölling, I. Cirac, G. V. Shlyapnikov, T. W. Hänsch, and I. Bloch. Tonks–girardeau gas of ultracold atoms in an optical lattice. Nature, 429:277, 2004.

[25] J. I. Gillen. The Quantum Gas Microscope. PhD thesis, Harvard University, 2009.

[26] M. Pasienski and B. DeMarco. A high-accuracy algorithm for designing arbitrary holographic atom traps. Optics Express, 16:2176, 2008.

[27] W. S. Bakr, A. Peng, M. E. Tai, R. Ma, J. Simon, J. I. Gillen, S. Foelling, L. Pollet, and M. Greiner. Probing the superfluid–to–mott insulator transition at the single-atom level. Science, 329:547, 2010.

[28] J. F. Sherson, C. Weitenberg, M. Endres, M. Cheneau, I. Bloch, and S. Kuhr. Single-atom-resolved fluorescence imaging of an atomic mott insulator. Nature, 2010.

[29] C. Weitenberg, M. Endres, J. F. Sherson, M. Cheneau, P. Schauß, T. Fukuhara, I. Bloch, and S. Kuhr. Single-spin addressing in an atomic mott insulator. Nature, 471:319, 2011.

[30] P. Würtz, T. Langen, T. Gericke, A. Koglbauer, and H. Ott. Experimental demonstration of single-site addressability in a two-dimensional optical lattice. Phys. Rev. Lett., 103(8):80404, 2009.

[31] W. Zwerger. Mott–hubbard transition of cold atoms in optical lattices. Journal of Optics B, 5:S9, 2003.

[32] A. L. Fetter and J. D. Walecka. Quantum Theory of Many-Particle Systems. Dover, 2003.

[33] W. H. Louisell. Quantum Statistical Properties of Radiation. John Wiley and Sons, Inc., New York, 1973.

[34] P. Meystre and M. Sargent. Elements of Quantum Optics. Springer Verlag, 2007.

[35] D. F. Walls, G. J. Milburn, and J. C. Garrison. Quantum Optics. Springer, 1995.

[36] C. J. Hood, H. J. Kimble, and J. Ye. Characterization of high-finesse mirrors: Loss, phase shifts, and mode structure in an optical cavity. Phys. Rev. A, 64:033804, 2001.

[37] K. M. Birnbaum, A. Boca, R. Miller, A. D. Boozer, T. E. Northup, and H. J. Kimble. Photon blockade in an optical cavity with one trapped atom. Nature, 436:87, 2005.

[38] A. E. Siegman. Lasers. University Science Books, 1986.

[39] C. W. Gardiner and M. J. Collett. Input and output in damped quantum systems: Quantum stochastic differential equations and the master equation. Phys. Rev. A, 31:3761, Jun 1985.

[40] T. Aoki, B. Dayan, E. Wilcut, W. P. Bowen, A. S. Parkins, T. J. Kippenberg, K. J. Vahala, and H. J. Kimble. Observation of strong coupling between one atom and a monolithic microresonator. Nature, 443:671, 2006.

[41] S. M. Spillane, T. J. Kippenberg, O. J. Painter, and K. J. Vahala. Ideality in a fiber-taper-coupled microresonator system for application to cavity quantum electrodynamics. Phys. Rev. Lett., 91:43902, 2003.

[42] S. M. Spillane, T. J. Kippenberg, K. J. Vahala, K. W. Goh, E. Wilcut, and H. J. Kimble. Ultrahigh-Q toroidal microresonators for cavity quantum electrodynamics. Phys. Rev. A, 71:013817, 2005.

[43] J. Sweet, B. C. Richards, J. D. Olitzky, J. Hendrickson, G. Khitrova, H. M. Gibbs, D. Litvinov, D. Gerthsen, D. Z. Hu, D. M. Schaadt, et al. GaAs photonic crystal slab nanocavities: Growth, fabrication, and quality factor. Photonics and Nanostructures-Fundamentals and Applications, 8:1, 2009.

[44] K. Hennessy, A. Badolato, A. Tamboli, P. M. Petroff, E. Hu, M. Atatüre, J. Dreiser, and A. Imamoğlu. Tuning photonic crystal nanocavity modes by wet chemical digital etching. App. Phys. Lett., 87:021108, 2005.

[45] B. S. Ham, P. R. Hemmer, and M. S. Shahriar. Efficient electromagnetically induced transparency in a rare-earth doped crystal. Opt. Commun., 144:227, 1997.

[46] A. V. Turukhin, V. S. Sudarshanam, M. S. Shahriar, J. A. Musser, B. S. Ham, and P. R. Hemmer. Observation of ultraslow and stored light pulses in a solid. Phys. Rev. Lett., 88:23602, 2002.

[47] H. Schmidt and A. Imamoğlu. Giant Kerr nonlinearities obtained by electromagnetically induced transparency. Opt. Lett., 21:1936, 1996.

[48] M. Fleischhauer, A. Imamoğlu, and J. P. Marangos. Electromagnetically induced transparency: Optics in coherent media. Rev. Mod. Phys., 77:633, 2005.

[49] S. E. Harris. Electromagnetically induced transparency. Phys. Today, 50:36, 1997.

[50] S. E. Harris, J. E. Field, and A. Imamoğlu. Nonlinear optical processes using electromagnetically induced transparency. Phys. Rev. Lett., 64:1107, 1990.

[51] M. O. Scully and M. S. Zubairy. Quantum Optics. Cambridge University Press, 1997.

[52] L. V. Hau, S. E. Harris, Z. Dutton, and C. H. Behroozi. Light speed reduction to 17 metres per second in an ultracold atomic gas. Nature, 397:594, 1999.

[53] K. M. Gheri, W. Alge, and P. Grangier. Quantum analysis of the photonic blockade mechanism. Phys. Rev. A, 60:2673, 1999.

[54] P. Grangier, D. F. Walls, and K. M. Gheri. Comment on "Strongly interacting photons in a nonlinear cavity". Phys. Rev. Lett., 81:2833, 1998.

[55] A. Imamoğlu, H. Schmidt, G. Woods, and M. Deutsch. Strongly interacting photons in a nonlinear cavity. Phys. Rev. Lett., 79:1467, 1997.

[56] S. Rebic, S. M. Tan, A. S. Parkins, and D. F. Walls. Large Kerr nonlinearity with a single atom. Journal of Optics B, 1:490, 1999.

[57] M. J. Werner and A. Imamoğlu. Photon-photon interactions in cavity electromagnetically induced transparency. Phys. Rev. A, 61:011801, 1999.

[58] J. Dalibard, Y. Castin, and K. Mølmer. Wave-function approach to dissipative processes in quantum optics. Phys. Rev. Lett., 68:580, 1992.

[59] R. Dum, P. Zoller, and H. Ritsch. Monte carlo simulation of the atomic master equation for spontaneous emission. Phys. Rev. A, 45:4879, 1992.

[60] C. W. Gardiner, A. S. Parkins, and P. Zoller. Wave-function quantum stochastic differential equations and quantum-jump simulation methods. Phys. Rev. A, 46:4363, 1992.

[61] K. Mølmer and Y. Castin. Monte carlo wavefunctions in quantum optics. Quantum and Semiclassical Optics: Journal of the European Optical Society Part B, 8:49, 1996.

[62] C. Cohen-Tannoudji, J. Dupont-Roc, and G. Grynberg. Atom-Photon Interactions. Wiley-Interscience, 1998.

[63] C.W. Gardiner and P. Zoller. Quantum Noise. Springer, 1991.

[64] D. N. Zubarev, V. A. Morozov, and G. Röpke. Relaxation and Hydrodynamic Processes Vol. 2. Akademie Verlag, Berlin, 1997.

[65] R. Shankar. Principles of Quantum Mechanics. Springer, 1994.

[66] R. A. Pepino, J. Cooper, D. Meiser, D. Z. Anderson, and M. J. Holland. Open quantum systems approach to atomtronics. Phys. Rev. A, 82:013640, 2010.

[67] S. Jang, J. Cao, and R. J. Silbey. Fourth-order quantum master equation and its Markovian bath limit. J. Chem. Phys., 116:2705, 2002.

[68] M. J. Buckingham. Noise in Electronic Devices and Systems. JOHN WILEY & SONS, 1983.

[69] B. T. Seaman, M. Krämer, D. Z. Anderson, and M. J. Holland. Atomtronics: Ultracold-atom analogs of electronic devices. Phys. Rev. A, 75:023615, 2007.

[70] A. T. Georges. Resonance fluorescence in Markovian stochastic fields. Phys. Rev. A, 21:2034, 1980.

[71] M. Khudaverdyan, W. Alt, I. Dotsenko, T. Kampschulte, K. Lenhard, A. Rauschenbeutel, S. Reick, K. Schörner, A. Widera, and D. Meschede. Controlled insertion and retrieval of atoms coupled to a high-finesse optical resonator. New J. Phys., 10:073023, 2008.

[72] G. Müller, M. Müller, A. Wicht, R. H. Rinkleff, and K. Danzmann. Optical resonator with steep internal dispersion. Phys. Rev. A, 56:2385, 1997.

[73] M. D. Lukin, M. Fleischhauer, M. O. Scully, and V. L. Velichansky. Intracavity electromagnetically induced transparency. Opt. Lett., 23:295, 1998.

[74] K. J. Vahala. Optical microcavities. Nature, 424:839, 2003.

[75] M. J. Hartmann and M. B. Plenio. Strong photon nonlinearities and photonic Mott insulators. Phys. Rev. Lett., 99:103601, 2007.

[76] M. J. Hartmann, F. G. S. L. Brandao, and M. B. Plenio. Quantum many-body phenomena in coupled cavity arrays. Laser & Photonics Reviews, 2:527, 2008.

[77] F. G. S. L. Brandao, M. J. Hartmann, and M. B. Plenio. Light-shift-induced photonic nonlinearities. New Journal of Physics, 10:043010, 2008.

[78] K. Hennessy, A. Badolato, M. Winger, D. Gerace, M. Atatüre, S. Gulde, S. Fält, E. L. Hu, and A. Imamoğlu. Quantum nature of a strongly coupled single quantum dot–cavity system. Nature, 445:896, 2007.

[79] A. Badolato, K. Hennessy, M. Atat
"ure, J. Dreiser, E. Hu, P. M. Petroff, and A. Imamoğlu. Deterministic coupling of single quantum dots to single nanocavity modes. Science, 308:1158, 2005.

[80] M. Bayindir, B. Temelkuran, and E. Ozbay. Tight-binding description of the coupled defect modes in three-dimensional photonic crystals. Phys. Rev. Lett., 84:2140, 2000.

[81] I. Fushman, D. Englund, A. Faraon, N. Stoltz, P. Petroff, and J. Vučković. Controlled phase shifts with a single quantum dot. Science, 320:769, 2008.

[82] E. Weidner, S. Combrié, A. De Rossi, J. Nagle, S. Cassette, A. Talneau, and H. Benisty. Achievement of ultrahigh quality factors in GaAs photonic crystal membrane nanocavity. App. Phys. Lett., 89:221104, 2006.

[83] E. Kuramochi, M. Notomi, S. Mitsugi, A. Shinya, T. Tanabe, and T. Watanabe. Ultrahigh-q photonic crystal nanocavities realized by the local width modulation of a line defect. App. Phys. Lett., 88:041112, 2006.

[84] C. W. Gardiner. Handbook of Stochastic Methods. Springer Berlin, 1985.

[85] P. Bermel, A. Rodriguez, S. G. Johnson, J. D. Joannopoulos, and M. Soljačić. Single-photon all-optical switching using waveguide-cavity quantum electrodynamics. Phys. Rev. A, 74:043818, 2006.

[86] S. E. Harris and L. V. Hau. Nonlinear optics at low light levels. Phys. Rev. Lett., 82:4611, 1999.

[87] H. Kang and Y. Zhu. Observation of large Kerr nonlinearity at low light intensities. Phys. Rev. Lett., 91:93601, 2003.

[88] D. Roy. Few-photon optical diode. Phys. Rev. B, 81:155117, 2010.

[89] P. B. Deotare, M. W. McCutcheon, I. W. Frank, M. Khan, and M. Lončar. Coupled photonic crystal nanobeam cavities. App. Phys. Lett., 95:031102, 2009.

[90] N. Na, S. Utsunomiya, L. Tian, and Y. Yamamoto. Strongly correlated polaritons in a two-dimensional array of photonic crystal microcavities. Phys. Rev. A, 77:031803, 2008.

[91] A. D. Greentree, C. Tahan, J. H. Cole, and L. C. L. Hollenberg. Quantum phase transitions of light. Nature Physics, 2:856, 2006.

[92] C. J. Hood, M. S. Chapman, T. W. Lynn, and H. J. Kimble. Real-time cavity QED with single atoms. Phys. Rev. Lett., 80:4157, 1998.

[93] M. J. Hartmann, F. G. S. L. Brandão, and M. B. Plenio. Strongly interacting polaritons in coupled arrays of cavities. Nat. Phys., 2:849, 2006.

[94] D. Jaksch and P. Zoller. The cold atom hubbard toolbox. Ann. Phys., 315:52, 2005.

[95] S. G. Bhongale, R. Walser, and M. J. Holland. Memory effects and conservation laws in the quantum kinetic evolution of a dilute bose gas. Phys. Rev. A, 66:043618, 2002.

[96] K. Burnett, J. Cooper, R. J. Ballagh, and E. W. Smith. Collisional redistribution of radiation. i. the density matrix. Phys. Rev. A, 22:2005, 1980.

[97] D. N. Zubarev and V. P. Kalashnikov. The derivation of time-irreversible generalized master equation. Physica, 56:345, 1971.

[98] Q. Shi and E. Geva. A new approach to calculating the memory kernel of the generalized quantum master equation for an arbitrary system–bath coupling. J. Chem. Phys., 119:12063, 2003.

[99] U. Fano. Pressure broadening as a prototype of relaxation. Phy. Rev., 131:259, 1963.

[100] W. Min, G. Luo, B. J. Cherayil, S. C. Kou, and X. S. Xie. Observation of a power-law memory kernel for fluctuations within a single protein molecule. Phys. Rev. Lett., 94:198302, 2005.

[101] E. W. Smith, J. Cooper, and C. R. Vidal. Unified classical-path treatment of stark broadening in plasmas. Phys. Rev., 185:140, 1969.

[102] T. Stöferle, H. Moritz, C. Schori, M. Köhl, and T. Esslinger. Transition from a strongly interacting 1d superfluid to a mott insulator. Phys. Rev. Lett., 92:130403, 2004.

[103] R. Walser, J. Cooper, and M. Holland. Reversible and irreversible evolution of a condensed bosonic gas. Phys. Rev. A, 63:013607, 2000.

[104] H. A. Kim, H. S. Moon, J. B. Kim, A. S. Choe, and J. Lee. Expanded concept of the adiabatic population transfer using dressed states. Phys. Rev. A, 59:1404, 1999.

[105] A. Aspect, E. Arimondo, R. Kaiser, N. Vansteenkiste, and C. Cohen-Tannoudji. Laser cooling below the one-photon recoil energy by velocity-selective coherent population trapping: theoretical analysis. JOSA B, 6:2112, 1989.

[106] W. S. Bakr, J. I. Gillen, A. Peng, S. Fölling, and M. Greiner. A quantum gas microscope for detecting single atoms in a hubbard-regime optical lattice. Nature, 462:74, 2009.

[107] M. B. Plenio and P. L. Knight. The quantum-jump approach to dissipative dynamics in quantum optics. Rev. Mod. Phys., 70:101, 1998.

[108] G. Nienhuis. Time-dependent spectra of colliding atoms in an intense radiation field. J. Phys. B, 16:2677, 1983.

[109] G. Nienhuis. Time and frequency dependence of nearly resonant light scattered from collisionally perturbed atoms. Physica B+C, 96:391, 1979.

[110] J. H. Eberly and K. Wodkiewicz. The time-dependent physical spectrum of light. JOSA, 67:1252, 1977.

[111] V. G. Morozov and G. Röpke. Non-markovian quantum kinetics and conservation laws. J. Stat. Phys., 102:285, 2001.

[112] R. Zwanzig. On the identity of three generalized master equations. Physica, 30:1109, 1964.

[113] H. Haug and L. Banyai. Improved spectral functions for quantum kinetics. Solid State Commun., 100:303, 1996.

[114] J. Wong. Results on certain non-hermitian hamiltonians. J. Math. Phys., 8:2039, 1967.

[115] L. Armstrong Jr and H. C. Baker. An adiabatic and near-adiabatic model of multiphoton ionisation. J. Phys. B, 13:4727, 1980.

[116] M. Baranger. Problem of overlapping lines in the theory of pressure broadening. Phys. Rev., 111:494, 1958.

[117] M. Elk and P. Lambropoulos. Spontaneous emission in a cavity driven by a strong bichromatic field. Phys. Rev. A, 50:1490, 1994.

[118] J. Cooper, A. Charlton, D. R. Meacher, P. Ewart, and G. Alber. Revised theory of resonant degenerate four-wave mixing with broad-bandwidth lasers. Phys. Rev. A, 40:5705, 1989.

[119] M. Antezza, L. P. Pitaevskii, and S. Stringari. New asymptotic behavior of the surface-atom force out of thermal equilibrium. Phys. Rev. Lett., 95:113202, 2005.

[120] S. Raghavan, A. Smerzi, S. Fantoni, and S. R. Shenoy. Coherent oscillations between two weakly coupled bose-einstein condensates: Josephson effects, π oscillations, and macroscopic quantum self-trapping. Phys. Rev. A, 59:620, 1999.

[121] S. Haroche and J. M. Raimond. Exploring the Quantum: Atoms, Cavities, and Photons. Oxford University Press, New York, 2007.

[122] R. A. Pepino, J. Cooper, D. Z. Anderson, and M. J. Holland. Atomtronic Circuits of Diodes and Transistors. Phys. Rev. Lett., 103:140405, 2009.

[123] D. K. Armani, T. J. Kippenberg, S. M. Spillane, and K. J. Vahala. Ultra-high-q toroid microcavity on a chip. Nature, 8:37, 2003.

Appendix A

Master Equation Solution Methods

In this appendix we present our method for solving for the matrix elements of the steady-state system reduced density operator. For simplicity, we develop the technique from a master equation in the standard Lindblad form. Consider the following master equation:

$$\frac{d\hat{\rho}_S}{dt} = -\frac{i}{\hbar}[\hat{H}_S, \hat{\rho}_S] - \frac{\Gamma}{2}\left(\hat{a}^\dagger\hat{a}\hat{\rho}_S + \hat{\rho}_S\hat{a}^\dagger\hat{a} - 2\hat{a}\hat{\rho}_S\hat{a}^\dagger\right). \tag{A.1}$$

Projecting this equation the system eigenbasis, the $\langle a|\hat{\rho}_S|b\rangle$ matrix element becomes

$$\frac{d}{dt}\langle a|\hat{\rho}_S|b\rangle = -i\omega_{ab}\langle a|\hat{\rho}_S|b\rangle - \frac{\Gamma}{2}\left(\hat{A}^\dagger_{an}\hat{A}_{nm}\langle m|\hat{\rho}_S|b\rangle + \langle a|\hat{\rho}_S|n\rangle\hat{A}^\dagger_{nm}\hat{A}_{mb} - 2\hat{A}_{an}\langle n|\hat{\rho}_S|m\rangle\hat{A}^\dagger_{mb}\right) \tag{A.2}$$

where $|a\rangle$, $|b\rangle$, $|n\rangle$, and $|m\rangle$ are all eigenstates of $\hat{H}_S$, $\hat{A}_{nm} = \langle n|\hat{a}|m\rangle$, and $\omega_{ab} = \omega_a - \omega_b$ are eigenenergies of $\hat{H}_S$.

In matrix form, we get the following system of equations:

$$\frac{d}{dt}\hat{\mathbf{P}} = -i\mathbf{\Omega} * \hat{\mathbf{P}} - \frac{\Gamma}{2}\left(\hat{\mathbf{A}}^\dagger\hat{\mathbf{A}}\hat{\mathbf{P}} + \hat{\mathbf{P}}\hat{\mathbf{A}}^\dagger\hat{\mathbf{A}} - 2\hat{\mathbf{A}}\hat{\mathbf{P}}\hat{\mathbf{A}}^\dagger\right) \tag{A.3}$$

where $\langle a|\hat{\mathbf{P}}|b\rangle = \langle a|\hat{\rho}_S|b\rangle$, $\langle a|\mathbf{\Omega}|b\rangle = \omega_{ab}$, $\langle a|\hat{\mathbf{A}}|b\rangle = \langle a|\hat{a}|b\rangle$ and $\mathbf{\Omega} * \hat{\mathbf{P}}$ is understood to be element-by-element multiplication of $\mathbf{\Omega}$ and $\hat{\mathbf{P}}$, *i.e.* $\langle a|\mathbf{\Omega} * \hat{\mathbf{P}}|b\rangle = \omega_{ab}\langle a|\hat{\rho}_S|b\rangle$.

We are concerned with steady-state behavior of equation (A.3). Thus we need to solve

$$\mathbf{0} = -i\mathbf{\Omega} * \hat{\mathbf{P}} - \frac{\Gamma}{2}\left(\hat{\mathbf{A}}^\dagger\hat{\mathbf{A}}\hat{\mathbf{P}} + \hat{\mathbf{P}}\hat{\mathbf{A}}^\dagger\hat{\mathbf{A}} - 2\hat{\mathbf{A}}\hat{\mathbf{P}}\hat{\mathbf{A}}^\dagger\right). \tag{A.4}$$

Let's assume that the dimensionality of the Hilbert space is n. Then, all of these matrices are $n \times n$. Instead of 'brute force' solving this system of equations for $\hat{\mathbf{P}}$, we move into a Liouville

representation where the $n \times n$ matrix $\hat{\mathbf{P}}$ is stretched to an $n^2 \times 1$ vector denoted as $\hat{\hat{\mathbf{P}}}$. In this framework, we derive a super operator $\hat{\hat{\mathbf{M}}}$ whose dimension is $n^2 \times n^2$ such that equation (A.4) can be written as

$$\mathbf{0} = \hat{\hat{\mathbf{M}}}\hat{\hat{\mathbf{P}}} \tag{A.5}$$

Then, we can employ standard linear algebra tricks to solve this equation. Namely, the eigenvector that corresponds to the zero eigenvalue is the steady-state solution. Once this is found, we can repack $\hat{\hat{\mathbf{P}}} \rightarrow \hat{\mathbf{P}}$, the $n \times n$ density matrix, and normalize it, yielding

$$\frac{1}{\mathrm{Tr}\left\{\hat{\mathbf{P}}\right\}}\hat{\mathbf{P}}, \tag{A.6}$$

which is the density matrix solution.

This method is much more numerically efficient than solving for the coupled system directly due to the fact that the matrices that we're dealing with are typically sparse. The trick is to generate $\hat{\hat{\mathbf{M}}}$ properly, which we derive below.

We first define our unpacking algorithm. Given the density operator with elements $\hat{\mathrm{P}}_{bc}$, we map it onto the super operator space by

$$\hat{\hat{\mathrm{P}}}_{\beta} = \hat{\hat{\mathrm{P}}}_{[n(b-1)+c]} = \hat{\mathrm{P}}_{bc} \tag{A.7}$$

That is, the column vector $\hat{\hat{\mathbf{P}}}$ consists of taking the rows of matrix $\hat{\mathbf{P}}$, transposing them, and then stacking them on top of each other in order. In this appendix, we use Roman letters for Hilbert space elements and Greek letters for Liouville space elements throughout this derivation.

With the definition of $\hat{\hat{\mathbf{P}}}$ in place, we can construct $\hat{\hat{\mathbf{M}}}$, which we do term-by-term. Consider the first term of equation (A.4).

$$\begin{aligned} -i\Omega_{ab} * \hat{\mathrm{P}}_{ab} &= -i\hat{\hat{\Omega}}_{\beta}\hat{\hat{\mathrm{P}}}_{\beta} \\ &= -i\hat{\hat{\Omega}}_{\alpha}\delta_{\alpha\beta}\hat{\hat{\mathrm{P}}}_{\beta} \\ &\equiv \hat{\hat{\mathbf{M}}}_1\hat{\hat{\mathbf{P}}} \end{aligned} \tag{A.8}$$

where $\delta_{\alpha\beta}$ is the Kronecker delta, or identity matrix for the $n^2 \times n^2$ Liouville space. Therefore,

$$\hat{\hat{\mathbf{M}}}_1 = -i\hat{\hat{\Omega}}_{\alpha}\delta_{\alpha\beta} \tag{A.9}$$

Since the Kronecker tensor product is needed for the remaining terms, we define it here as

$$\hat{\hat{\mathbf{W}}} = \hat{\mathbf{U}} \otimes \hat{\mathbf{V}} \tag{A.10}$$

such that

$$\hat{\hat{\mathrm{W}}}_{\alpha\beta} = \hat{\hat{\mathrm{W}}}_{[n(a-1)+c][n(b-1)+d]} = \hat{\mathrm{U}}_{ab}\hat{\mathrm{V}}_{cd} \tag{A.11}$$

In this convention, the tensor product multiplies every element of $\hat{\mathbf{U}}$ by the matrix $\hat{\mathbf{V}}$.

Now consider second term of equation (A.4), which is of the form $\hat{\mathbf{X}}\hat{\mathbf{P}}$ where $\hat{\mathbf{X}}$ is the combined matrix of all the operators on the left. Then,

$$\hat{\mathrm{X}}_{ab}\hat{\mathrm{P}}_{bc} = \hat{\hat{\mathrm{X}}}_{\alpha\beta}\hat{\hat{\mathrm{P}}}_{\beta} \tag{A.12}$$

where $\beta = n(b-1)+c$ implies that $\alpha = n(a-1)+c$. Therefore

$$\hat{\hat{\mathrm{X}}}_{\alpha\beta} = \hat{\hat{\mathrm{X}}}_{[n(a-1)+c][n(b-1)+c]} = \hat{\mathrm{X}}_{ab}\delta_{cd} = \hat{\mathrm{X}} \otimes \hat{\mathbb{1}}. \tag{A.13}$$

Thus

$$\hat{\hat{\mathbf{M}}}_2 = -\left(\frac{\Gamma}{2}\hat{\mathbf{A}}^{\dagger}\hat{\mathbf{A}}\right) \otimes \hat{\mathbb{1}}. \tag{A.14}$$

Next, consider the form

$$\hat{\mathbf{P}}\hat{\mathbf{X}} = \hat{\mathrm{P}}_{ab}\hat{\mathrm{X}}_{bc} = \hat{\hat{\mathrm{X}}}_{\alpha\beta}\hat{\hat{\mathrm{P}}}_{\beta}. \tag{A.15}$$

This time $\beta = n(a-1)+b$ and $\alpha = n(a-1)+c$. Consequently,

$$\hat{\hat{\mathrm{X}}}_{\alpha\beta} = \hat{\hat{\mathrm{X}}}_{[n(a-1)+c][n(a-1)+b]} = \delta_{ad}\hat{\mathrm{X}}_{cb} = \delta_{ad}\hat{\mathrm{X}}_{bc} = \hat{\mathbb{1}} \otimes (\hat{\mathbf{X}}^T), \tag{A.16}$$

where $(\hat{\mathbf{X}}^T)$ is the transpose of $\hat{\mathbf{X}}$. Therefore

$$\hat{\hat{\mathbf{M}}}_3 = -\hat{\mathbb{1}} \otimes \left(\left(\frac{\Gamma}{2}\hat{\mathbf{A}}^{\dagger}\hat{\mathbf{A}}\right)^T\right). \tag{A.17}$$

Finally, we consider the expression of the form

$$\hat{\mathbf{X}}\hat{\mathbf{P}}\hat{\mathbf{Y}} = \hat{\mathrm{X}}_{ab}\hat{\mathrm{P}}_{bc}\hat{\mathrm{Y}}_{cd} = \hat{\hat{\mathrm{Z}}}_{\alpha\beta}\hat{\hat{\mathrm{P}}}_{\beta}. \tag{A.18}$$

The implication of $\beta = n(b-1)+c$ and $\alpha = n(a-1)+d$ is

$$\hat{\hat{\mathrm{Z}}}_{\alpha\beta} = \hat{\hat{\mathrm{Z}}}_{[n(a-1)+d][n(b-1)+c]} = \hat{\mathrm{X}}_{ab}\hat{\mathrm{Y}}_{dc} = \hat{\mathrm{X}}_{ab}\hat{\mathrm{Y}}^T_{cd} = \hat{\mathbf{X}} \otimes \left(\hat{\mathbf{Y}}^T\right) \tag{A.19}$$

Thus,

$$\hat{\hat{\mathbf{M}}}_4 = \Gamma \hat{\mathbf{A}} \otimes \left(\left(\hat{\mathbf{A}}^\dagger \right)^T \right). \tag{A.20}$$

Putting everything together, we get the following superoperator matrix equation:

$$\mathbf{0} = \hat{\hat{\mathbf{M}}} \hat{\hat{\mathbf{P}}} \tag{A.21}$$

where $\hat{\hat{\mathbf{M}}} = \hat{\hat{\mathbf{M}}}_1 + \hat{\hat{\mathbf{M}}}_2 + \hat{\hat{\mathbf{M}}}_3 + \hat{\hat{\mathbf{M}}}_4$.

Once the super operator $\hat{\hat{\mathbf{M}}}$ is constructed, its zero eigenvalue corresponds to the eigenvector that is the steady-state of $\hat{\hat{\mathbf{P}}}$. $\hat{\hat{\mathbf{P}}}$ can then be repacked $\hat{\hat{\mathbf{P}}} \rightarrow \hat{\mathbf{P}}$, and then normalized as described above to yield the steady-state solution to $\hat{\rho}_S$ projected onto the system eigenbasis. Once this is done relevant observables can be calculated by tracing over the system degrees of freedom. For example, the expectation value of system observable $\hat{\Theta}_S$ is then

$$\langle \hat{\Theta} \rangle = \mathrm{Tr}_s[\hat{\Theta} \hat{\rho}_S] \tag{A.22}$$